

AD-A012 537

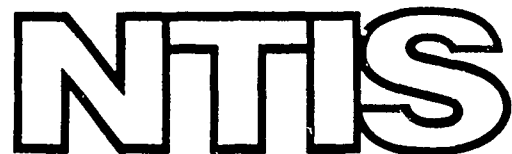
EXPERIMENTAL INVESTIGATION OF THREE
ROTOR HUB FAIRING SHAPES

Peter S. Montana

Naval Ship Research and Development Center
Bethesda, Maryland

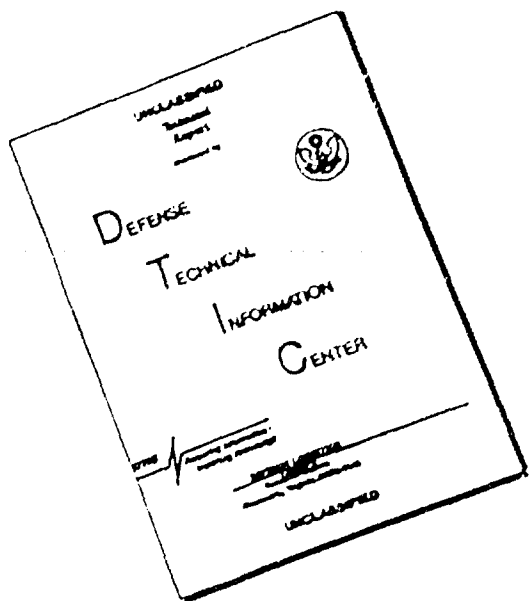
May 1975

DISTRIBUTED BY:



National Technical Information Service
U. S. DEPARTMENT OF COMMERCE

DISCLAIMER NOTICE



THIS DOCUMENT IS BEST
QUALITY AVAILABLE. THE COPY
FURNISHED TO DTIC CONTAINED
A SIGNIFICANT NUMBER OF
PAGES WHICH DO NOT
REPRODUCE LEGIBLY.

ADA012537

210125



**EXPERIMENTAL INVESTIGATION OF THREE
ROTOR HUB FAIRING SHAPES**

by

Peter S. Montana

APPROVED FOR PUBLIC RELEASE:
DISTRIBUTION UNLIMITED

Reproduced by
NATIONAL TECHNICAL
INFORMATION SERVICE
US Department of Commerce
Springfield, VA 22151

Report ASED 333

May 1975

NAVAL
SHIP
RESEARCH
AND
DEVELOPMENT
CENTER

BETHESDA
MARYLAND
20934

Unclassified

SECURITY CLASSIFICATION OF THIS PAGE (When Data Entered)

REPORT DOCUMENTATION PAGE		READ INSTRUCTIONS BEFORE COMPLETING FORM
1 REPORT NUMBER ASED 333	2 GOVT ACCESSION NO	3 RECIPIENT'S CATALOG NUMBER HID-A012 537
4 TITLE (and Subtitle) EXPERIMENTAL INVESTIGATION OF THREE ROTOR HUB FAIRING SHAPES		5 TYPE OF REPORT & PERIOD COVERED
7 AUTHOR/s Peter S. Montana		8 PERFORMING ORG REPORT NUMBER
9 PERFORMING ORGANIZATION NAME AND ADDRESS Naval Ship Research and Development Center Aviation and Surface Effects Department Bethesda, Maryland 20084		10 PROGRAM ELEMENT PROJECT * TASK AREA & WORK UNIT NUMBERS
11 CONTROLLING OFFICE NAME AND ADDRESS Naval Air Systems Command AIR-320D Washington, D.C. 20361		12 REPORT DATE
14 NAME, ADDRESS, AGENCY NAME & ADDRESS IF different from Controlling Office		13 NUMBER OF PAGES 57
		15 SECURITY CLASS of this report Unclassified
		16a DECLASSIFICATION/DOWNGRADING SCHEDULE
16 DISTRIBUTION STATEMENT (of the Report) Approved for Public Release: Distribution Unlimited		
17 DISTRIBUTION STATEMENT (in the abstract entered in Block 20, if different from Report)		
18 SUPPLEMENTARY NOTES		
19 KEY WORDS (Continue on reverse side if necessary and identify by block number) Helicopter, Rotor, Hub, Drag, Pressures, Fairings, Shanks		
20 ABSTRACT (Continue on reverse side if necessary and identify by block number) A series of subsonic wind tunnel evaluations were undertaken to establish minimum drag fairings for helicopter hubs as part of the Helicopter Drag Technology Program. The data reported herein were taken to investigate the flow phenomena affecting helicopter rotor hubs. Three large, 25 percent thick, analytically faired hubs were evaluated (both with and without simulated rotor blade shanks) over a wide range of angles of attack at full scale Reynolds numbers. Forces, moments, and pressures were measured on the hubs.		

Unclassified

SECURITY CLASSIFICATION OF THIS PAGE(When Data Entered)

20.

Of the three fairing shapes evaluated, the reflex curvature fairing was shown to have significantly lower drag at small angles of attack than the other shapes.

10

Unclassified

SECURITY CLASSIFICATION OF THIS PAGE(When Data Entered)

TABLE OF CONTENTS

	Page
ABSTRACT	1
ADMINISTRATIVE INFORMATION	1
INTRODUCTION	1
MODEL DESCRIPTION	2
TEST APPARATUS	2
DATA CORRECTION TECHNIQUES	3
RESULTS AND DISCUSSION	4
NON-ROTATING DATA VALIDATION	4
HUB DATA	6
CONCLUSIONS	8

LIST OF FIGURES

Figure 1 - Hub Fairing Cross Section Shapes	9
Figure 2 - Shank Fairing Shapes	9
Figure 3 - Typical Hub-Shank Assembly	10
Figure 4 - Experimental Evaluation Configuration	11
Figure 5 - Configuration Notation	12
Figure 6 - Drag Coefficients (C_D) Versus Angle of Attack	13
Figure 7 - Drag Coefficients (C_{D_V}) Versus Angle of Attack	15
Figure 8 - Drag Coefficients (C_D) Versus Dynamic Pressure	16
Figure 9 - Lift Coefficients Versus Angle of Attack	17
Figure 10 - Pitching Moment Coefficients Versus Angle of Attack	19
Figure 11 - Pressure Coefficients Along Model Centerlines	21
Figure 12 - Pressure Coefficient Contours on the Upper Surface of the Hub Fairings at a Dynamic Pressure of 50 Pounds Per Square Foot	58

Page

Figure 13 - Pressure Coefficient Contours on the Upper Surface
of the Elliptical Hub-Small Shank Fairing Configurations
at a Dynamic Pressure of 50 Pounds Per Square Foot 69

SYMBOLS

C_D	Drag coefficient, $\frac{D}{qs}$
C_{D_v}	Drag coefficient, $\frac{D}{qv^2/3}$
C_L	Lift coefficient, $\frac{L}{qs}$
C_{L_t}	Lift curve slope, $\frac{\partial C_L}{\partial \alpha}$
C_M	Pitching moment coefficient, $\frac{M}{qsd}$
C_p	Pressure coefficient, $\frac{P-P_\infty}{q}$
d	Diameter of hubs, ft
D	Drag force, lbs
L	Lift force, lbs
M	Pitching moment, lb-in
P	Static pressure, lb/ft ²
P_∞	Freestream static pressure, lb/ft ²
q	Dynamic pressure, $\frac{1}{2}\rho v_\infty^2$, lb/ft ²
S	Hub planform area, ft ²
V	Hub internal volume, ft ³
V_H	Rotational velocity at hub radius, ft/sec
V_T	Rotational velocity at rotor blade tip, ft/sec
V_∞	Freestream velocity, ft/sec
μ	Advance ration, $\frac{V_\infty}{V_T}$, $\frac{V_\infty}{V_H}$
ν_H	Hub advance ratio, $\frac{V_\infty}{V_H}$
ρ	Atmospheric density, slugs/ft ³

ABSTRACT

A series of subsonic wind-tunnel evaluations were undertaken to establish minimum drag fairings for helicopter hubs as part of the Helicopter Drag Technology Program. The data reported herein were taken to investigate the flow phenomena affecting helicopter rotor hubs. Three large, 25-percent thick, analytically faired hubs were evaluated (both with and without simulated rotor blade shanks) over a wide range of angles of attack at full scale Reynolds numbers. Forces, moments, and pressures were measured on the hubs. In addition, fluorescent oil flow visualization was used to aid in the qualitative understanding of the flow. Of the three fairing shapes evaluated, the reflex curvature fairing was shown to have significantly lower drag at small angles of attack than the other shapes.

ADMINISTRATIVE INFORMATION

The work reported herein was sponsored by the Naval Air Systems Command (AIR-320D). Funding was provided under Project F41.421.201, Work Unit 1-1690-105.

INTRODUCTION

The Helicopter Drag Technology Program¹ was developed to meet the growing need for aerodynamically refined helicopter fuselages. Since a large part of the drag of helicopter fuselages is due to the main rotor hub and pylon, a comprehensive analysis of the flow phenomena in this region was undertaken. The analysis is divided into two parts: theory and experiment. The theoretical portion is based on the use of potential flow analysis computer programs² with some simplified separation prediction along streamlines. The experimental portion of the program

¹Montana, P. S., "Helicopter Drag Technology Program Fiscal 1973 Progress Report", NSRDC Tech Note AL-310 (Sep 1973).

²Dawson, C. W. and J. S. Dean, "The XYZ Potential Flow Program," NSRDC Report 3892 (Jun 1972).

approaches the problem through a systematic series of wind tunnel tests. Throughout the program there is a correlation between experimental results and theory to improve prediction techniques and reduce the amount of wind tunnel testing necessary.

This report presents the results of the initial series of wind tunnel tests which were designed to explore the flow over three candidate rotor hub fairing shapes. Each of the shapes was tested both with and without two different size sets of four simulated rotor blade shanks. To accurately model the full-scale flow phenomena, the largest possible hub models and the highest possible dynamic pressures were used. As a result, the Reynolds numbers attained on the models approach those experienced by the SH-3 helicopter's rotor hub at a flight velocity of about 120 knots.

MODEL DESCRIPTION

The rotor hub models tested were all 25-percent thick (height to diameter), 44-inches in diameter, oblate bodies of revolution. Each was instrumented with up to 88 pressure taps located on 3 radii, 22.5 degrees apart. Each hub was provided a means of attaching four simulated rotor blade shanks. The hub fairing shapes, referred to by their cross section shapes of elliptical, circular arc, and reflex curvature, are shown in Figure 1. Two different size sets of four rotor shanks were used, each of which had a 30-percent thick elliptical cross section and a span of 22 inches. One shank in each set was instrumented with 42 pressure taps located at six spanwise stations over the semichord. The shank models are shown in Figure 2. A typical hub shank assembly is shown in Figure 3.

TEST APPARATUS

The test was conducted in NSRDC's 8-by 10-foot subsonic wind tunnel.³ Force and moment data were measured on the wind tunnel's Toledo balance

³Kidd, M. A., "Subsonic Wind-Tunnel Facilities," NSRDC Report 3782 (Jan 1972).

system and were recorded on punched paper tape. Pressure data were measured using a three-ganged S-size scanivalve mounted inside the model and were also recorded on paper tape. The models were supported on a single main support strut and were actuated in angle of attack by an airfoil shaped remotely driven pitch strut. The tunnel setup is shown in Figure 4. The hub fairing models were clamped to a circular aluminum plate attached to the main and pitch struts. This arrangement made it possible to index the azimuth angle of the hub fairing and thereby obtain a full surface pressure field survey.

DATA CORRECTION TECHNIQUES

Conventional corrections⁴ were applied to the measured freestream dynamic pressure to account for solid and wake blockage and buoyancy. Corrections were not made for streamline curvature or down-wash; however, an analysis made for the elliptical hub fairing revealed that for a dynamic pressure of 50 pounds per square foot and angle of attack of zero degrees, the corrections to angle of attack, lift coefficient, and drag coefficient were 0.09, 0.0015, and 0.0026 degrees, respectively. It was not possible to obtain complete support system tare and interference measurements. To obtain the corrections for tare and interference, an approximation to the normal procedure was made by mounting dummy support and pitch struts and wind shields on the tunnel ceiling and by bringing the struts as close to the models as possible without actually touching the models. Runs were made with this system installed for all hub-fairing-only configurations to establish support system interference values. The tare values were approximated by measuring the drag on the equivalent length of exposed struts without any hub fairing or mounting hardware attached.

⁴Pope, A. and J. J. Harper, "Low Speed Wind Tunnel Testing," John Wiley & Sons, Inc (1966).

RESULTS AND DISCUSSION

Non-Rotating Data Validation

The data presented in Figure 6 through 12 are, as stated previously, for nonrotating hub and hub shank fairing models. The use of this type of data for the prediction of the aerodynamic loads on rotating hubs and hub shank configurations can provide meaningful data. A brief survey of the literature has shown that stopped rotor data can be used to simulate rotating data provided that some prespicacity is used. The following conclusions can be deduced from references 5 through 10:

1. At rotor advance ratios, μ , greater than 0.5, the variation of parasite area, D/q , with μ is generally small (5 percent or less).
2. At rotor advance ratios less than 0.5, the variation of D/q with μ is significant (on the order of 15 percent), but an insufficient body of data is available to clearly establish trends for a wide variety of configurations.
3. For hub advance ratios, μ_H , greater than 10, stopped rotor data gives a good approximation of rotating data--especially for lift, roll, and pitching moment coefficients.

Reference 5 presents experimental data on five rotor hubs. For one of the hubs, data are presented for the parasite area as a function of shaft rpm's. When the rpm's are converted to advance ratio (rotor radius is assumed to be ten times the hub radius), the rotor advance ratio range is from 1.0 to infinity. Hence, Reference 5 supports conclusions 1 and 3 because the variation in parasite area with rpm is very small.

Reference 6, which presents hub and hub pylon parasite areas for a range of Mach numbers and rpm's. also supports conclusions 1 and 3. The equivalent rotor advance ratio range is from about 0.2 through infinity.

⁵ Churchill, G. B. and R. D. Harrington, "Parasite Drag Measurements of Five Helicopter Rotor Hub," NASA Memo 1.31-59L (Feb 1959).

⁶ Linville, J. C., "An Experimental Investigation of High Speed Rotorcraft Drag," U.S. Army Air Mobility Research and Development Laboratory Tech Report 71-46 (Feb 1972).

Reference 7 presents the results of a drag reduction program conducted on a hub-pylon model mounted to the floor of a wind tunnel. The data is plotted as parasite area versus advance ratios which ranged from 0.1 to 0.8. This report supports conclusions 1 and 2. For advance ratios less than 0.5, there is a noticeable increase in D/q at the lower of the two wind speeds (100 mph) tested for configurations including small rotating rotor controls. The nature of the D/q curve in Figure 2 (Reference 7) is suspiciously similar to that of Figure 46(c) (Reference 6) for $M_\infty = 0.2$. The model configuration of Figure 46(c) includes a wing at 8 degrees angle of attack in close proximity to the rotor hub. In all probability, the vortex sheet shed from the wing acted like a solid boundary and interacted with the large laminar separated wake from the hub fairing. This deduction could be applied to Reference 6 for the lower wind speed. The effect is further supported by noting that removing the wing or increasing the Mach number eliminated the decreasing nature of the curve in Reference 7. In Reference 6, removing the small rotor controls and blade stubs from the test configuration also eliminated most of the same characteristic. In addition, all of the configurations with wings in Reference 6 show inconsistencies in drag trends which further support the flow interference concept.

References 8, 9, and 10 present various data obtained in NSRDC's 8- by 10-foot subsonic wind tunnels on the Hughes rotor/wing aircraft model.

⁷ Foster, R. D., "Results of the 1/2 Scale HU-1 and High Speed Helicopter Pylon and Hub Model Wind Tunnel Investigation," Bell Helicopter Company (Mar 1961).

⁸ Reader, K. R., "Wind Tunnel Tests, at High Advance Ratios, of the Hughes Rotor/Wing Aircraft Model (Series X) with Wing Flaps." NSRDC Test Report AL-65 (Dec 1965).

⁹ White, H. E. and J. T. Matthews, "Wind Tunnel Tests of the Highs Rotor-Wing Model at High Advance Ratios," NSRDC Test Report AL-53 (Oct 1968).

¹⁰ Briandy, F. J. and F. S. Okamoto, "Rotor/Wing Series VIII Wind Tunnel Tests Concept Model High Advance Ratios," Hughes Tool Company HTC-AD67-49 (Sep 1967).

The data are primarily plots of force and moment coefficients and coefficient combinations plotted versus rotor azimuth angle for several advance ratios including stopped rotor. The data for the stopped rotor are in good agreement with the higher advance ratio data; they are in especially good agreement for the lift, pitch, and roll coefficients. Figure 14 (Reference 8) plots dynamic rotor data for three revolutions versus azimuth angle and discrete point data for the stopped rotor which were obtained by indexing the rotor azimuth angle. Although the stopped rotor drag data do not follow the dynamic data, the mean drag value obtained by indexing agrees with the mean drag obtained from the dynamic data.

With the above discussion in mind, it should be possible to make efficient use of the data presented herein.

HUB DATA

The drag coefficient, C_D , presented in Figure 6 as a function of angle of attack, α , shows that in all cases the reflex curvature hub fairing configurations have the least drag while the elliptical hub fairings have the most drag. It should be noted that C_D comparisons (also lift coefficients, C_L , and pitching moment coefficient, C_M , comparisons) are equivalent to parasite drag area, D/q , L/q , and M/q , comparisons because all of the coefficients are referenced to the hub fairing planform area which is the same for all three hub fairing configurations. A very interesting comparison of the drag characteristics of the three hub-fairing-only configurations is made in Figure 7. This figure presents a modified drag coefficient, C_{D_V} , referenced to the area derived from the volume enclosed by each hub fairing as a function of α . In effect, C_{D_V} is an efficiency rating which takes into account some of the practical packaging aspects of enclosing the rotor hub components. For advanced, high-speed helicopters with auxiliary propulsion, small negative, and even positive, rotor shaft angles are anticipated. In this situation, Figure 7 indicates that approximately a 20-percent reduction in drag is obtainable by using the reflex curvature fairing. For conventional helicopters which obtain their propulsion by tilting the rotor forward, Figure 7 indicates that the more sophisticated reflex and circular

arc shapes are less efficient than the elliptical fairing shape when the shaft angle is less than -6 degrees. All of this discussion presupposes that the presence of the fuselage and pylon does not greatly alter the character of the hub flow field which, of course, they always do to an extent dependent on the helicopter's configuration.

Figure 8 is a plot of the drag coefficient at zero angle of attack versus dynamic pressure. All of the configurations exhibit a sensitivity to q , with C_D decreasing as q increases. Of the three hub fairings, the circular arc fairing is the least sensitive. The data taken for the elliptical hub configurations usually had more data points. That data shows a marked drop in C_D between $20 \text{ psf} < q < 30 \text{ psf}$. This drop indicates that transition from laminar to turbulent flow has occurred and corresponds to a Reynolds number of about 3.1×10^6 based on hub diameter. This is about one order of magnitude higher than the Reynolds number for transition given in Reference 11 for a sphere in uniform flow.

The lift and pitching moment coefficient data which are presented in Figures 9 and 10, are basically linear functions of α over the ± 9 degree range tested. In fact, the C_L and C_M data for all of the hub and hub shank fairing configurations is very similar. For the hub-shank configurations, these C_L and C_M characteristics were expected because the shank aerodynamics were expected to be dominant. (For the drag, differences in hub-shank interference and in hub flow separation account for the different values between configurations.) One characteristic worth noting is the lift curve slopes, $C_{L\alpha}$, for the hub alone configurations. The reflex curvature fairing has about one and one-half times the $C_{L\alpha}$ of the elliptical fairing, with the circular arc fairing intermediate. If this data were referenced to the volume area, as was the drag in Figure 7, the differences in $C_{L\alpha}$ would be even greater. The significance to conventional helicopter configurations is that the reflex shape would contribute about three times more download than the elliptical hub.

¹¹ Schlichting, H., "Boundary Layer Theory," McGraw-Hill Book Company (1968).

In addition to the force data, a considerable amount of pressure data was taken. These data are presented as pressure coefficient, C_p , plots in Figures 11, 12, and 13. Figure 11 shows the C_p variation along the centerline for each configuration tested. Figure 12 shows curves of constant C_p on each hub-alone configuration, and Figure 13 shows curves of constant C_p for the elliptical hub fairing with small shanks configurations. These last three figures are presented for information only.

CONCLUSIONS

1. Rotating hub data may be simulated with stopped rotor hub experiments provided the rotor advance ratio is greater than 0.5 or the hub advance ratio is greater than 10.0.
2. The reflex curvature hub fairing had the lowest drag coefficient, and the highest lift coefficient of the three hub fairings evaluated.
3. The reflex curvature hub fairing was the most efficient hub fairing shape provided the angle of attack was greater than -6 degrees.
4. The elliptical hub fairing was the most efficient hub fairing shape for angles of attack less than -6 degrees.
5. Transition from laminar to turbulent separation occurred on the elliptical hub fairing at a dynamic pressure of about 25 psf. (Reynolds number of 3.1×10^6).
6. The circular arc hub fairing was the least sensitive to changes in Reynolds number.
7. Of the configurations with simulated rotor blade shanks, the reflex curvature hub fairing configurations had the lowest drag coefficient.
8. The lift coefficient and pitching moment coefficient characteristics of the configurations with simulated rotor blade shanks were dominated by the aerodynamics of the blade shanks.

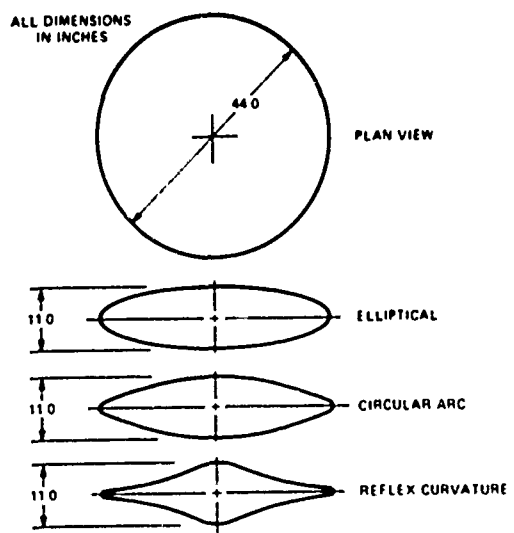


Figure 1 – Hub Fairing Cross Section Shapes

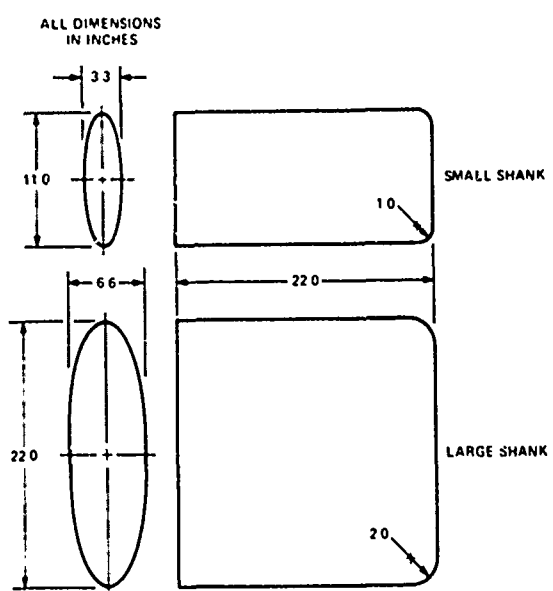


Figure 2 – Shank Fairing Shapes

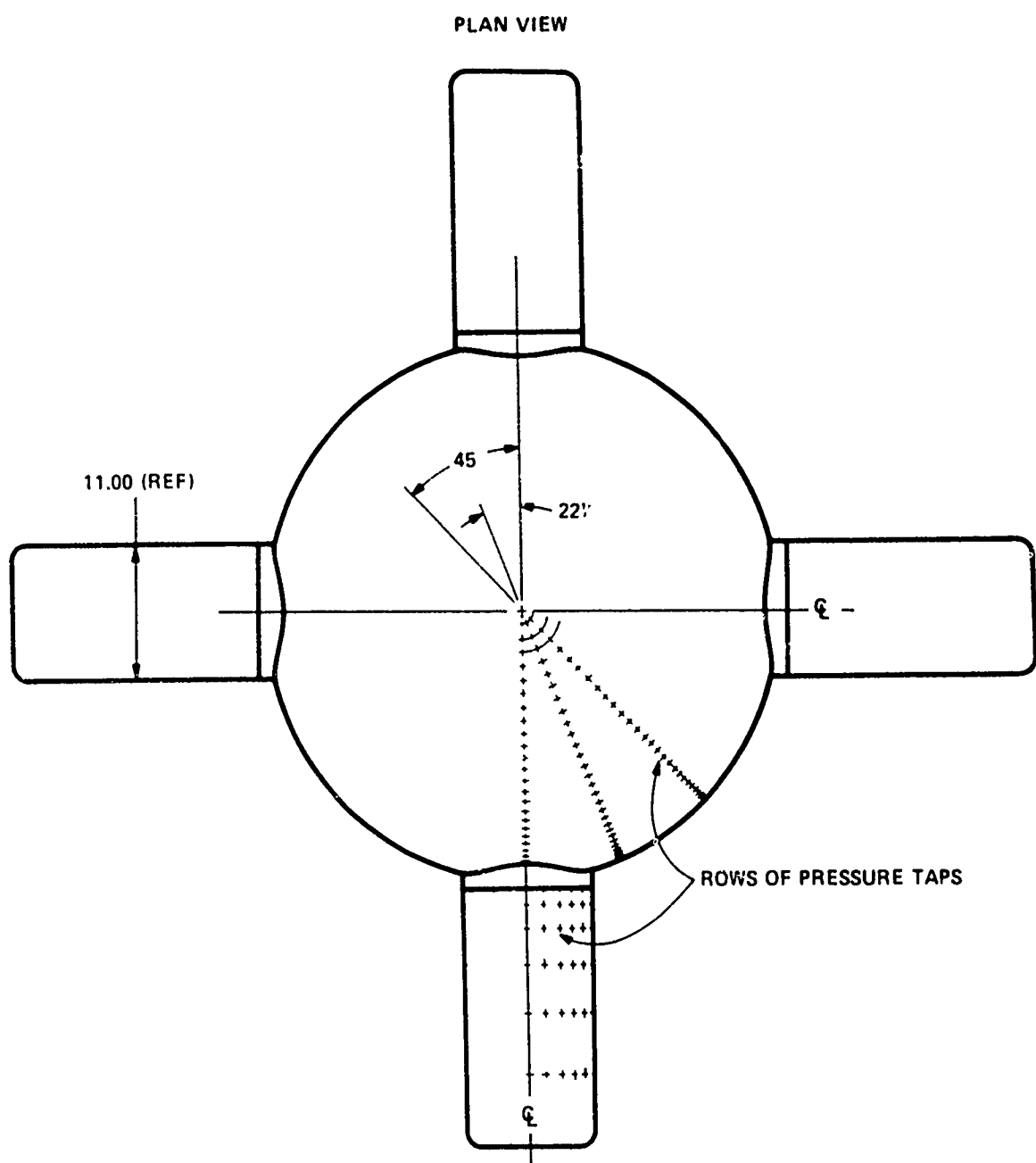


Figure 3 – Typical Hub-Shank Assembly

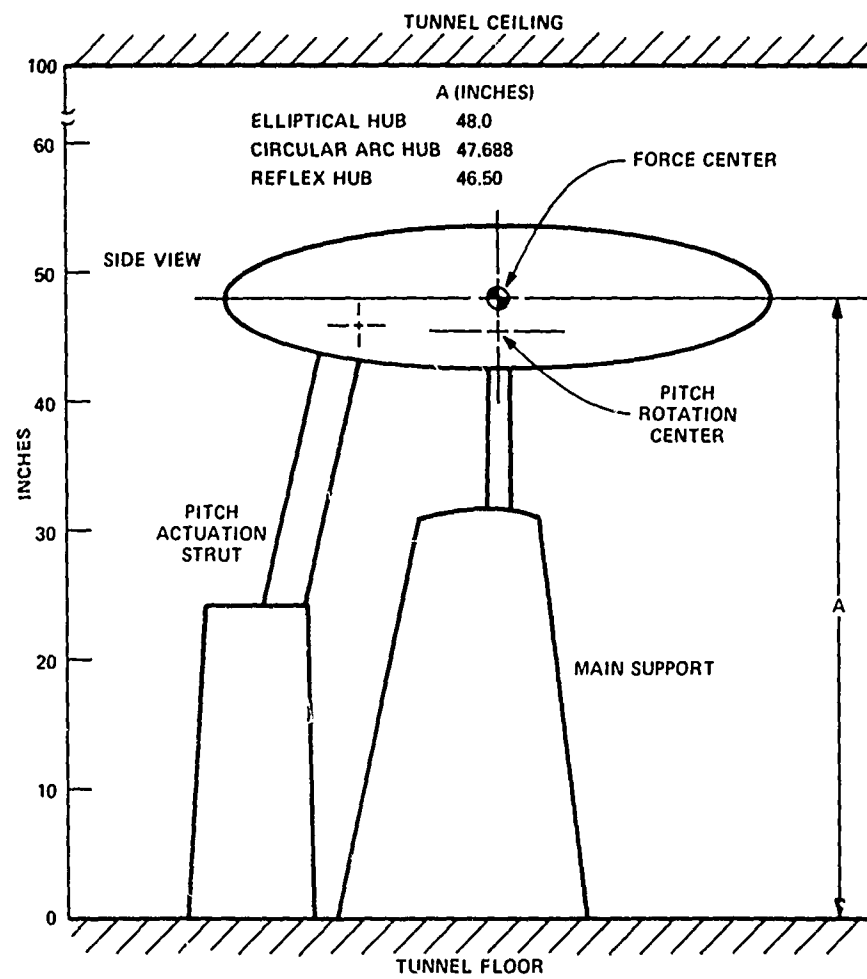
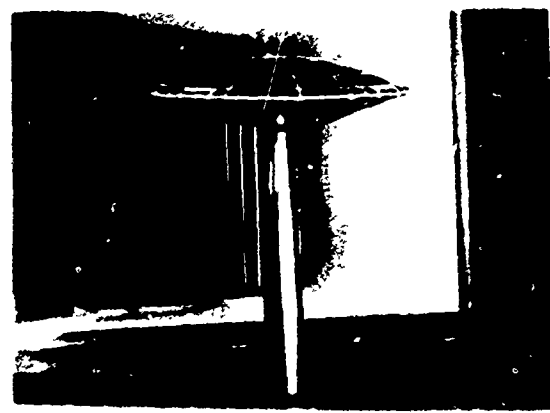
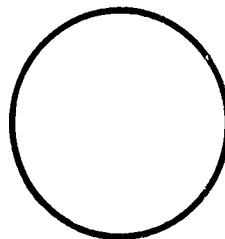


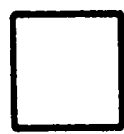
Figure 4 – Experimental Evaluation Configuration

PLAN VIEWS



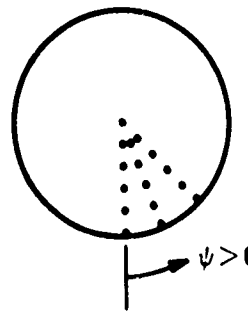
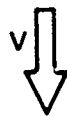
HUB FAIRINGS

- EH - ELLIPTICAL
- CH - CIRCULAR ARC
- RH - REFLEX CURVATURE



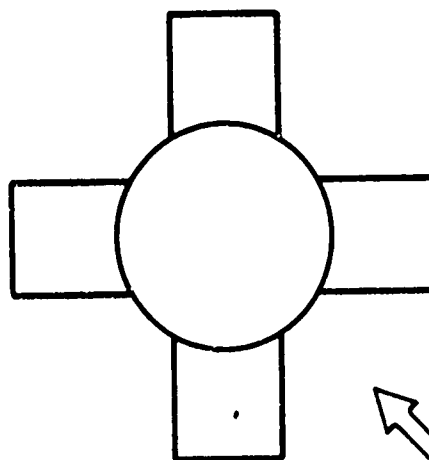
SHANK FAIRINGS

- SS - SMALL SHANK
- LS - LARGE SHANK



HUB ORIENTATION

- ψ - AZIMUTH ANGLE



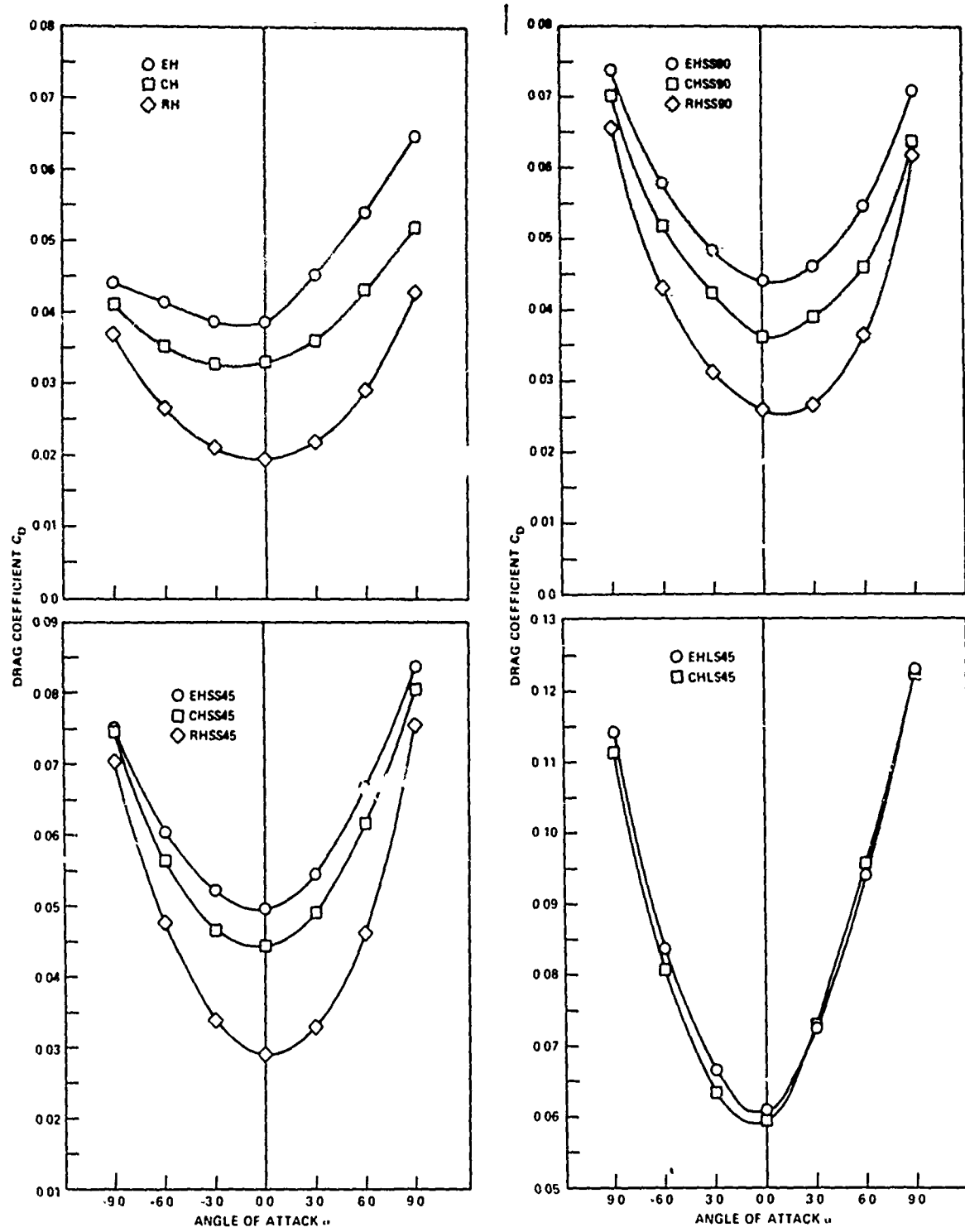
HUB SHANK ORIENTATION

EXAMPLES

- EHSS45°
- RH30°

Figure 5 – Configuration Notation

Figure 6 – Drag Coefficients (C_D) Versus Angle of Attack



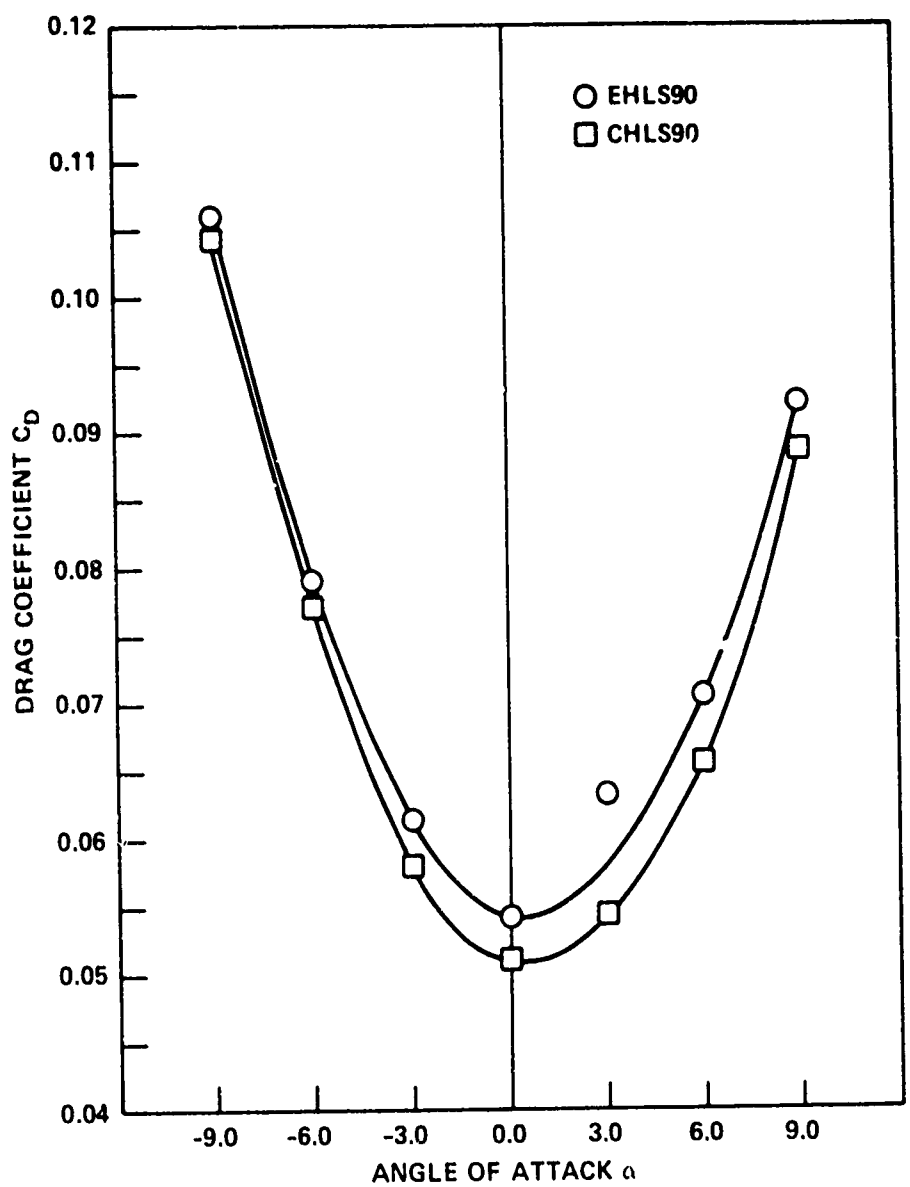


Figure 6 – (Concluded)

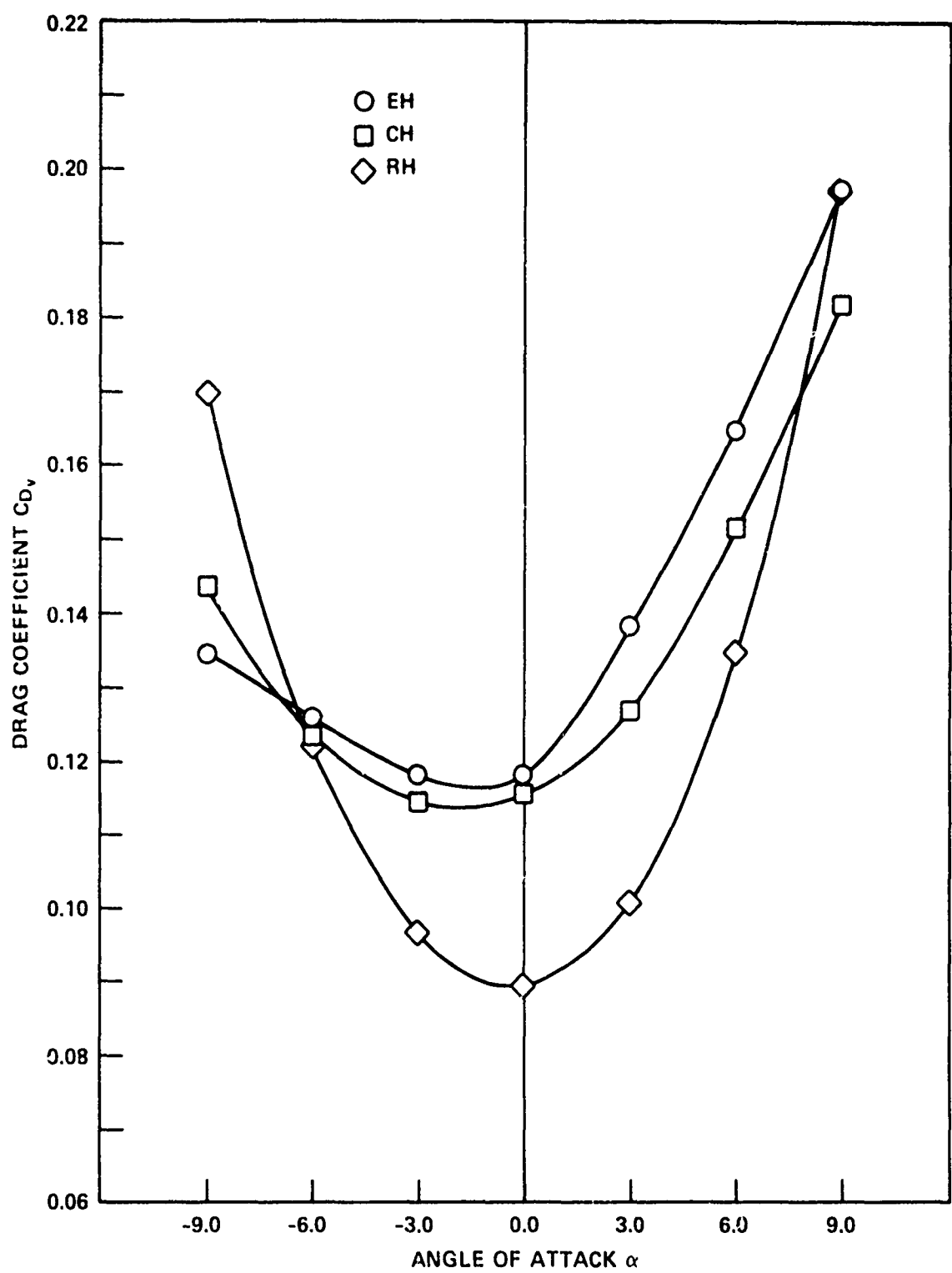


Figure 7 – Drag Coefficients (C_{Dv}) Versus Angle of Attack

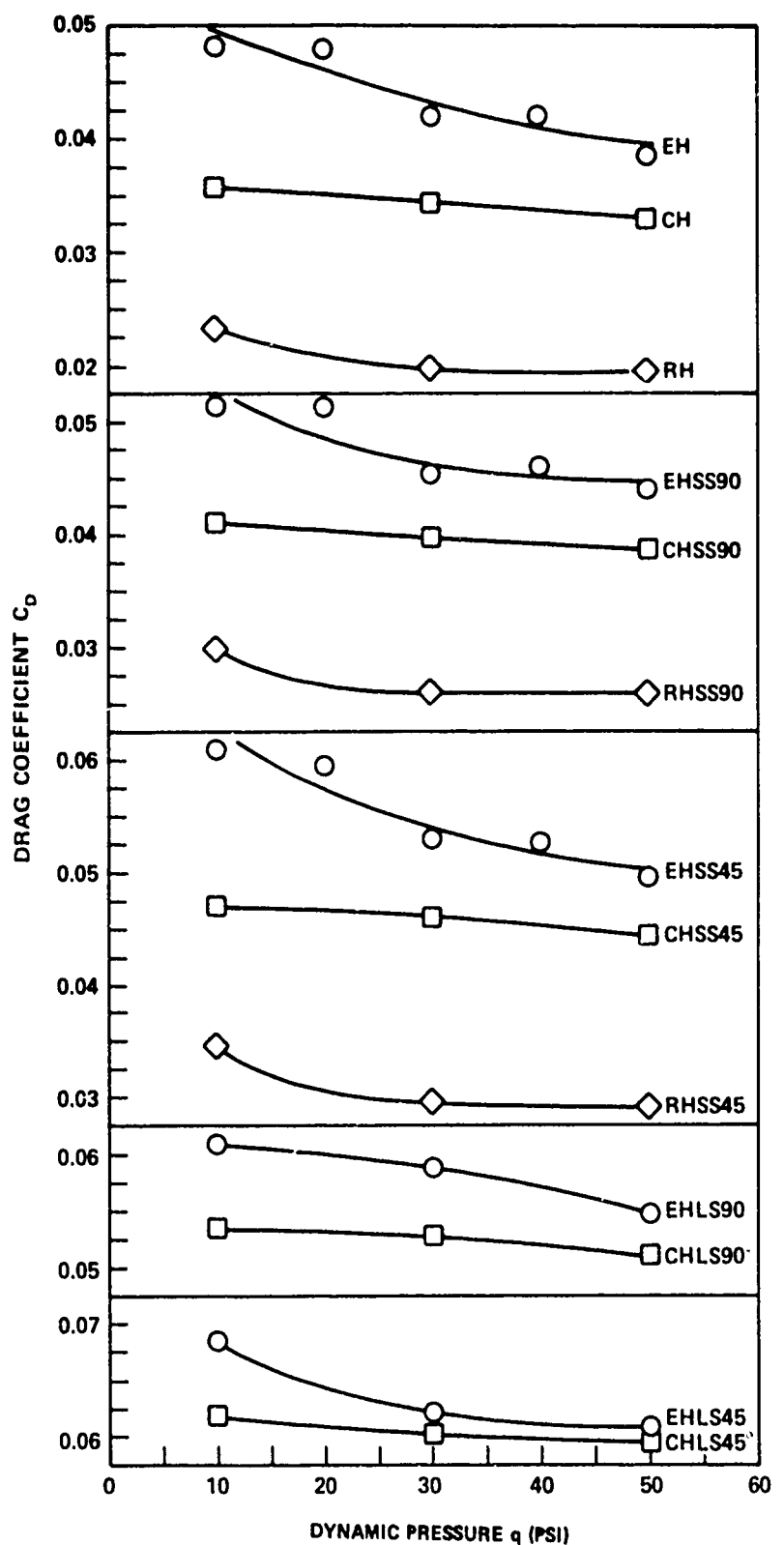
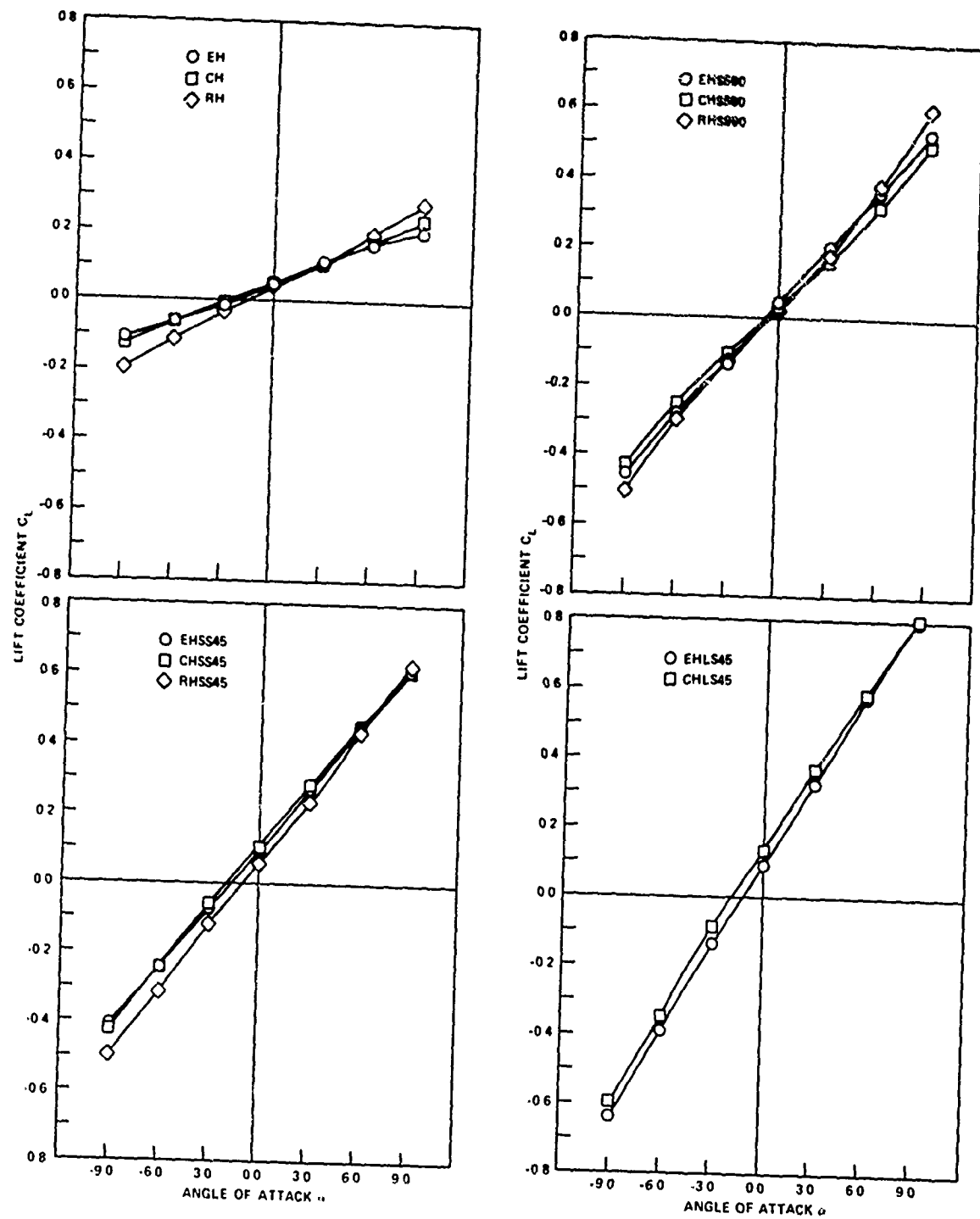


Figure 8 – Drag Coefficients (C_D) Versus Dynamic Pressure

Figure 9 – Lift Coefficients Versus Angle of Attack



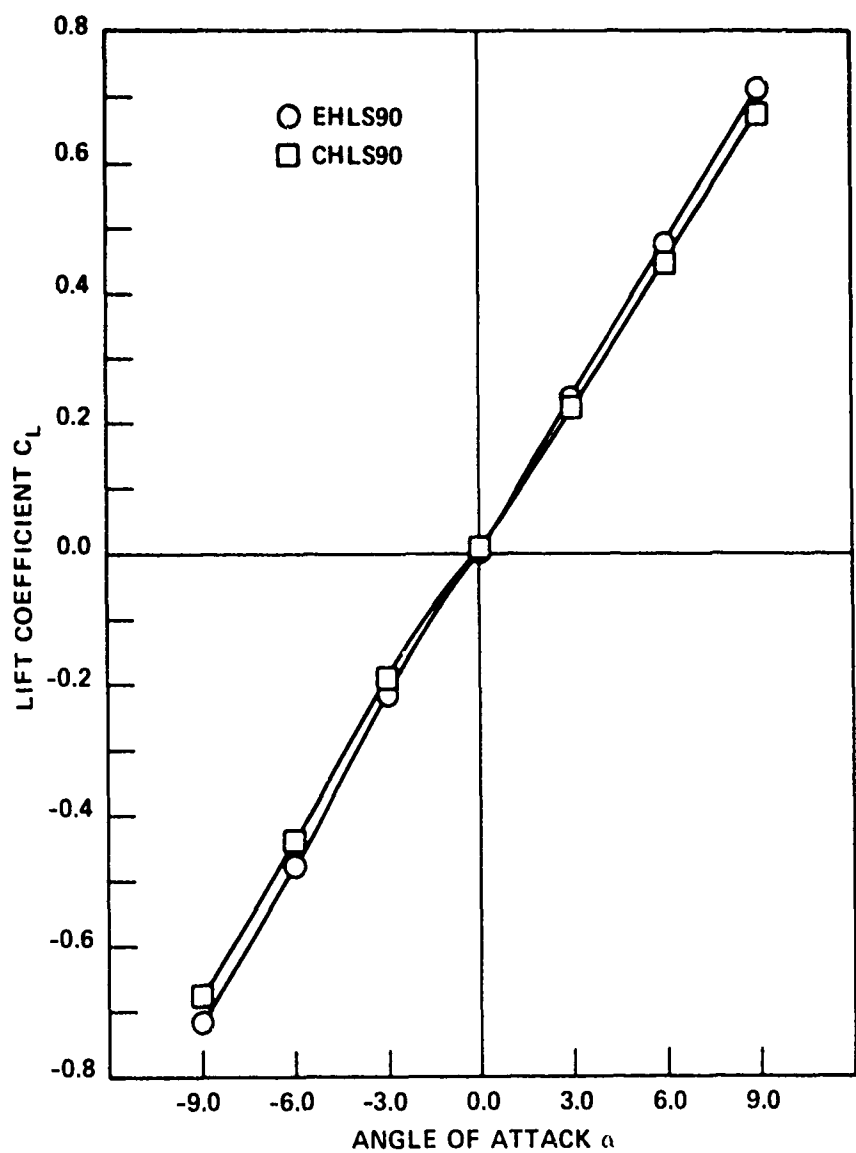
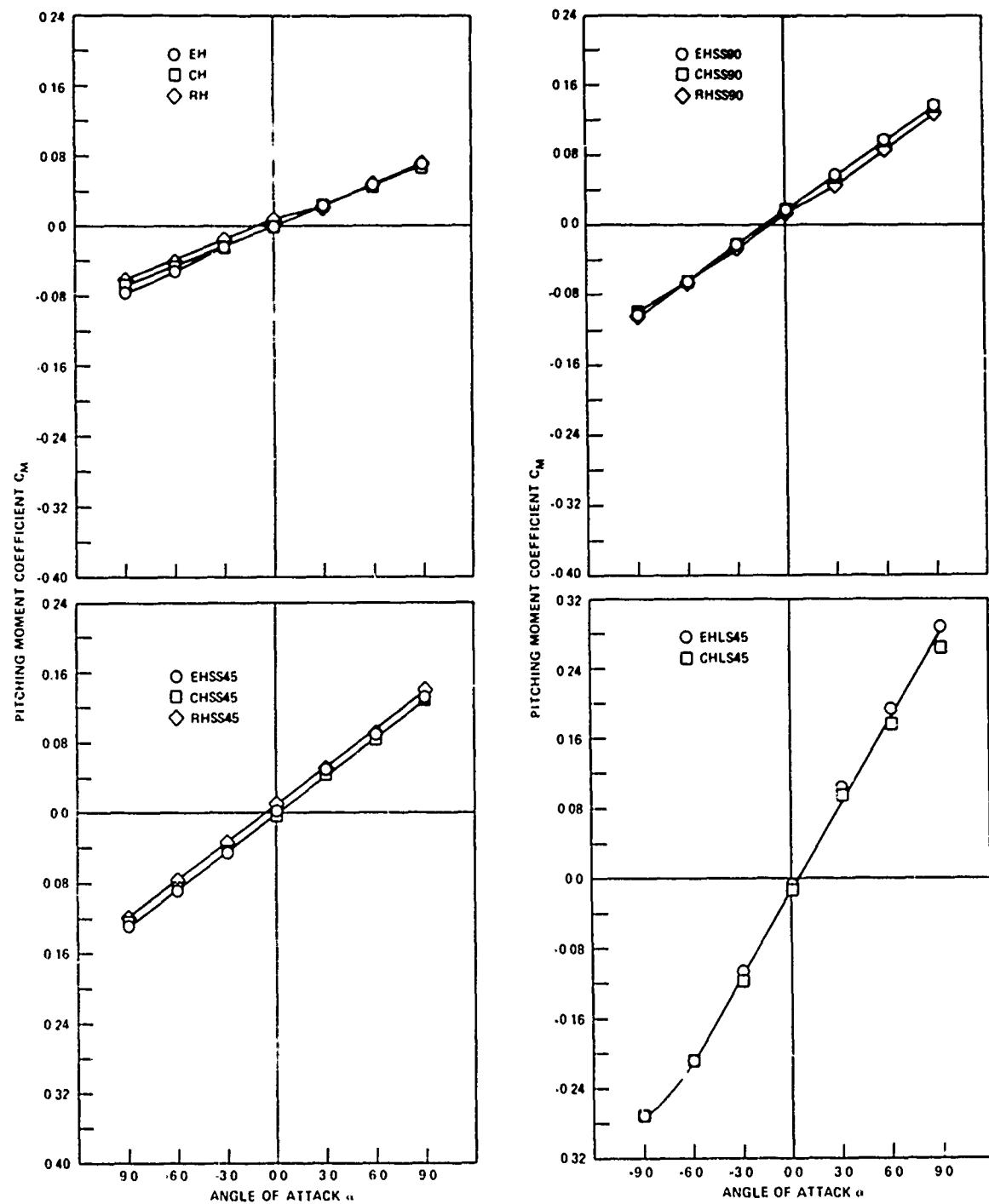


Figure 9 (Concluded)

Figure 10 – Pitching Moment Coefficients Versus Angle of Attack



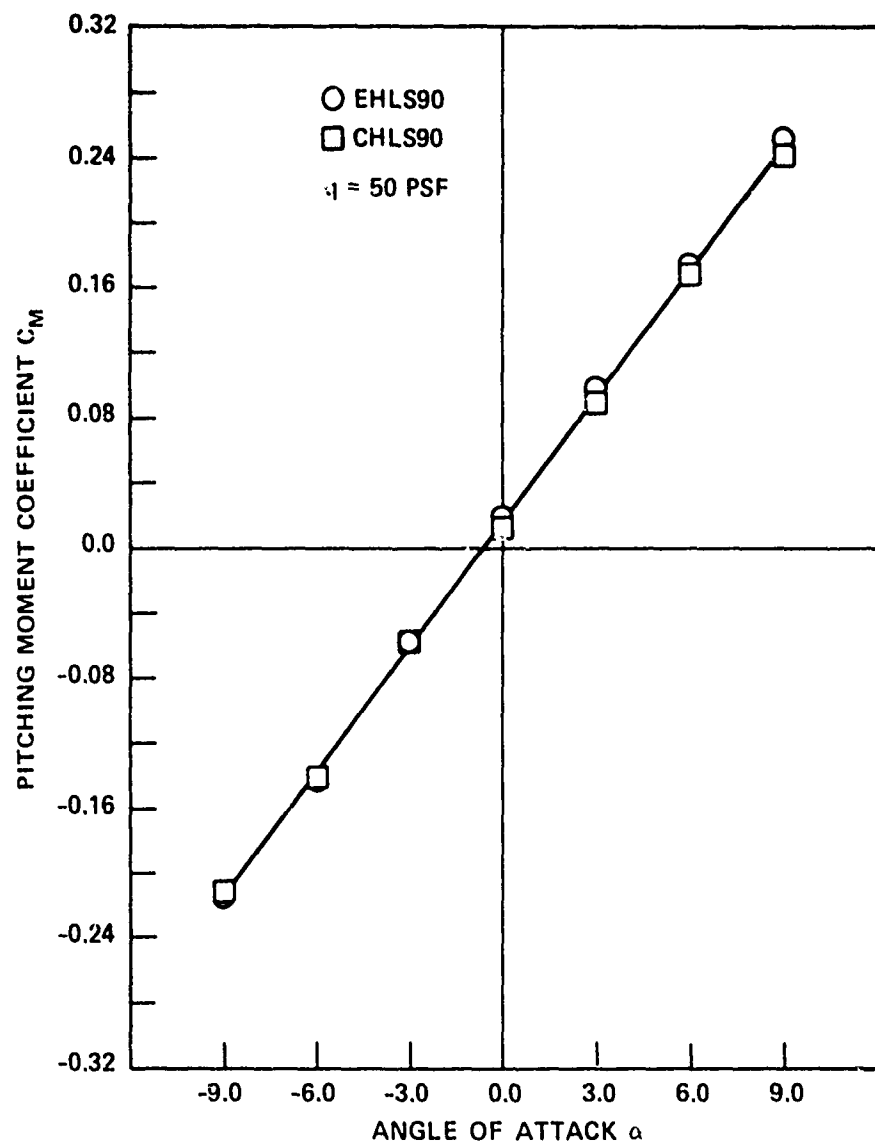
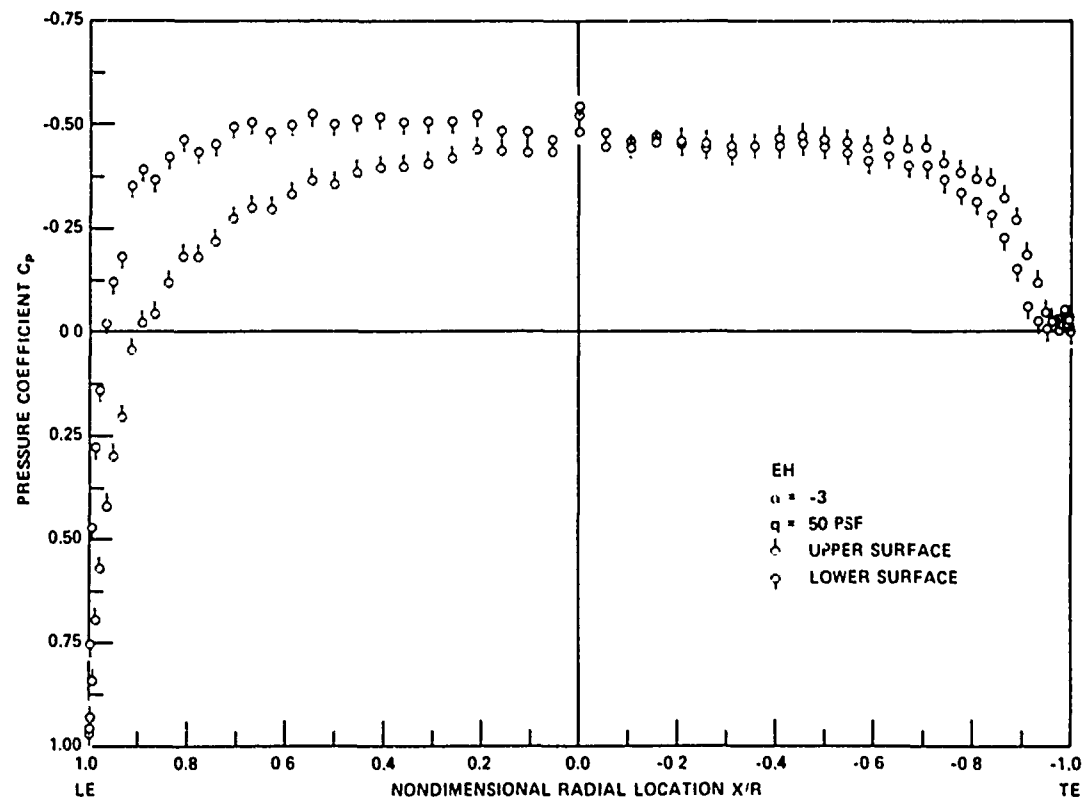
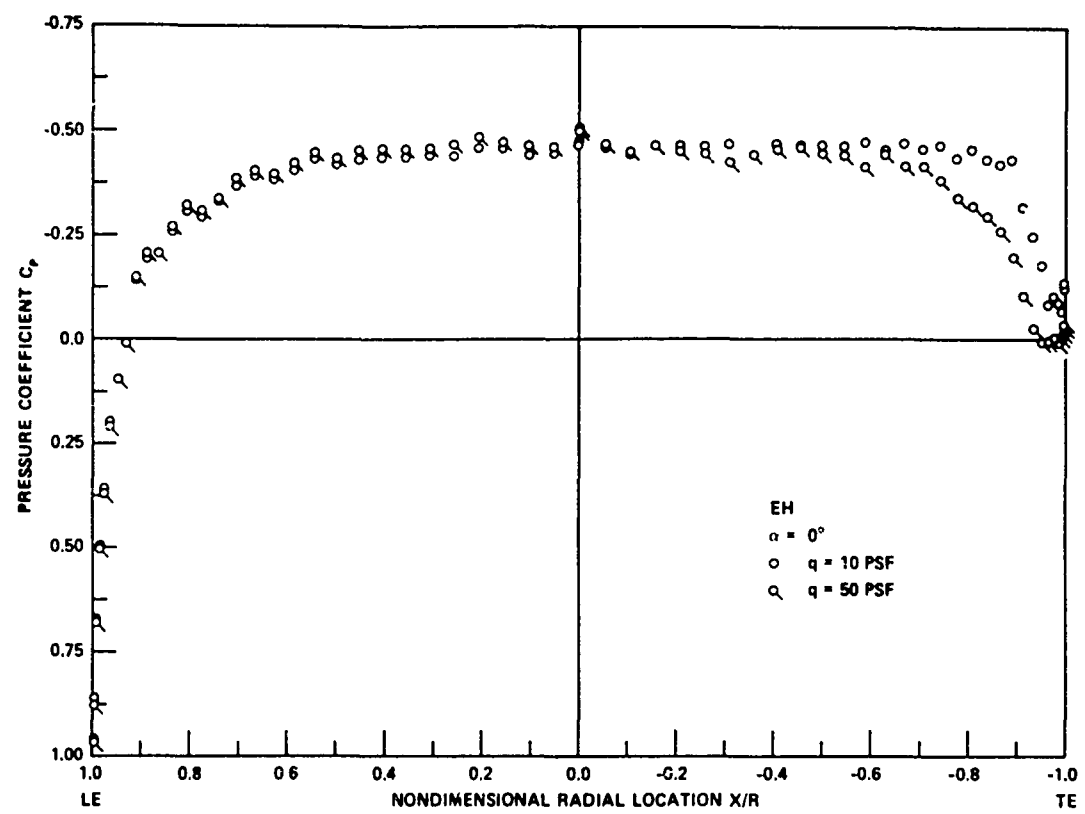


Figure 10 – (Concluded)

Figure 11 – Pressure Coefficients Along Model Centerlines



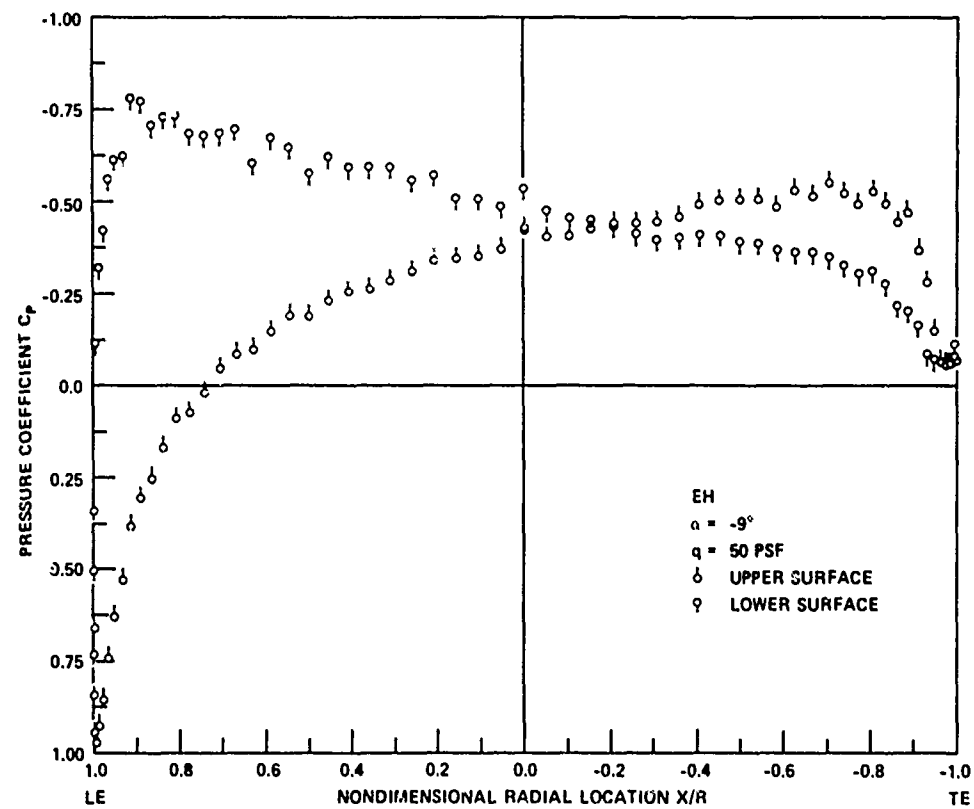
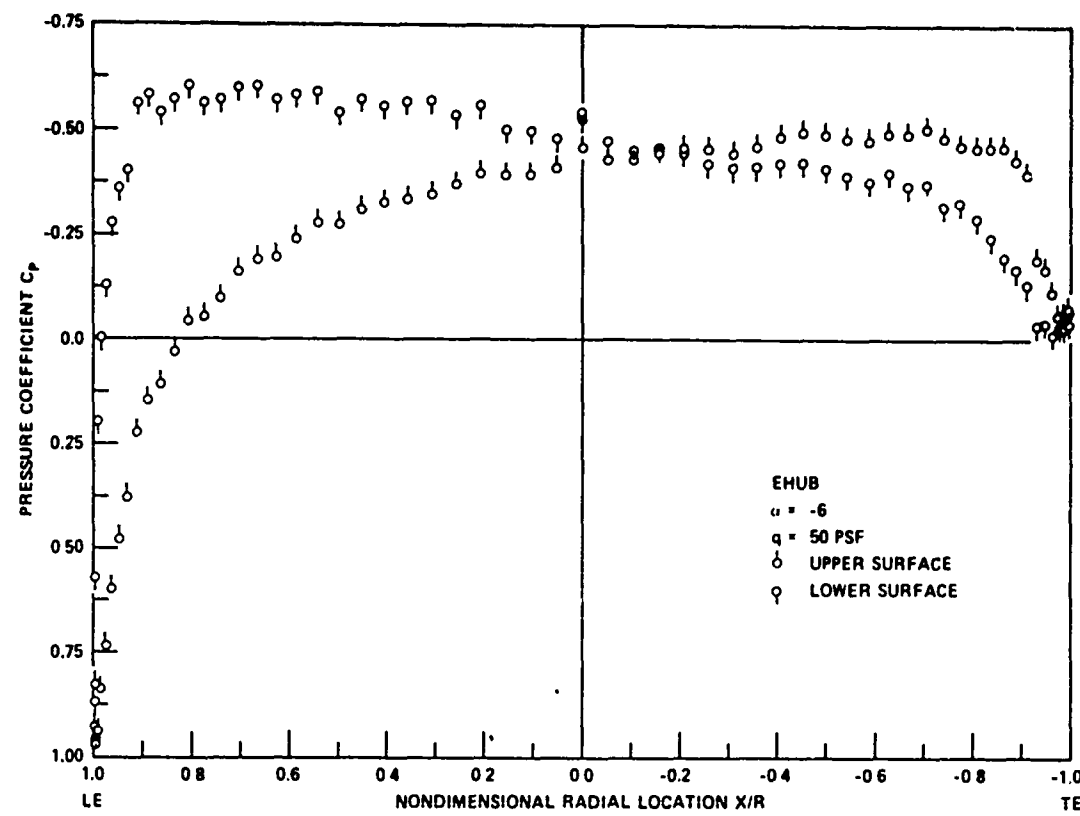


Figure 11 – (Continued)

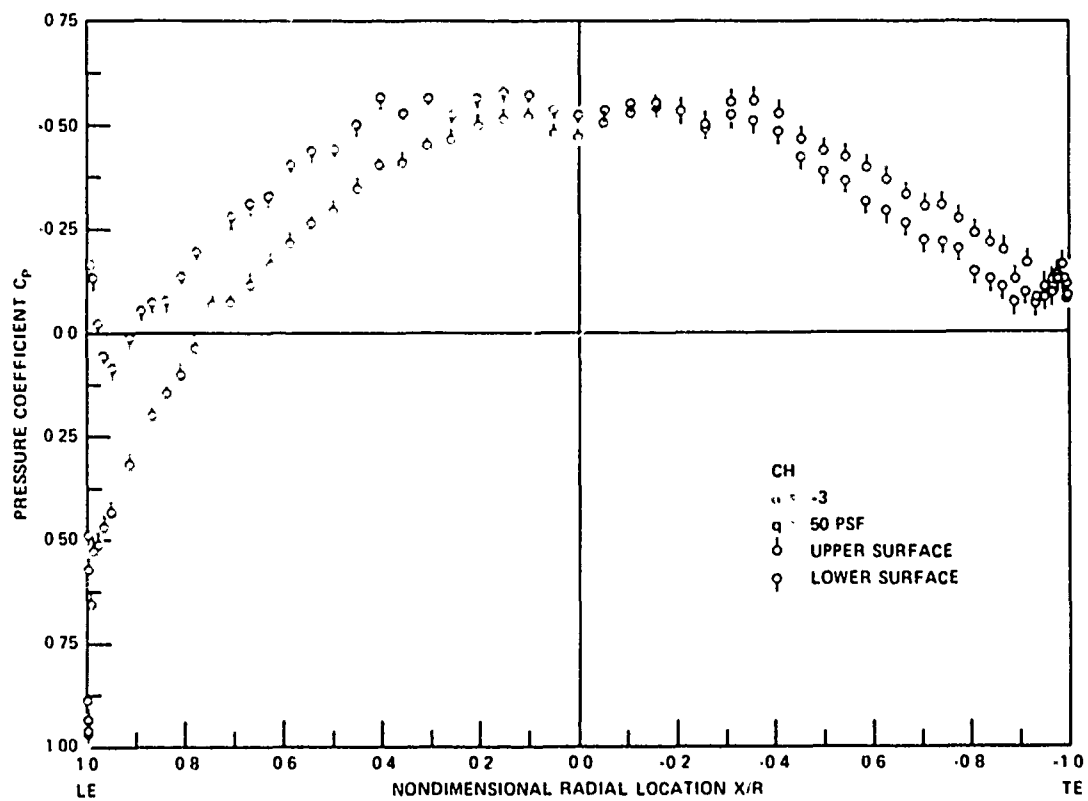
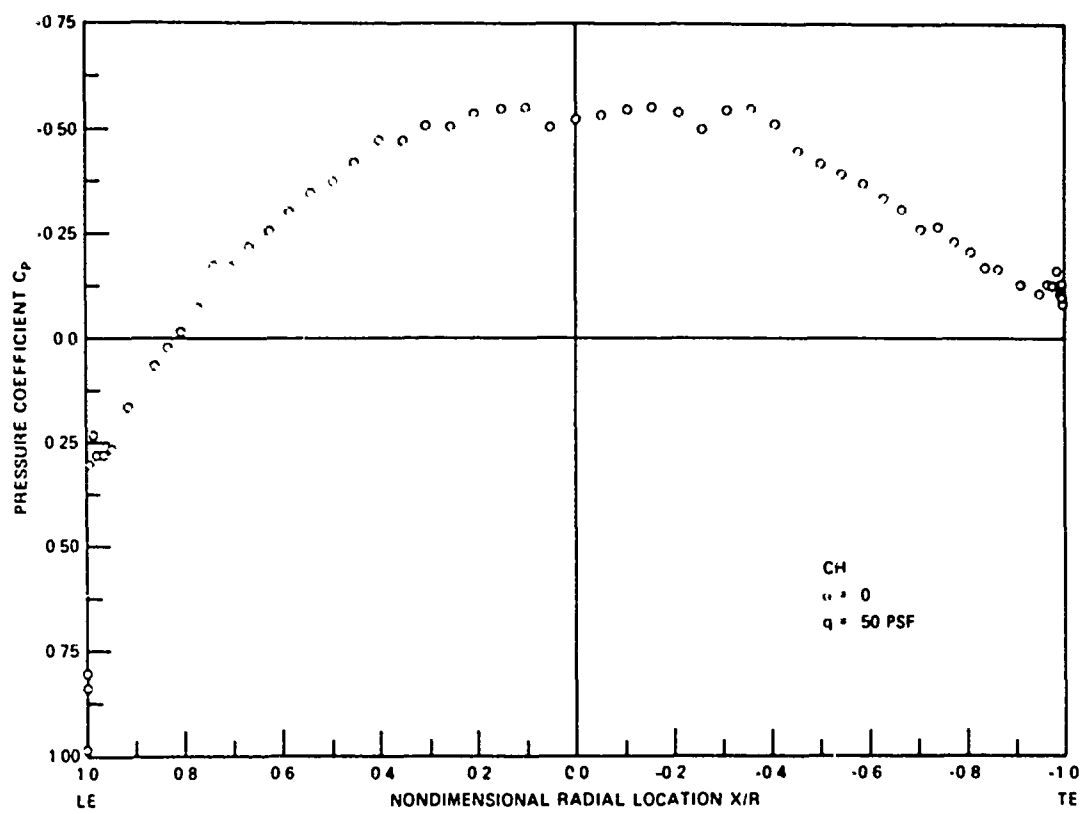


Figure 11 - (Continued)

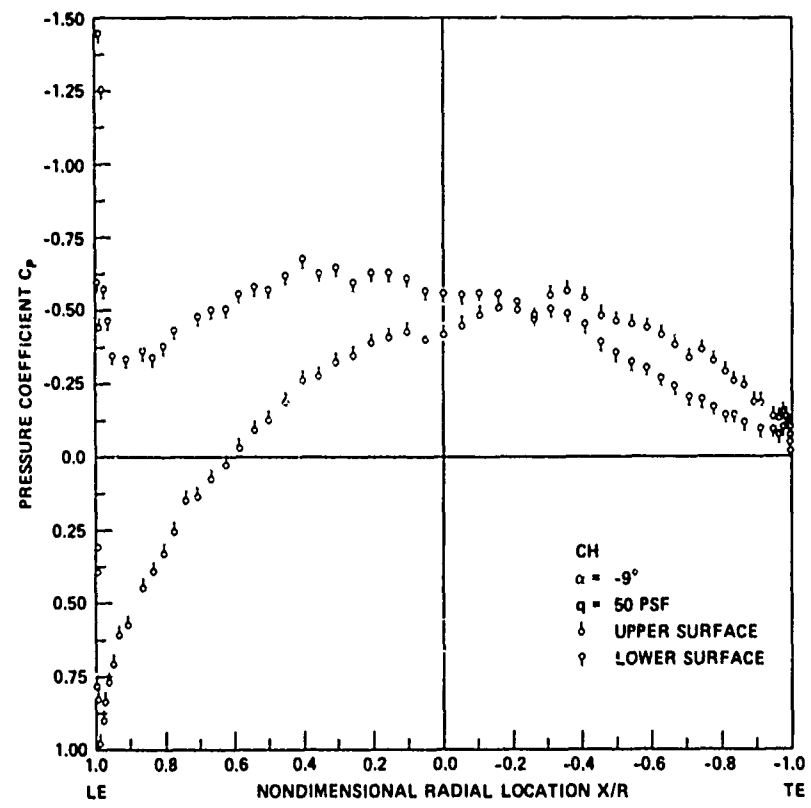
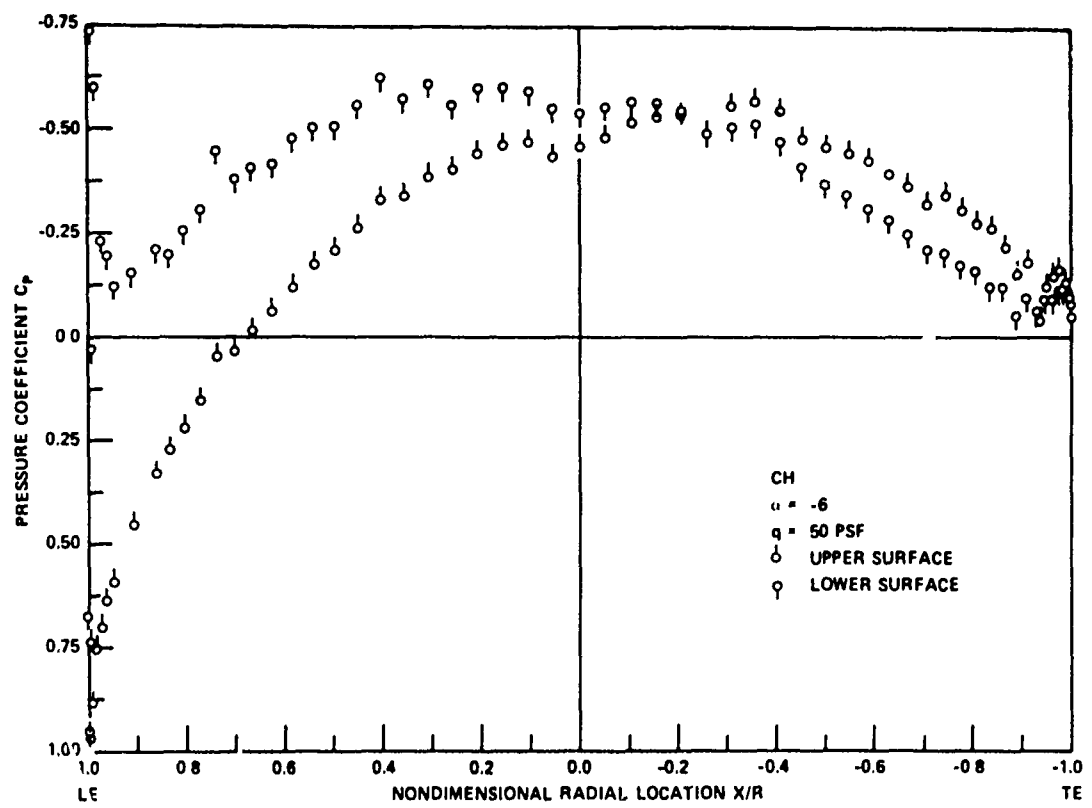


Figure 11 - (Continued)

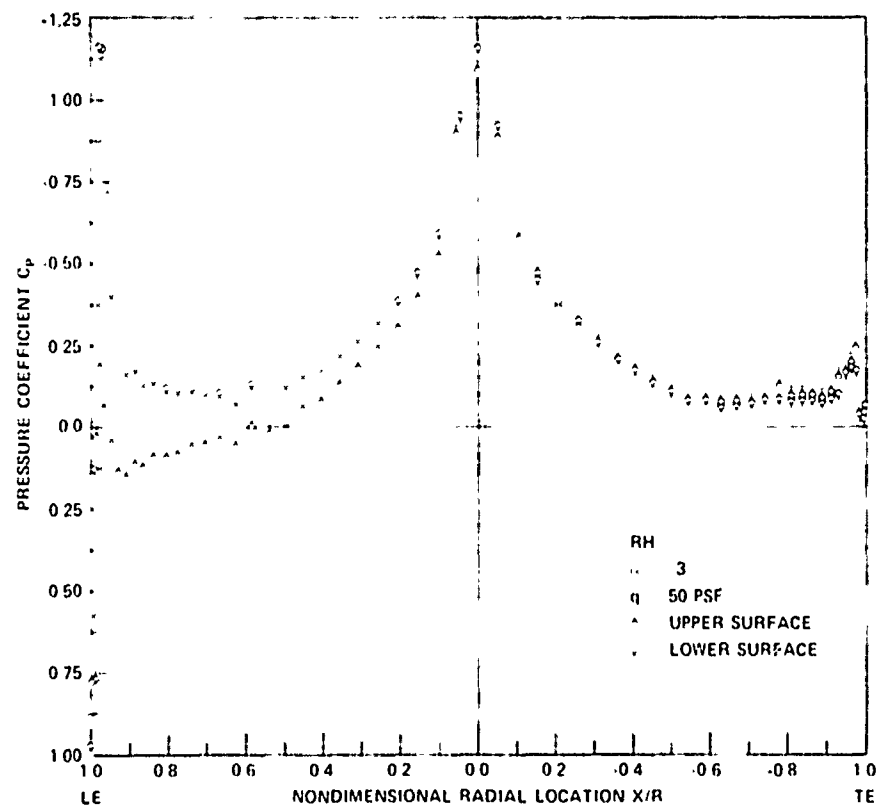
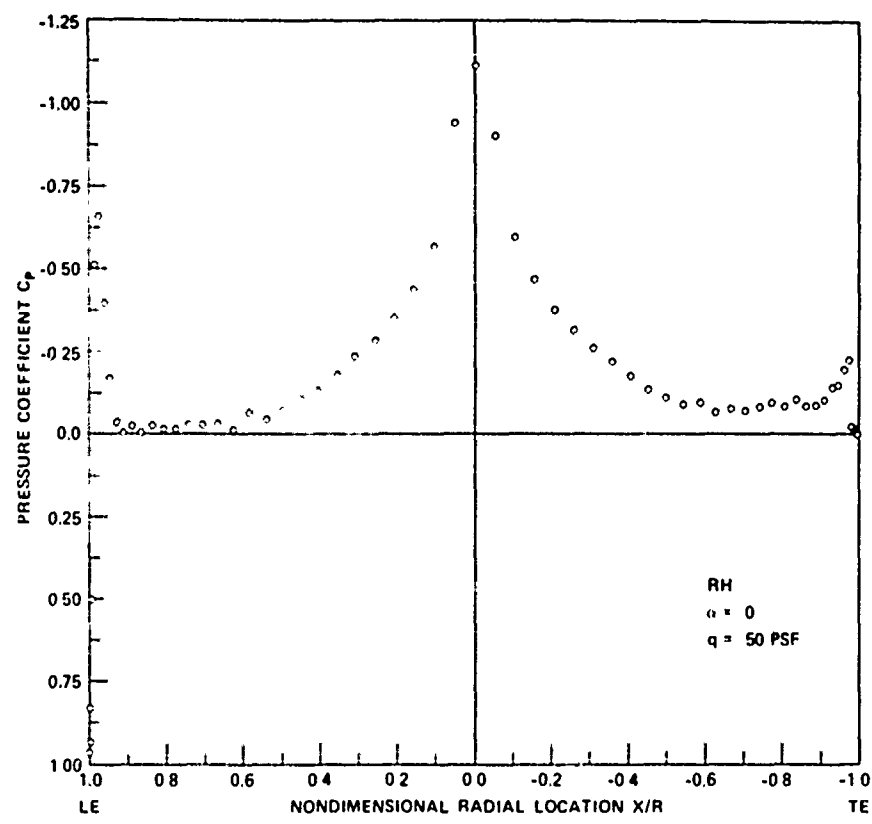


Figure 11 -- (Continued)

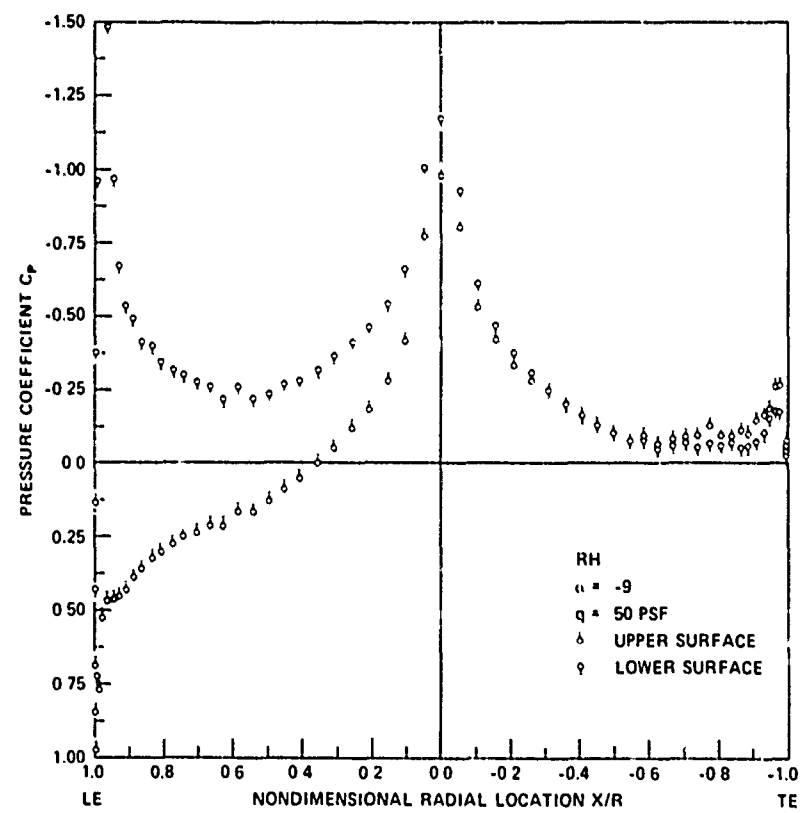
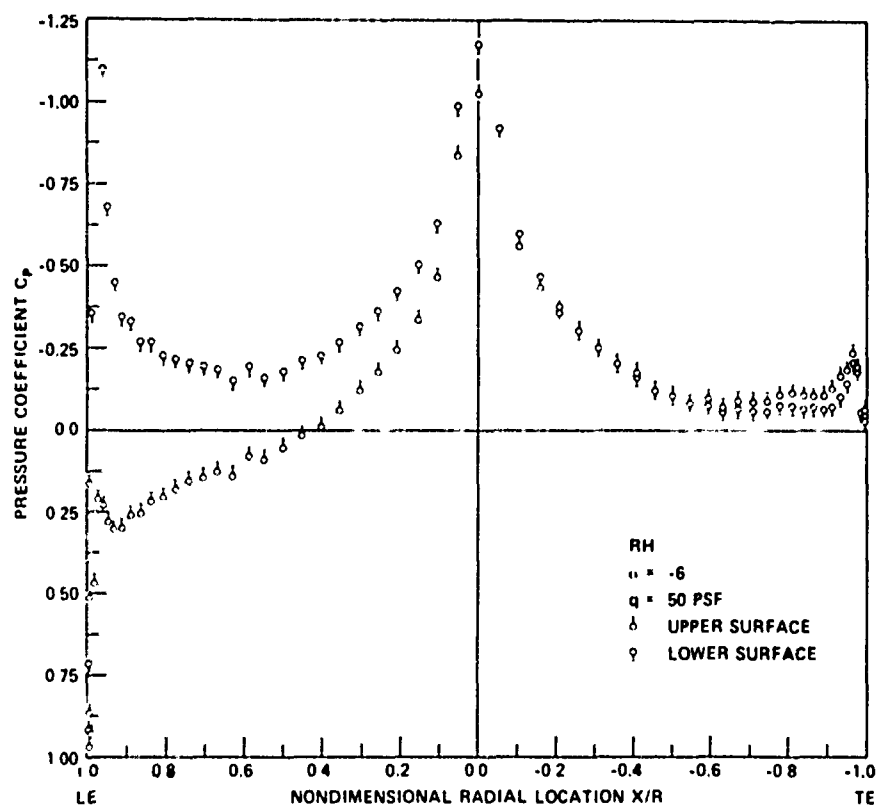


Figure 11 – (Continued)

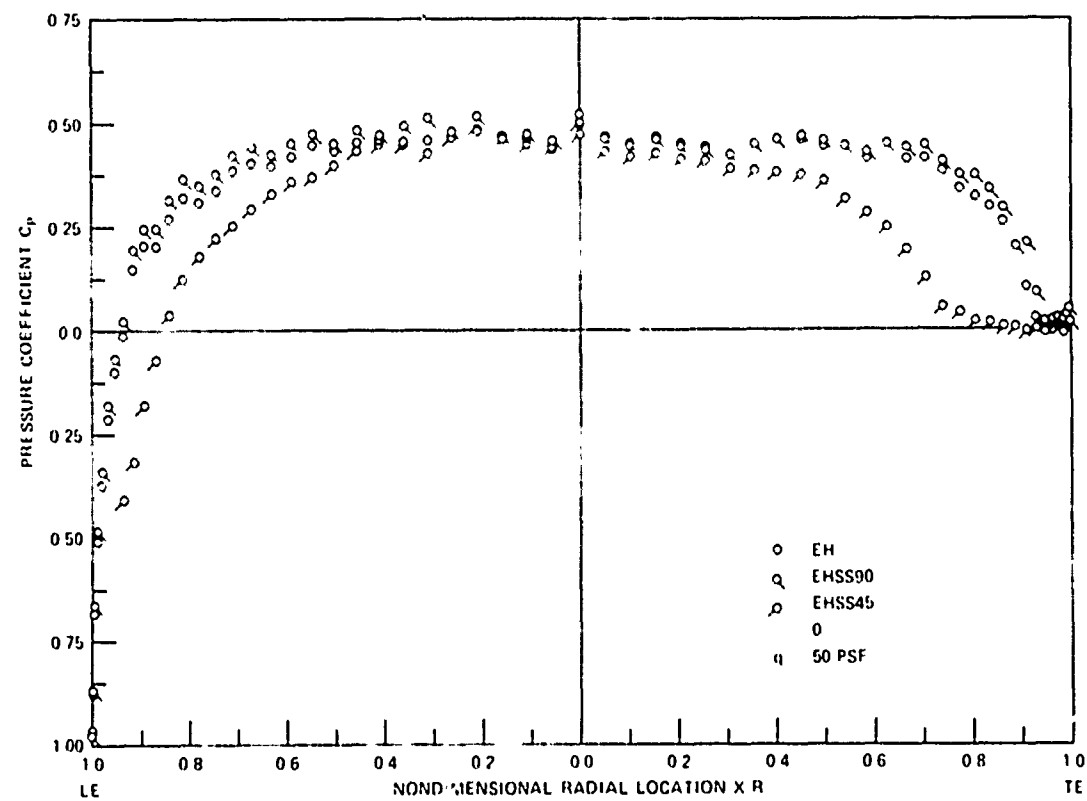
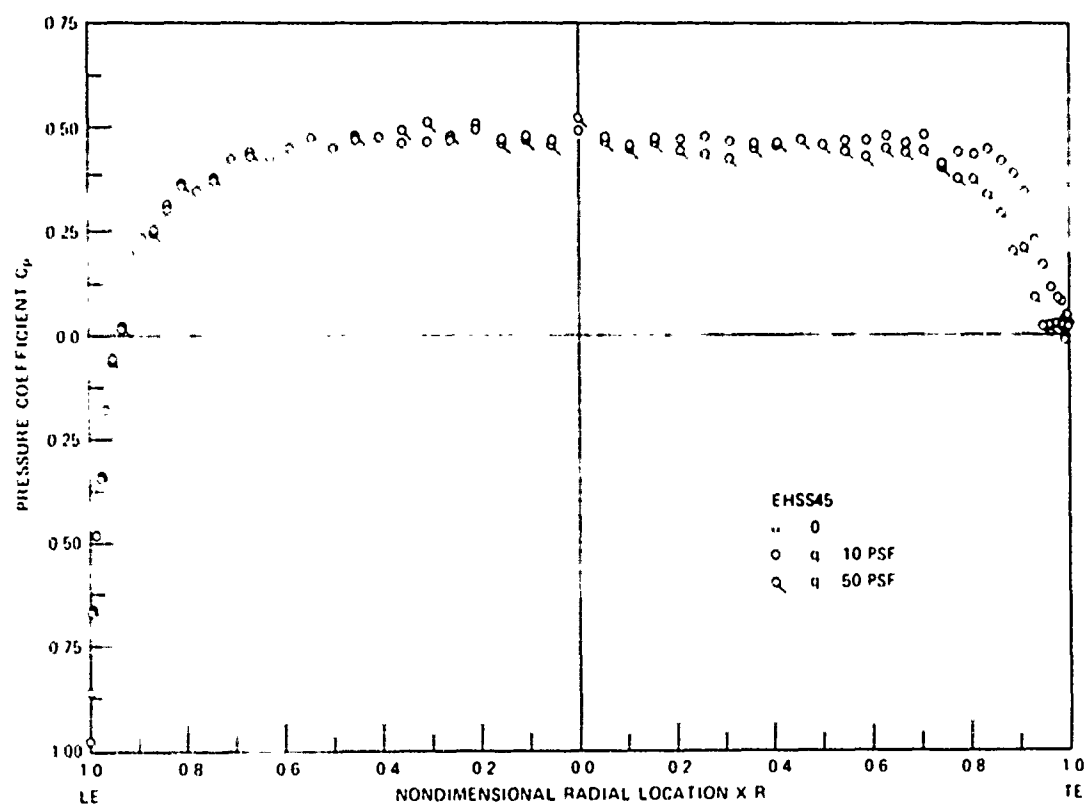


Figure 11 -- (Continued)

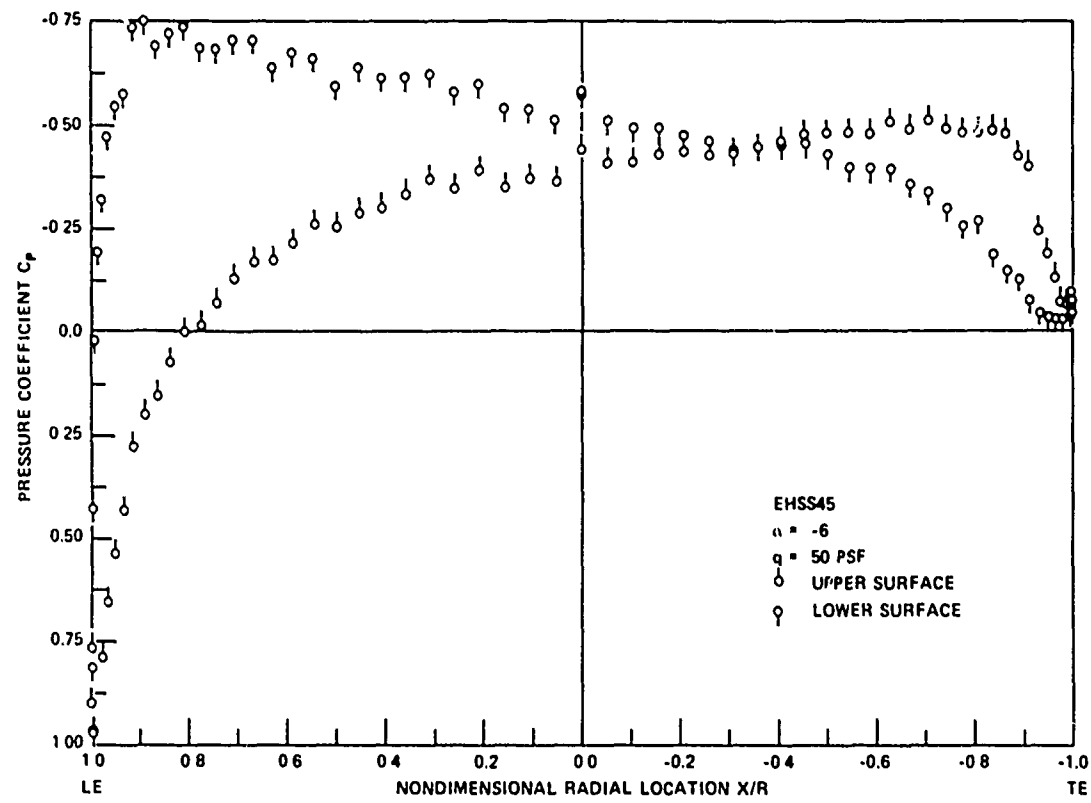
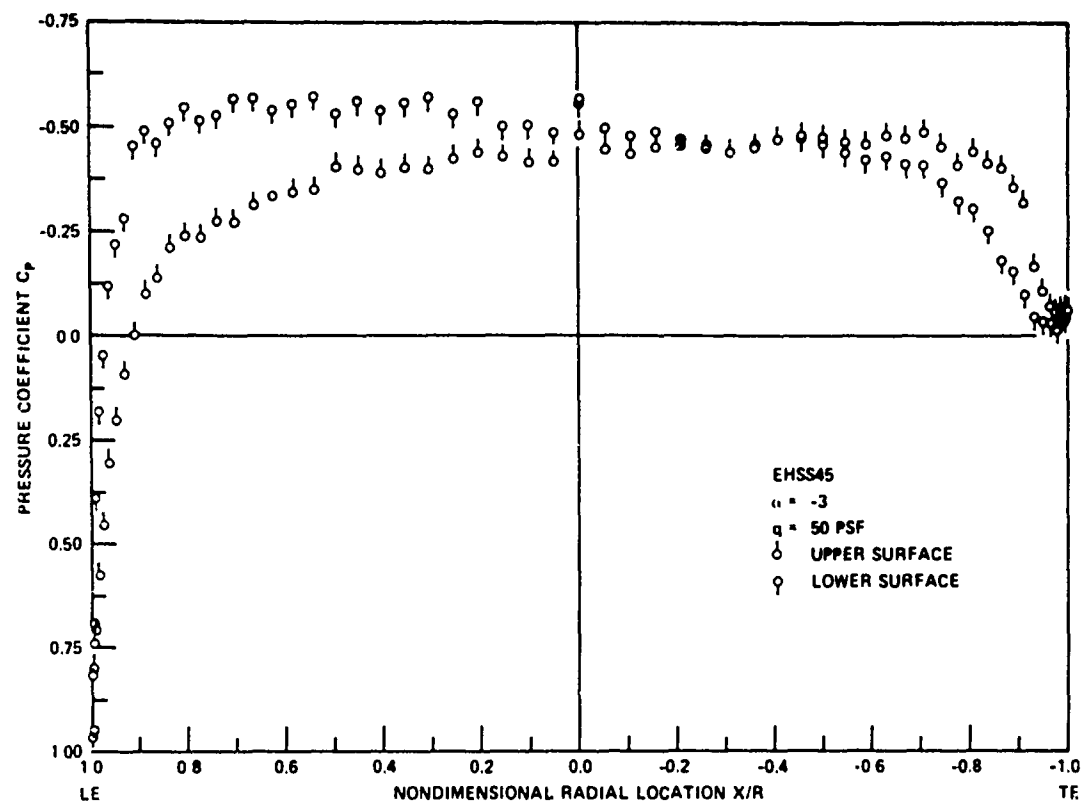
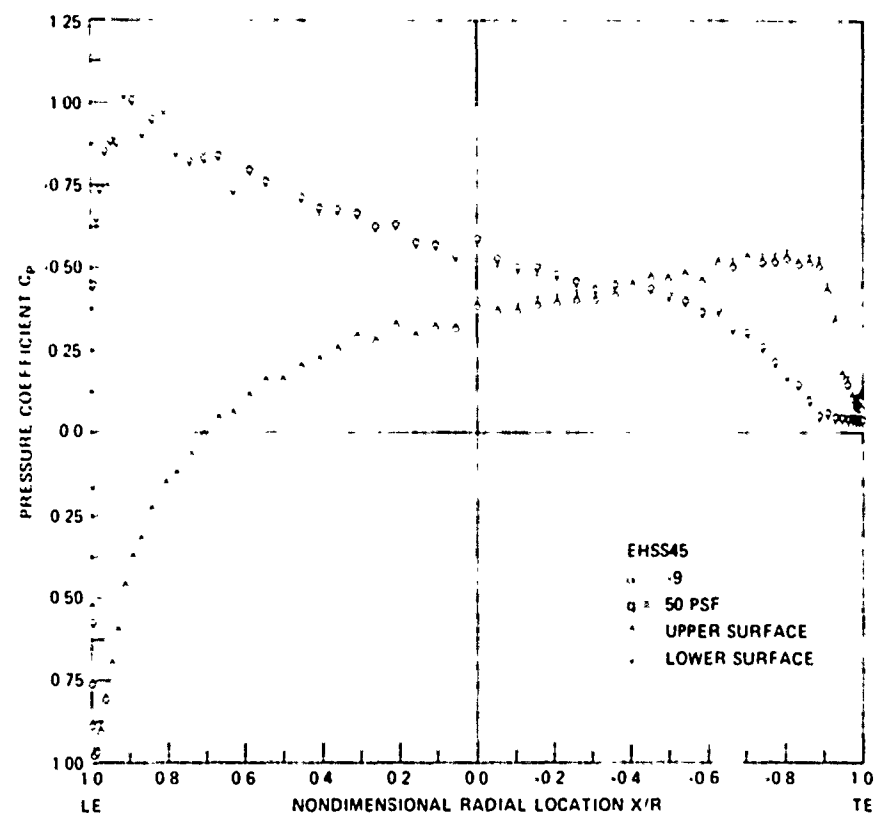


Figure 11 – (Continued)



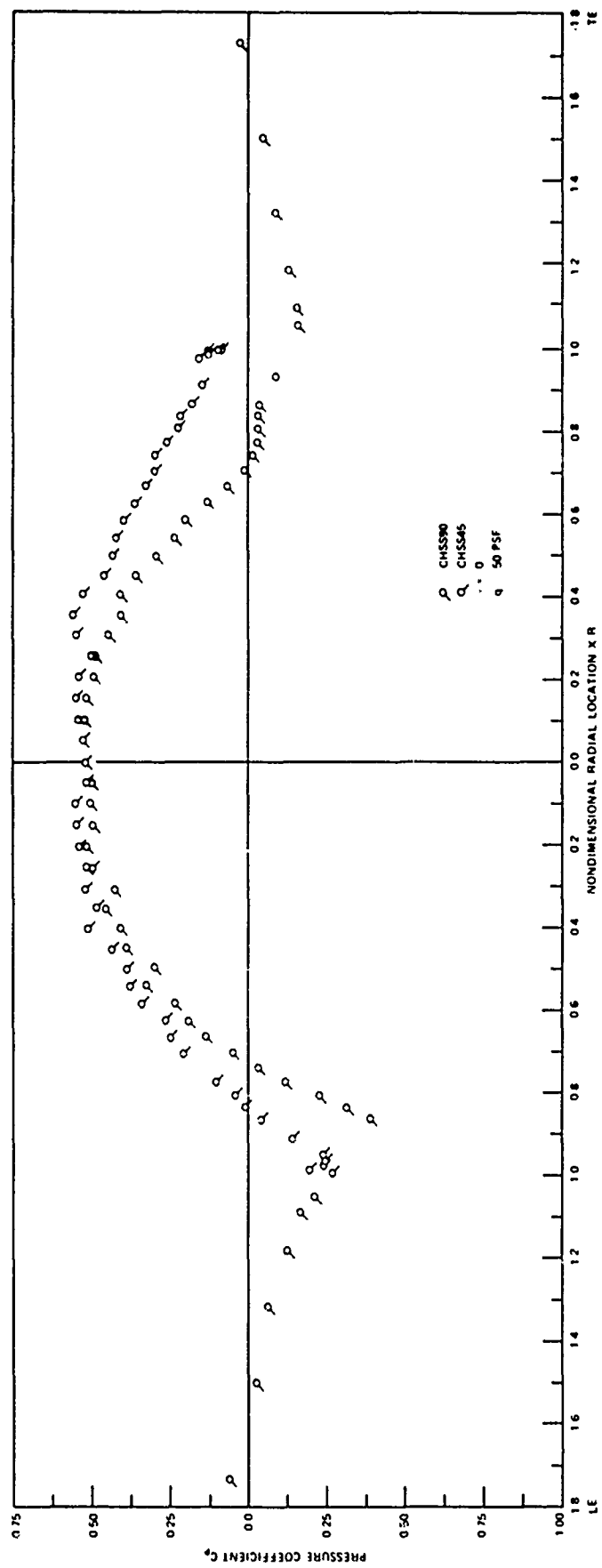


Figure 11 – (Continued)

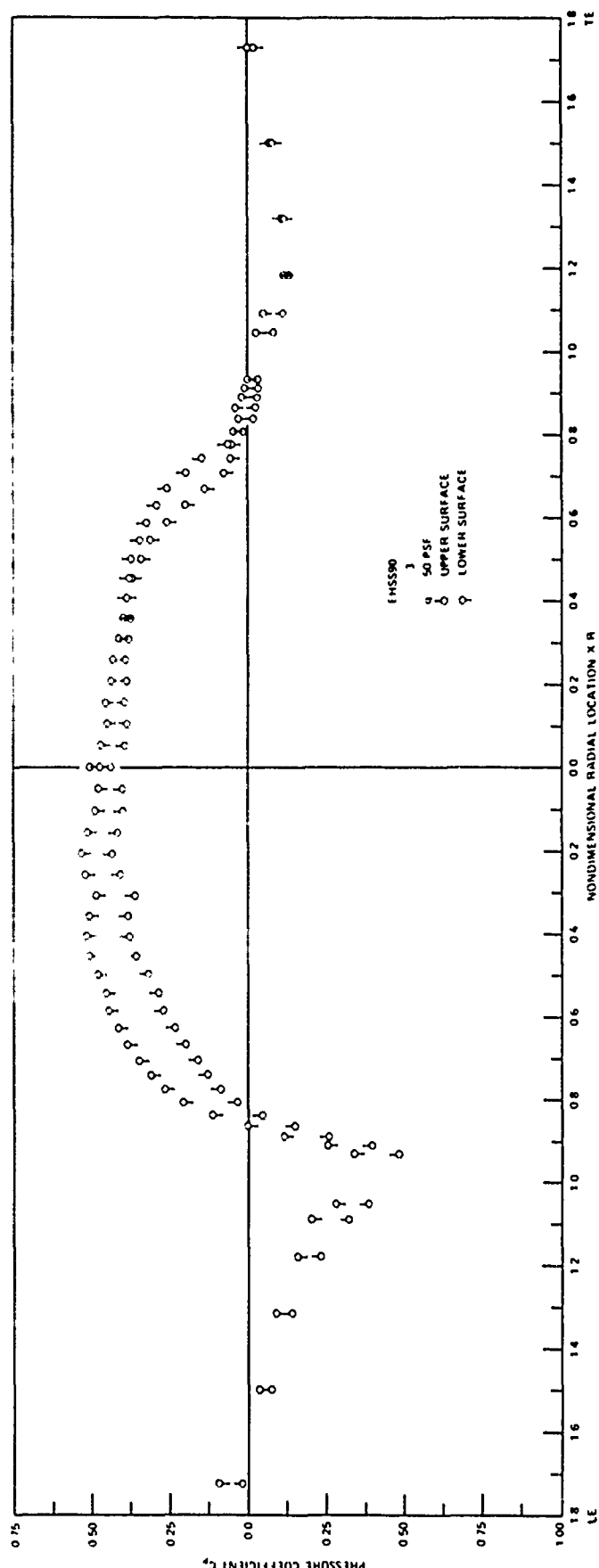


Figure 11 – (Continued)

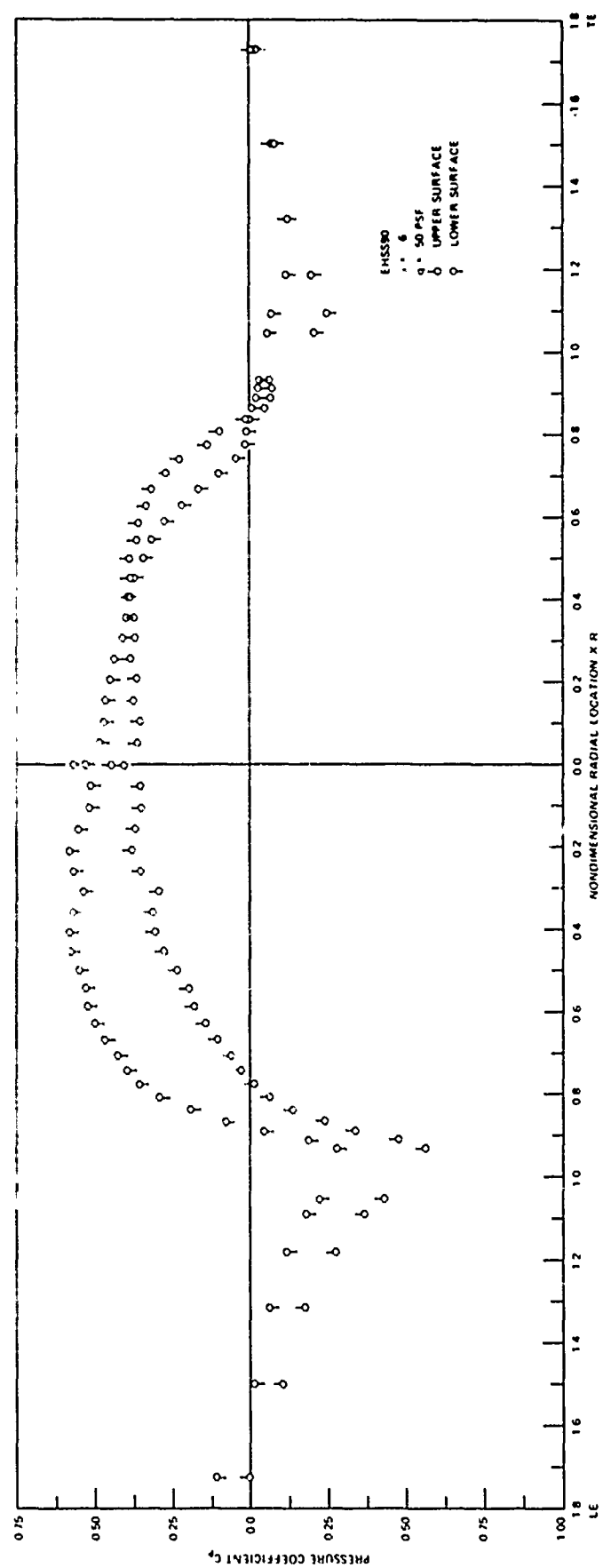


Figure 11 - (Continued)

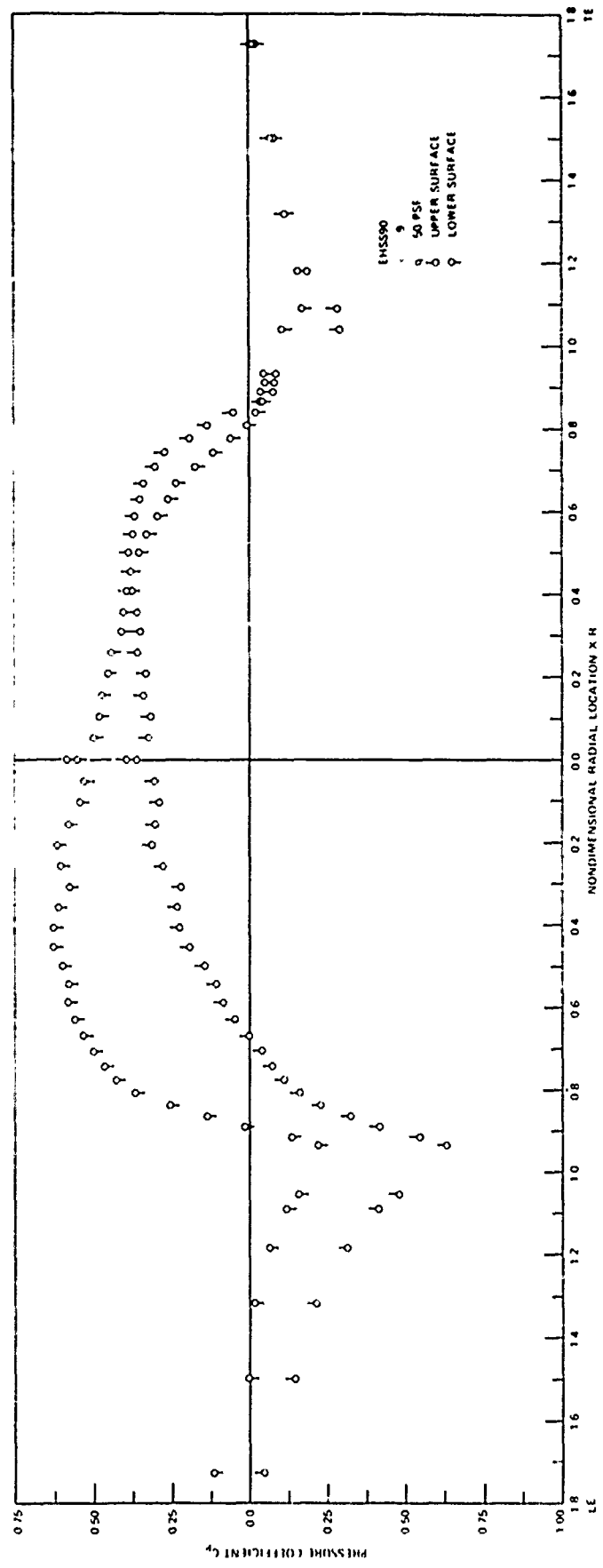


Figure 11 – (Continued)

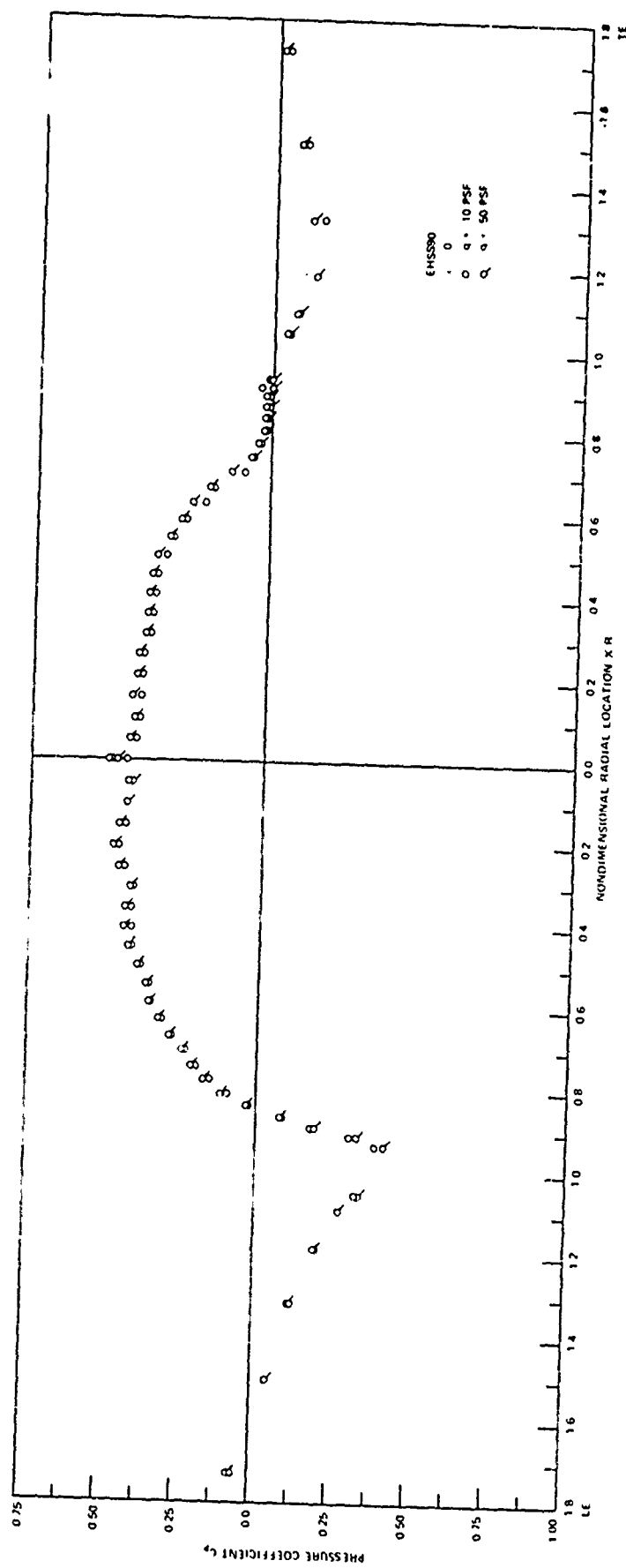


Figure 11 – (Continued)

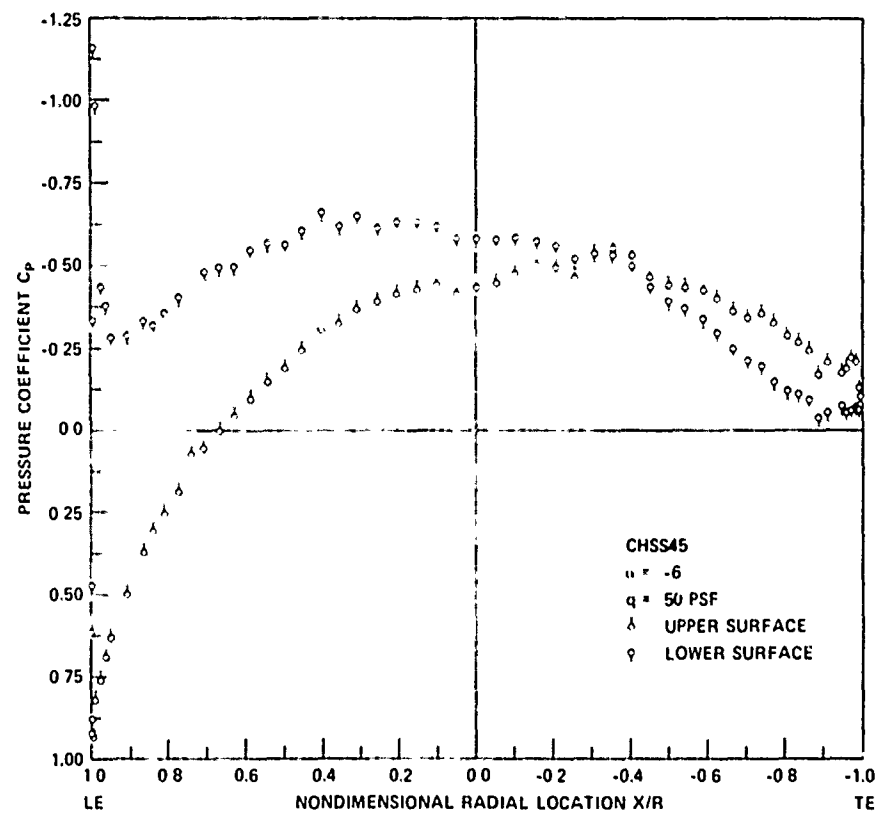
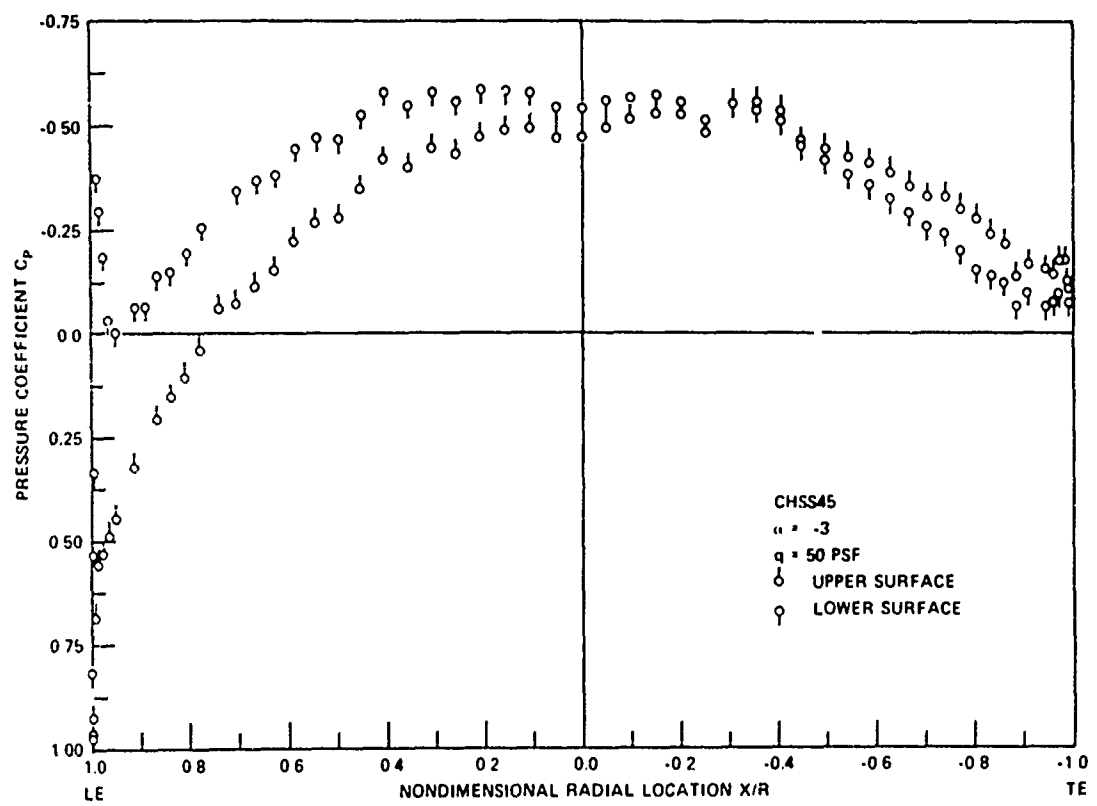


Figure 11 - (Continued)

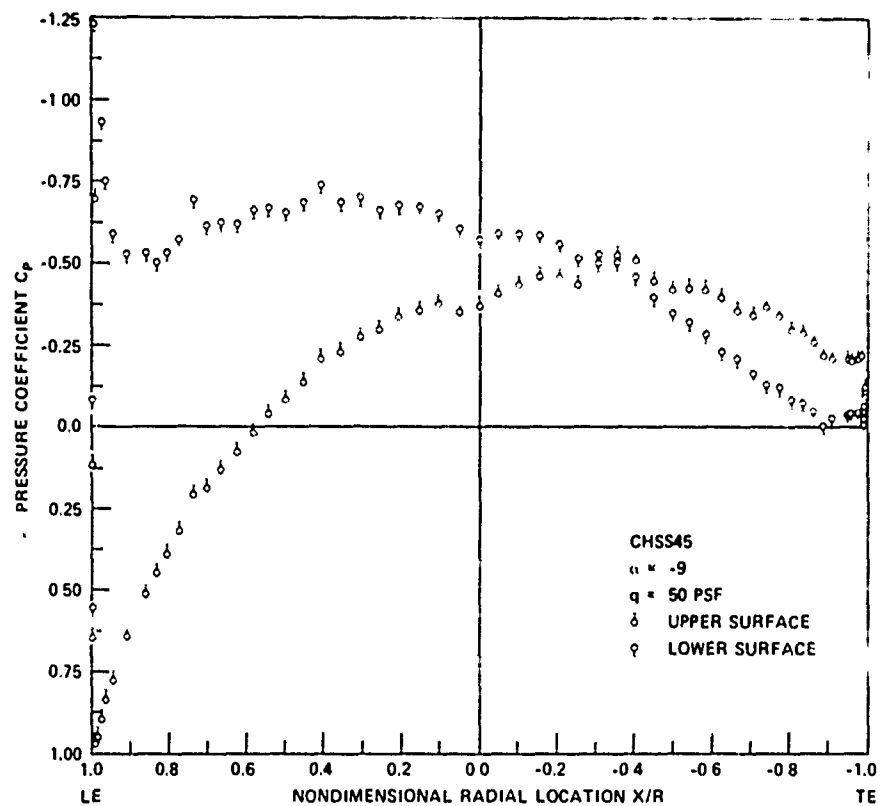


Figure 11 - (Continued)

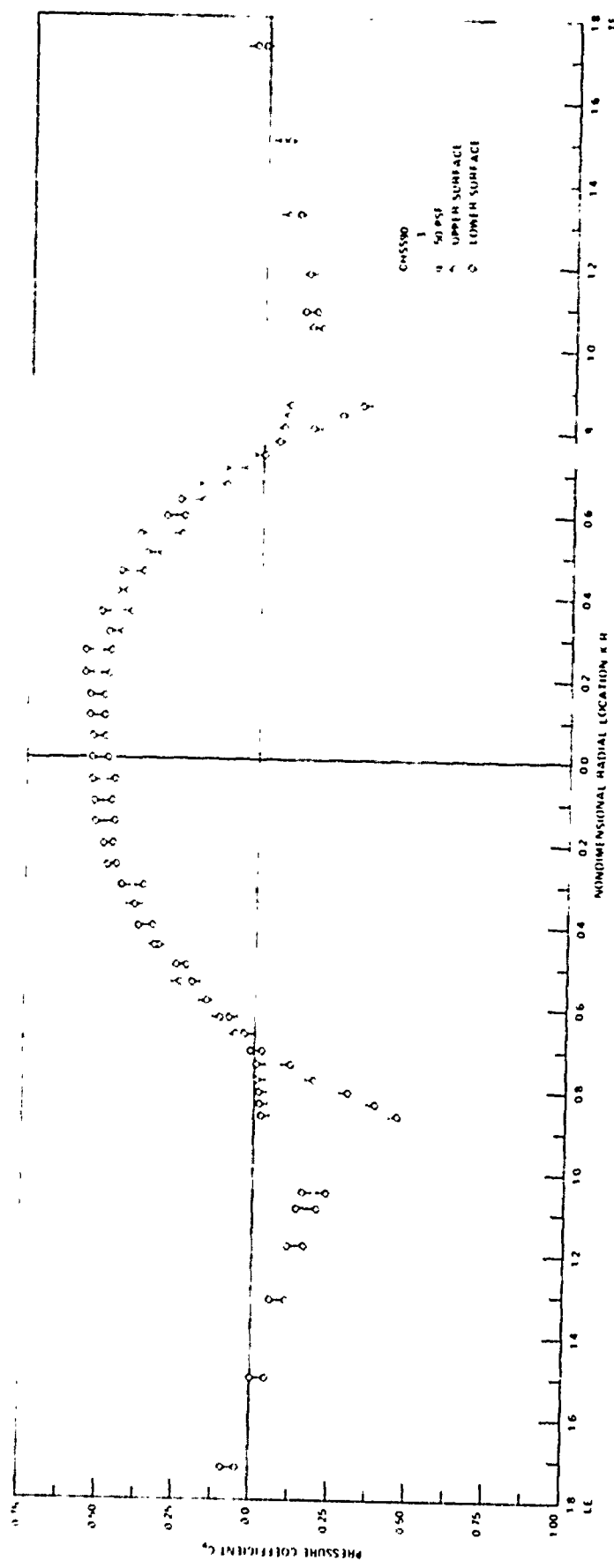


Figure 11 - (Continued)

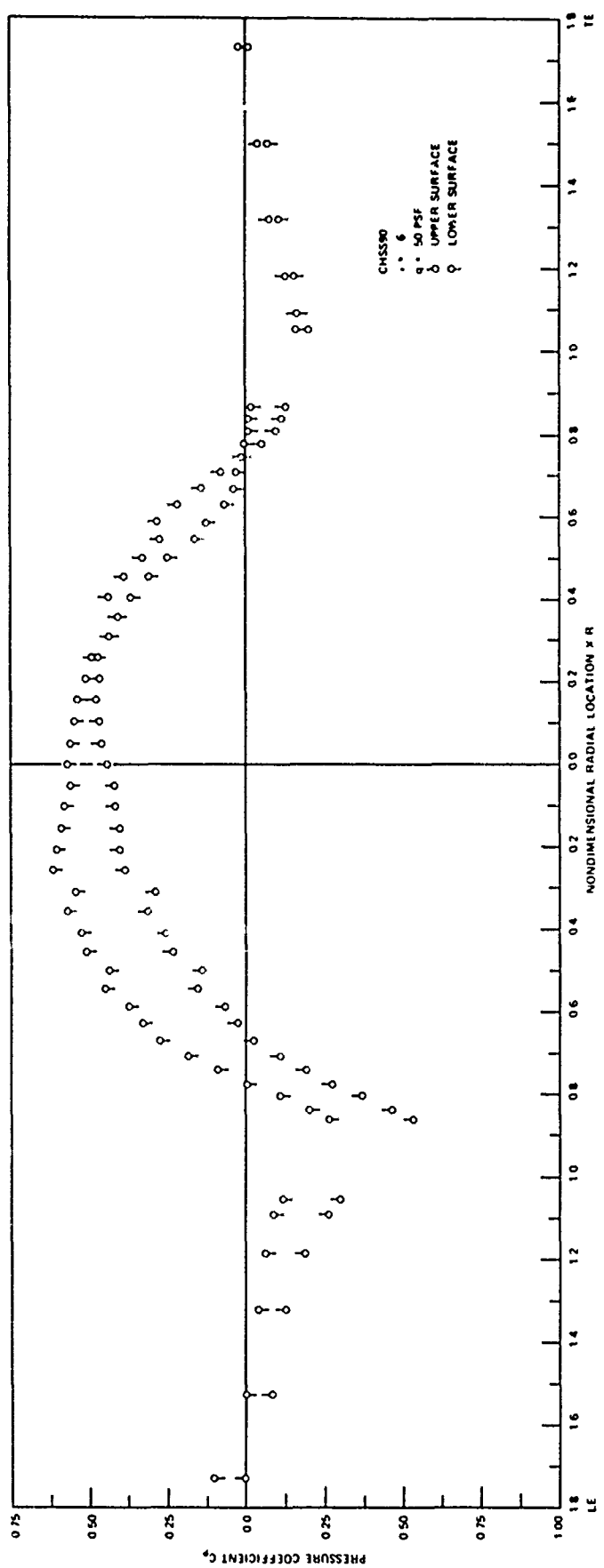


Figure 11 – (Continued)

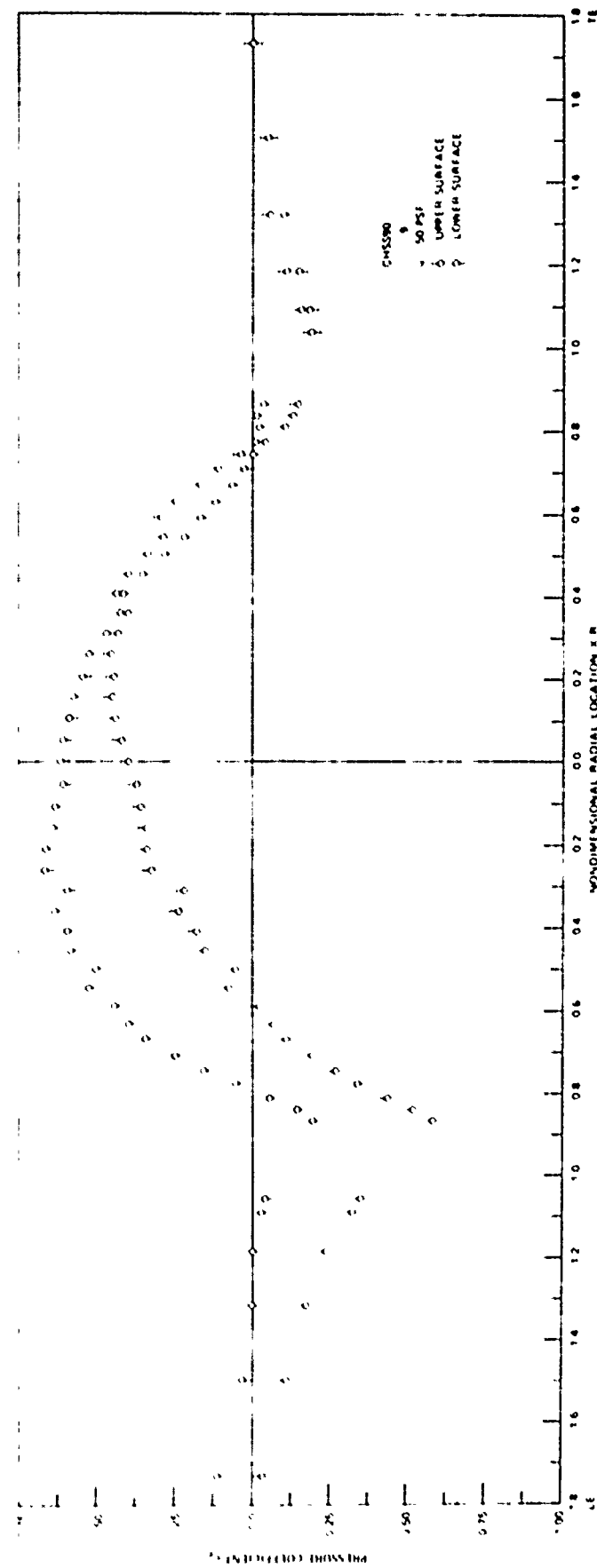


Figure 11 - (Continued)

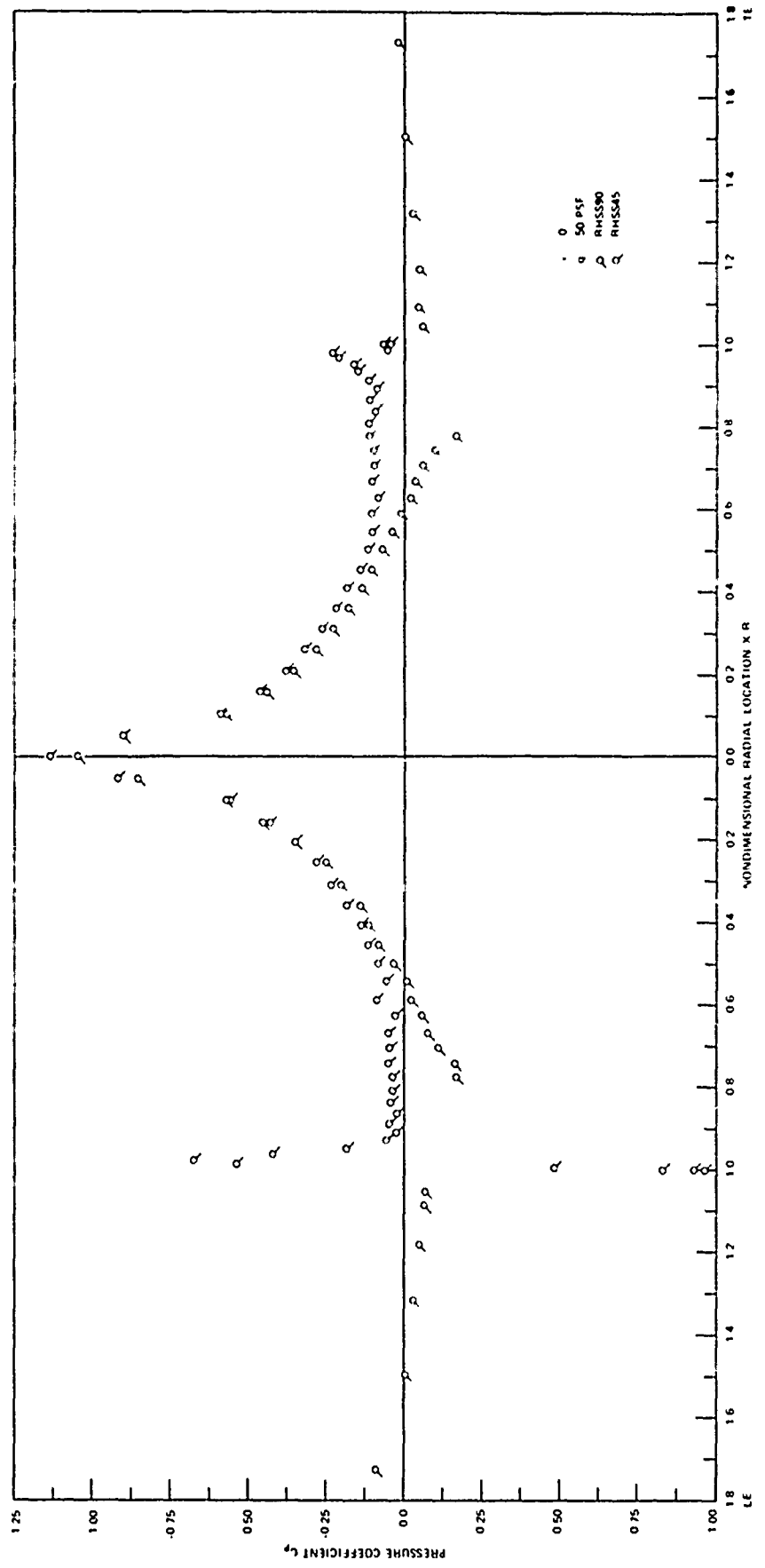


Figure 11 - (Continued)

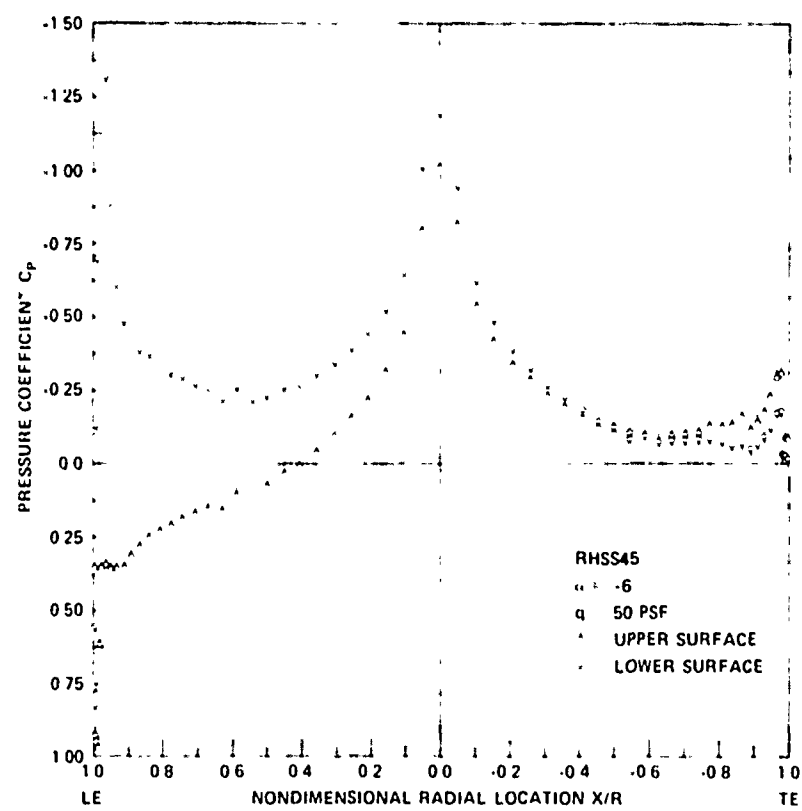
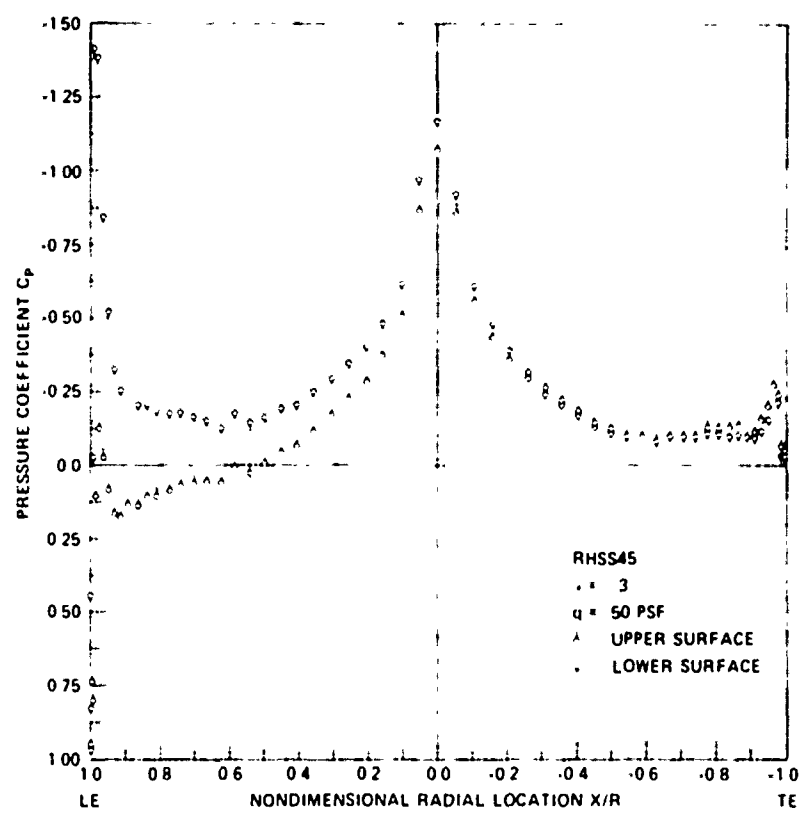


Figure 11 – (Continued)

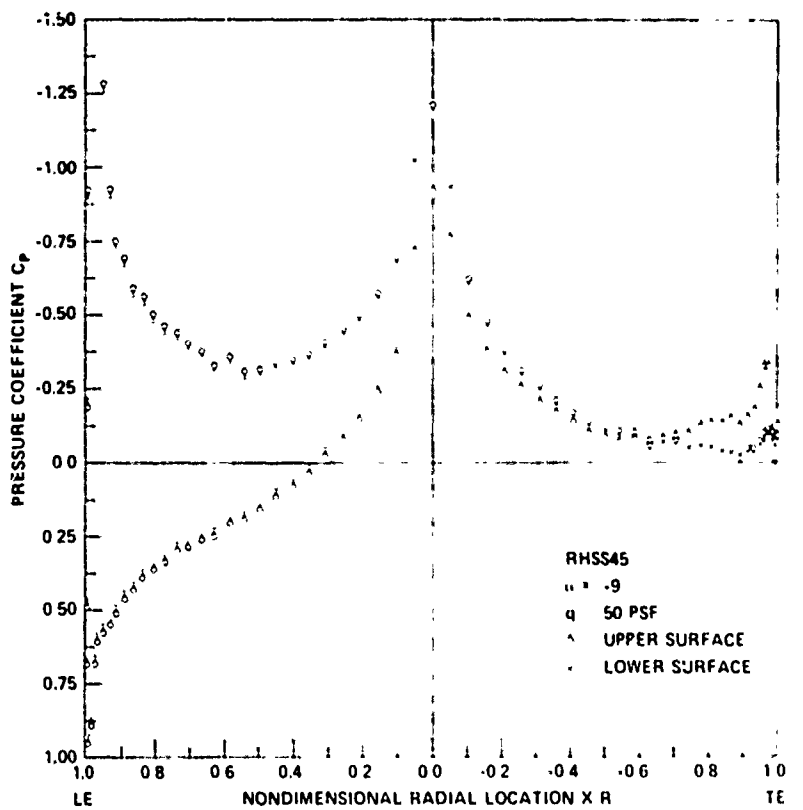


Figure 11 – (Continued)

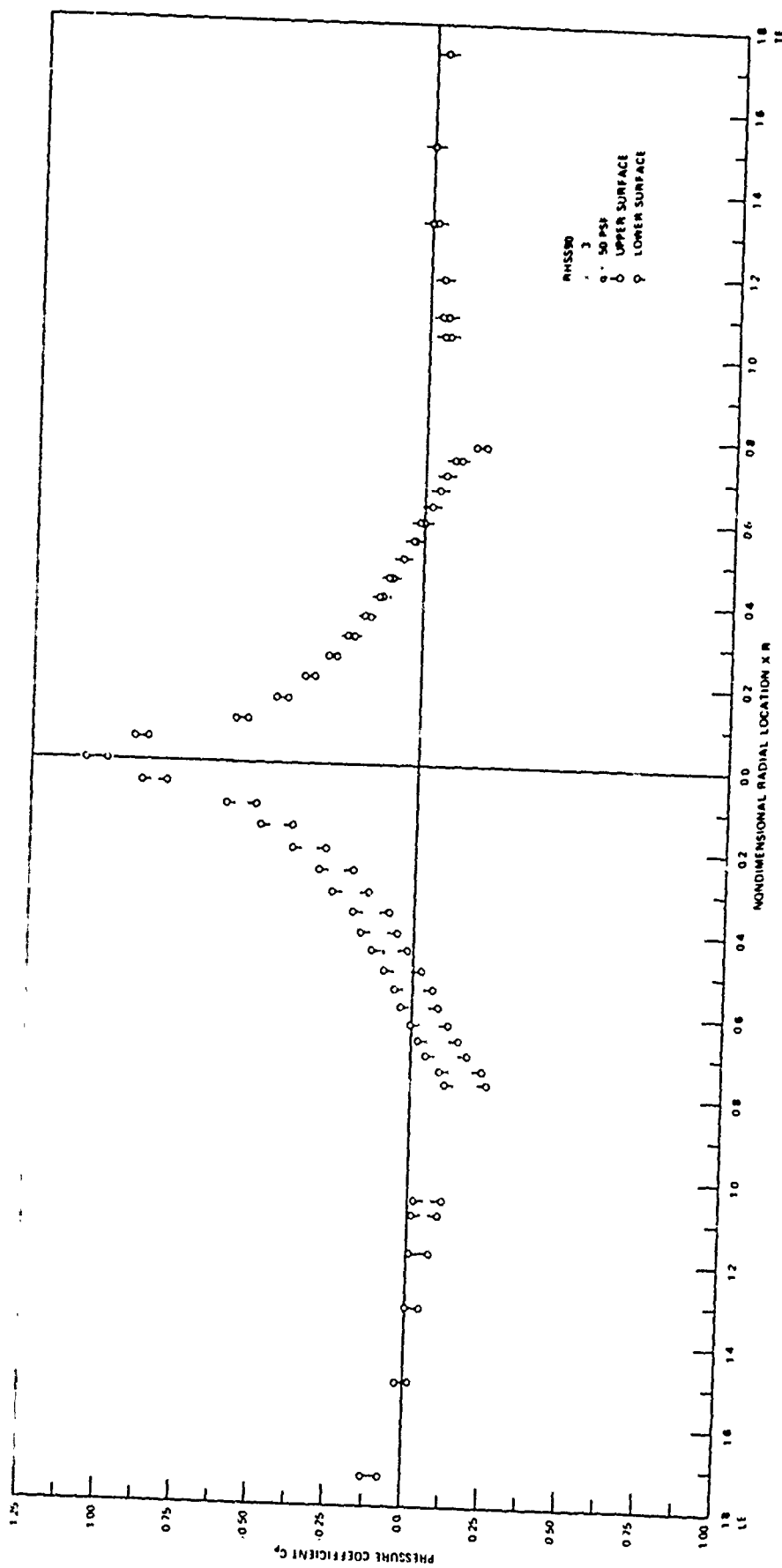


Figure 11 - (Continued)

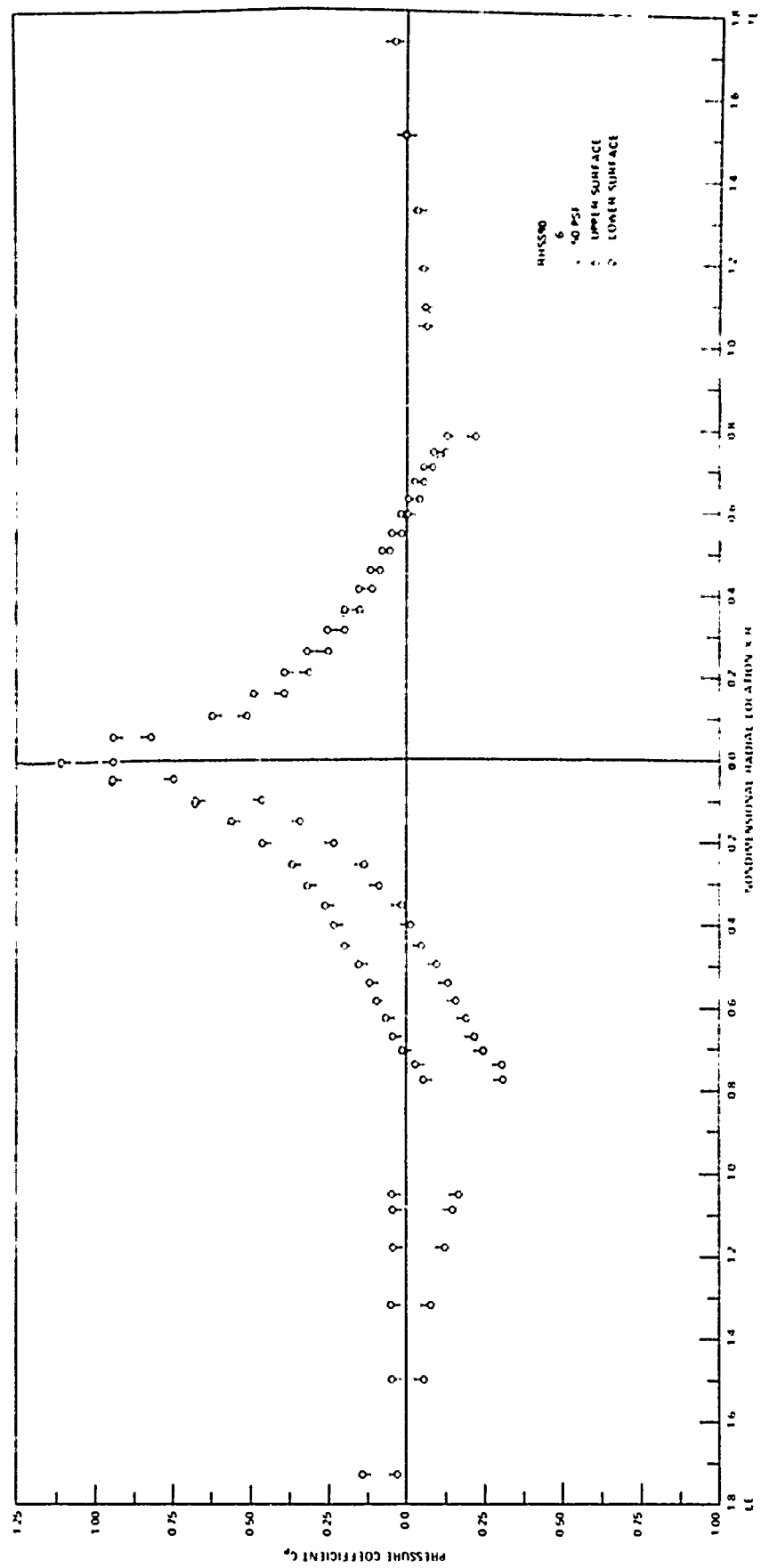
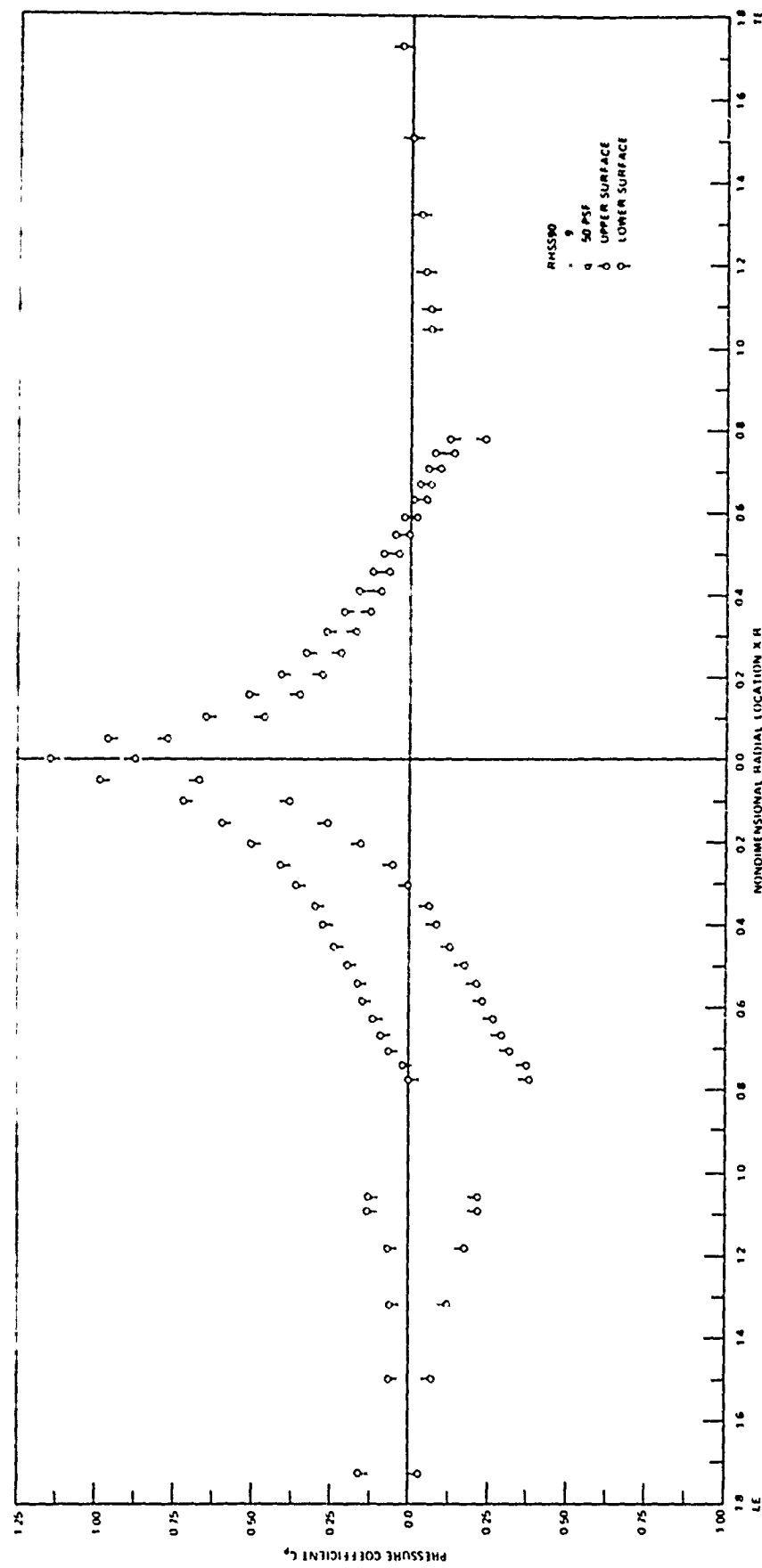


Figure 11 - (Continued)



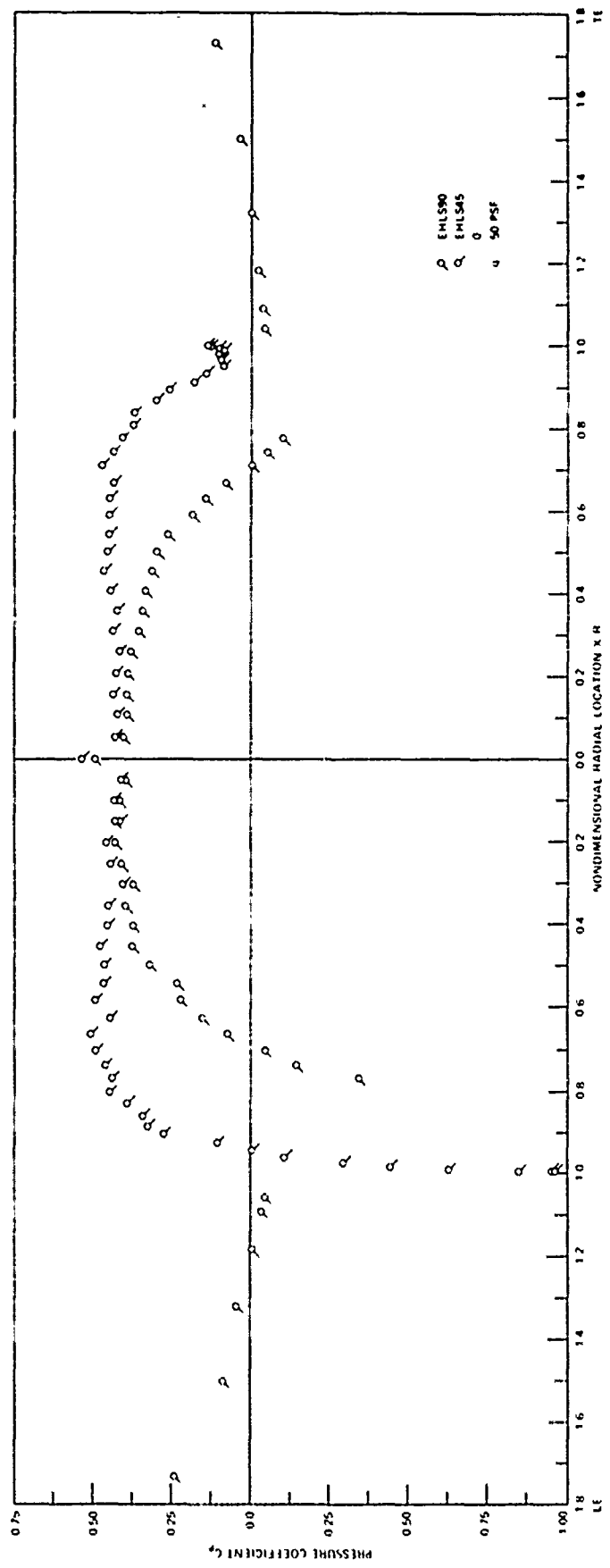


Figure 11 – (Continued)

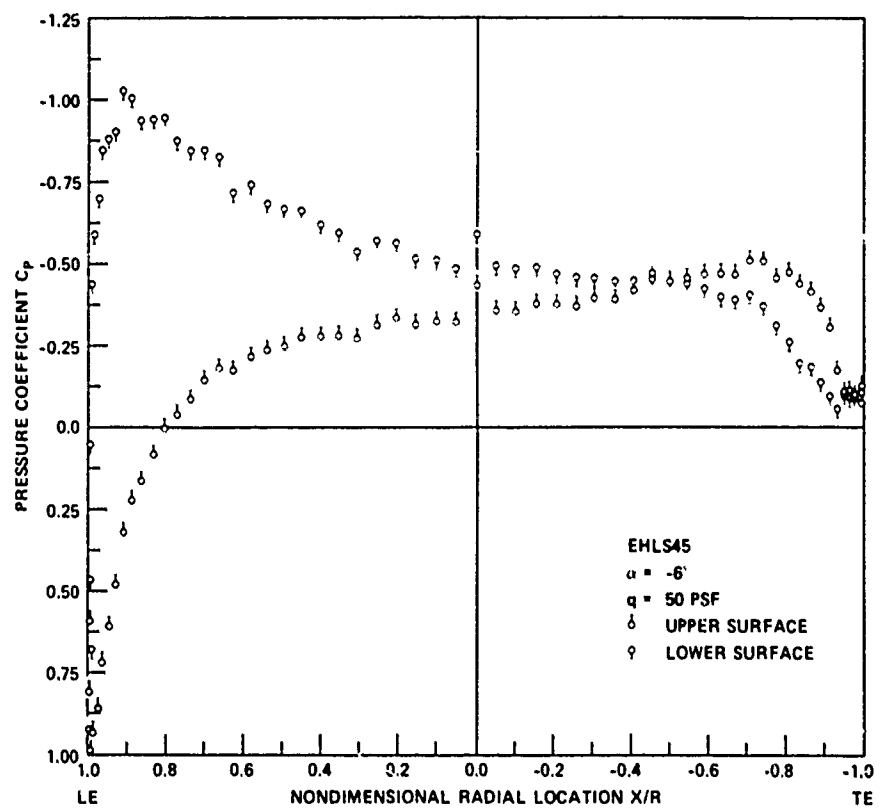
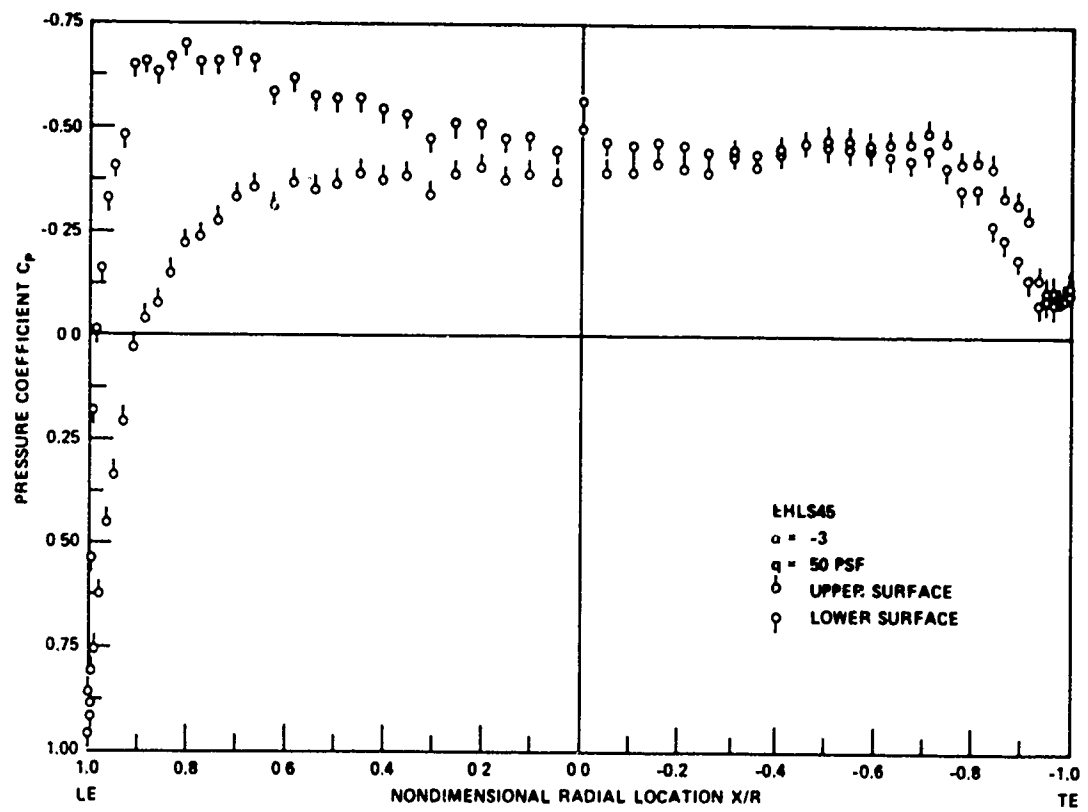


Figure 11 – (Continued)

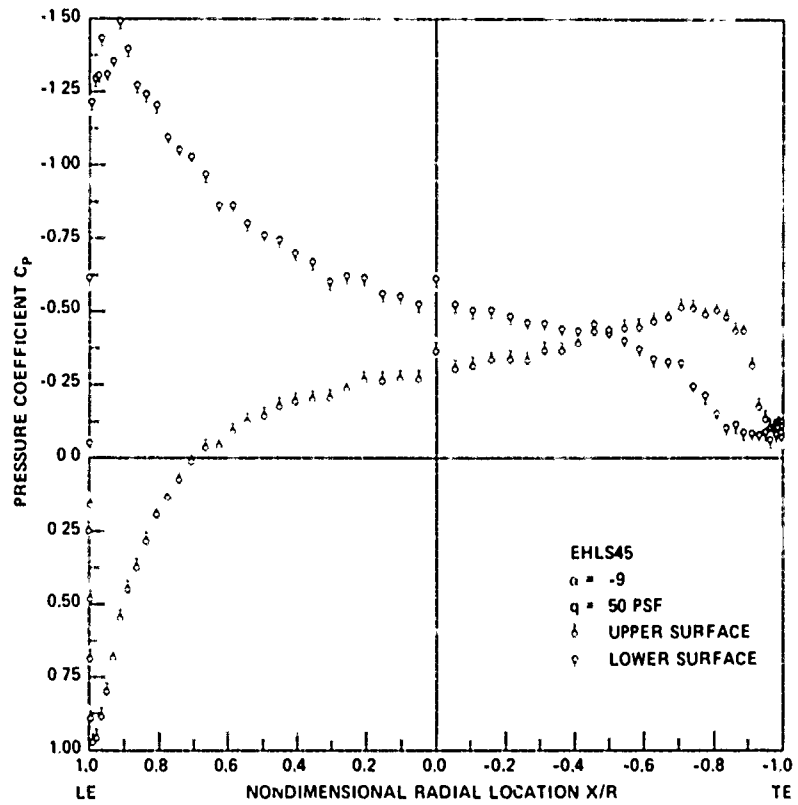


Figure 11 – (Continued)

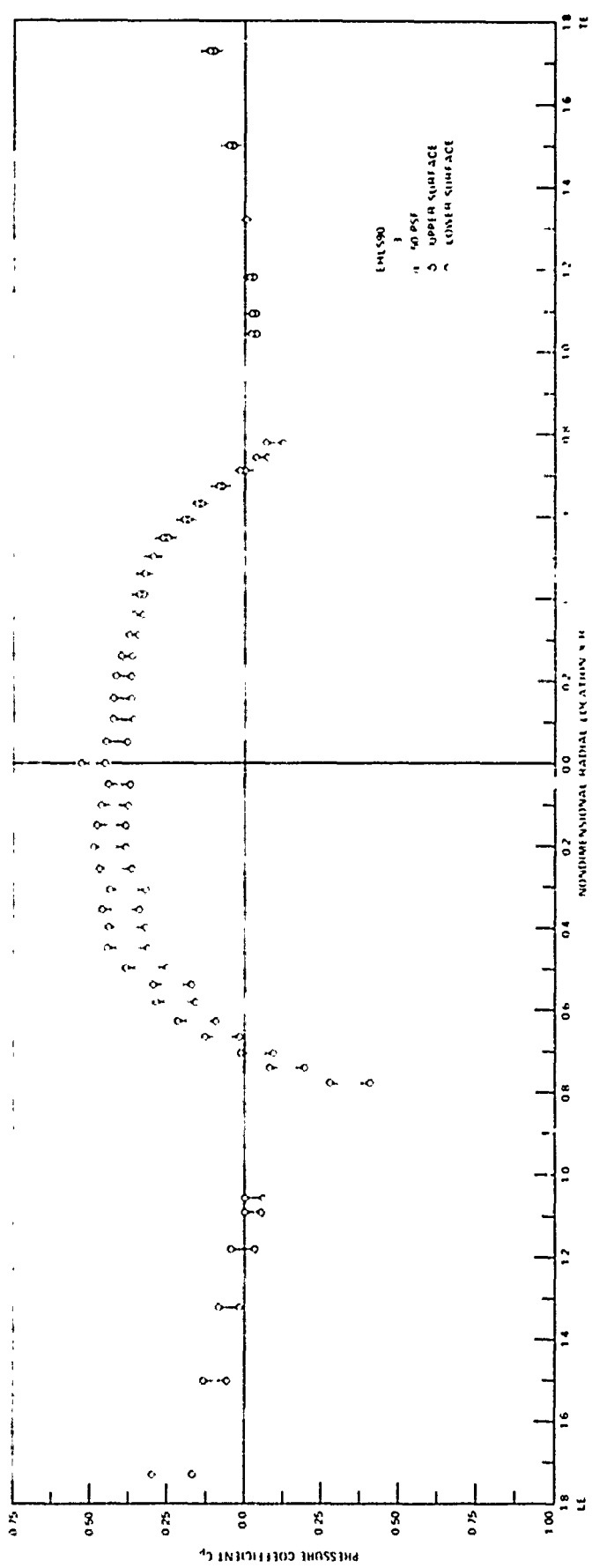
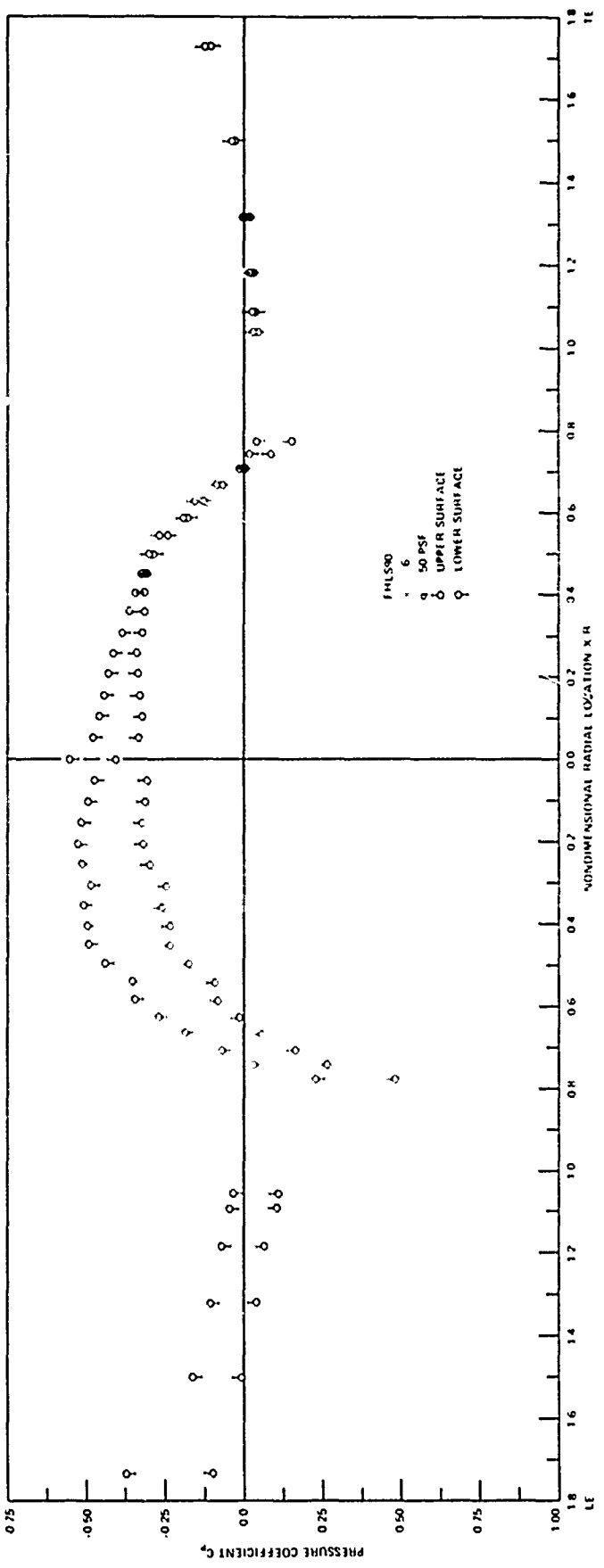


Figure 11 — (Continued)

Figure 11 - Continued



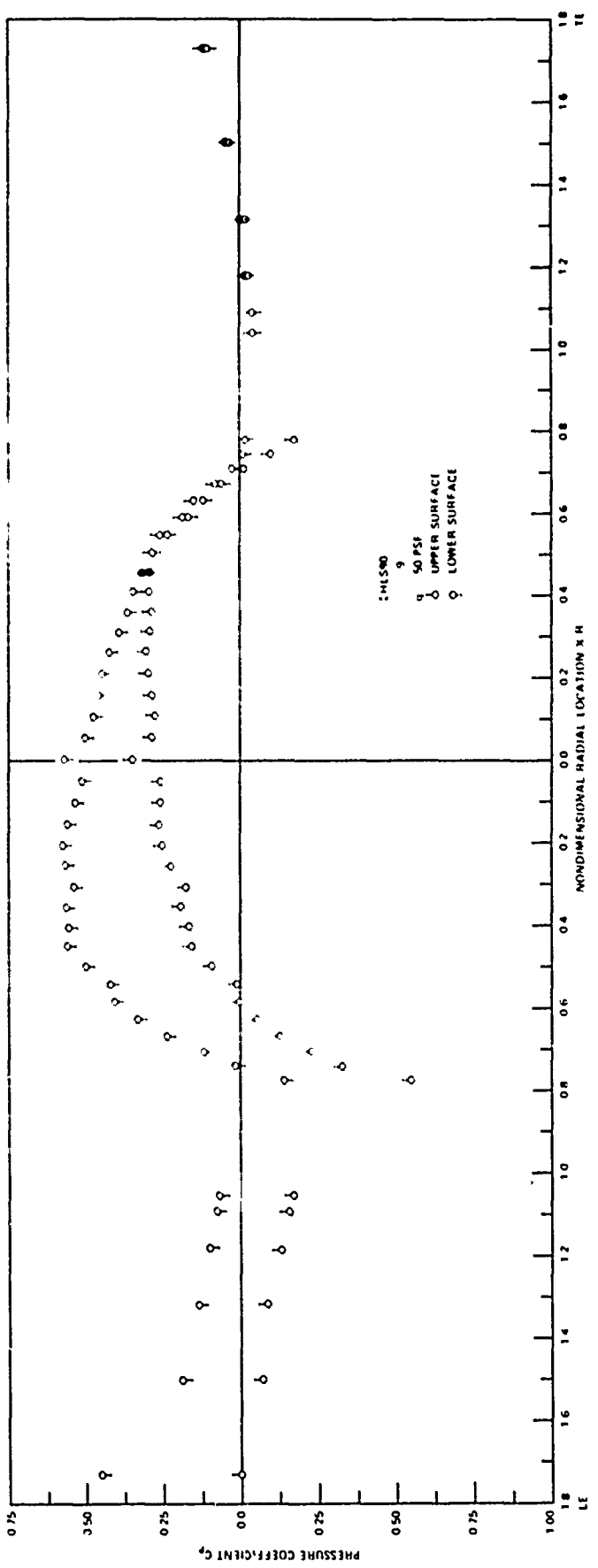


Figure 11 - (Continued)

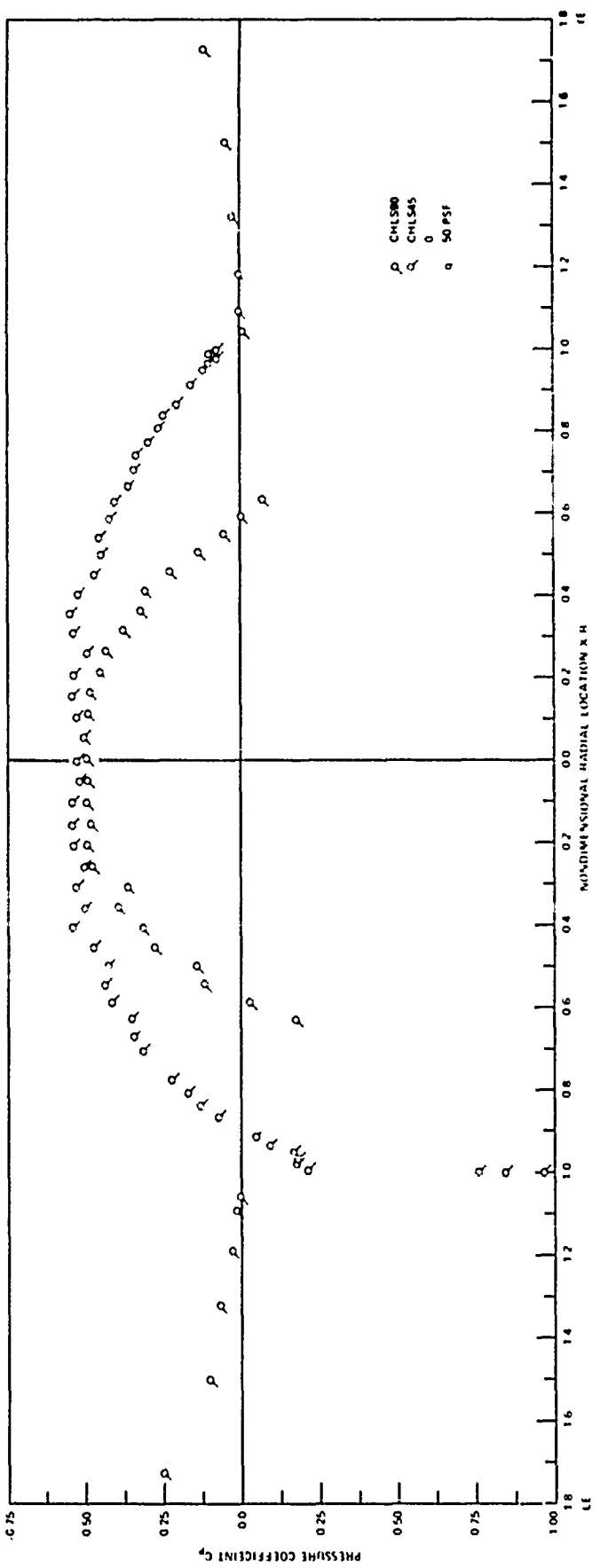


Figure 11 - (Continued)

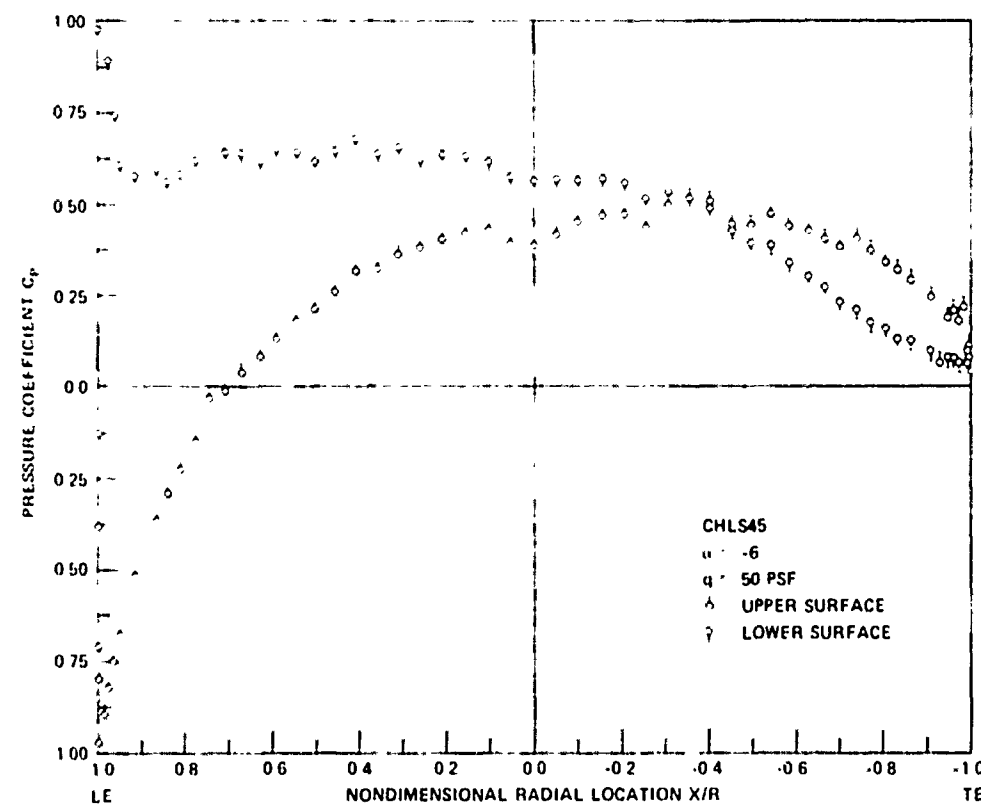
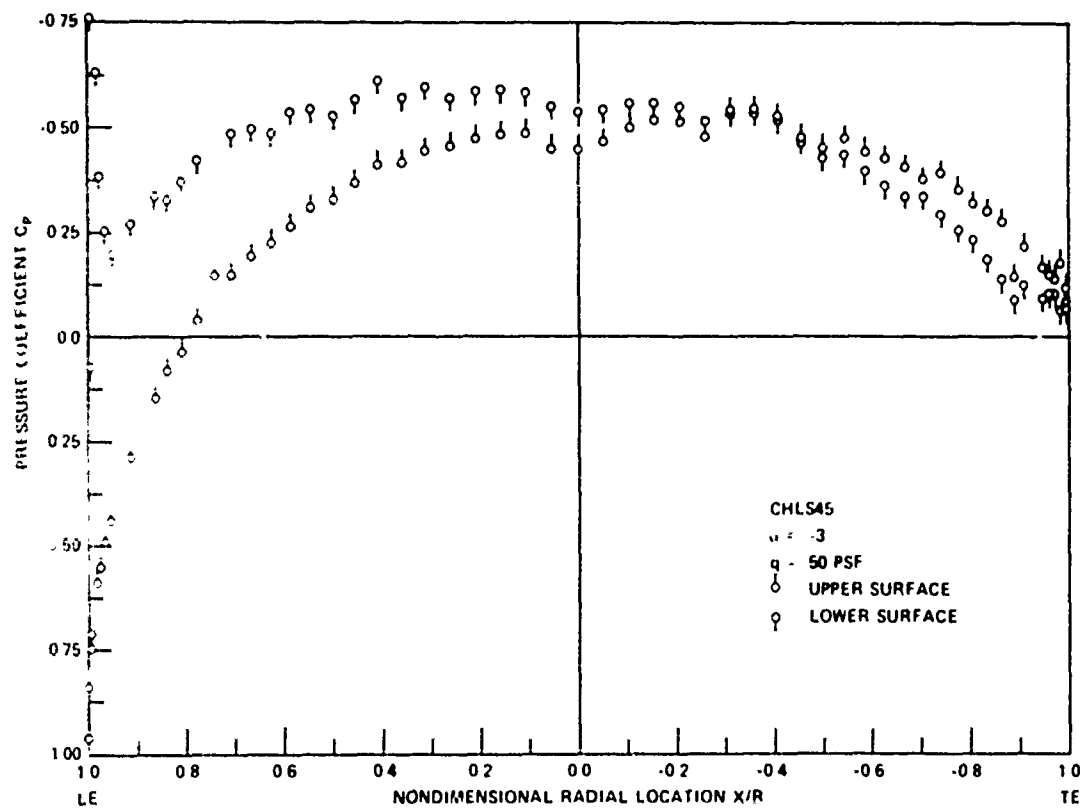


Figure 11 – (Continued)

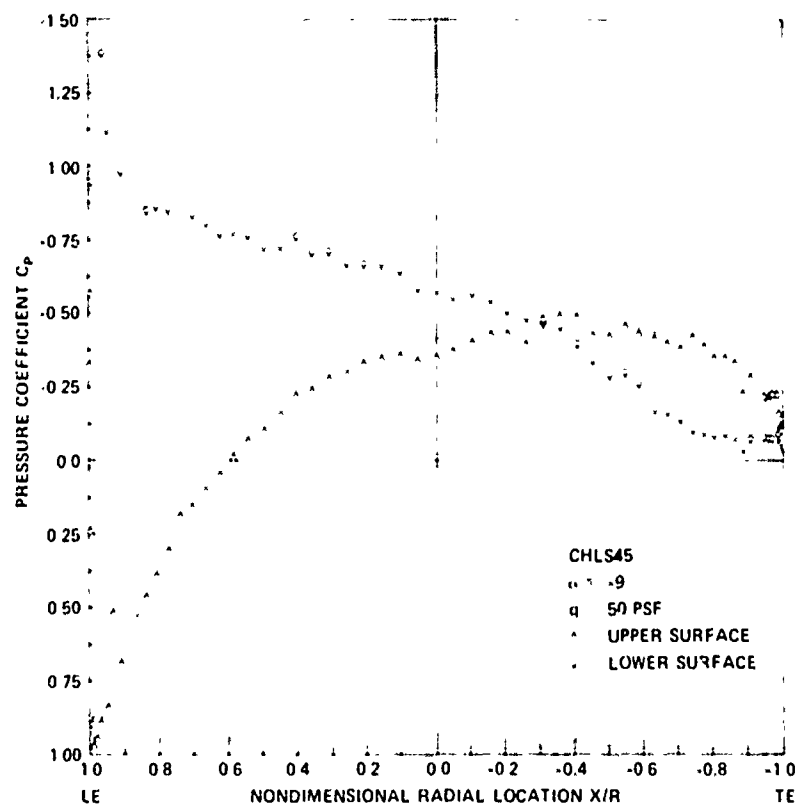


Figure 11 - (Continued)

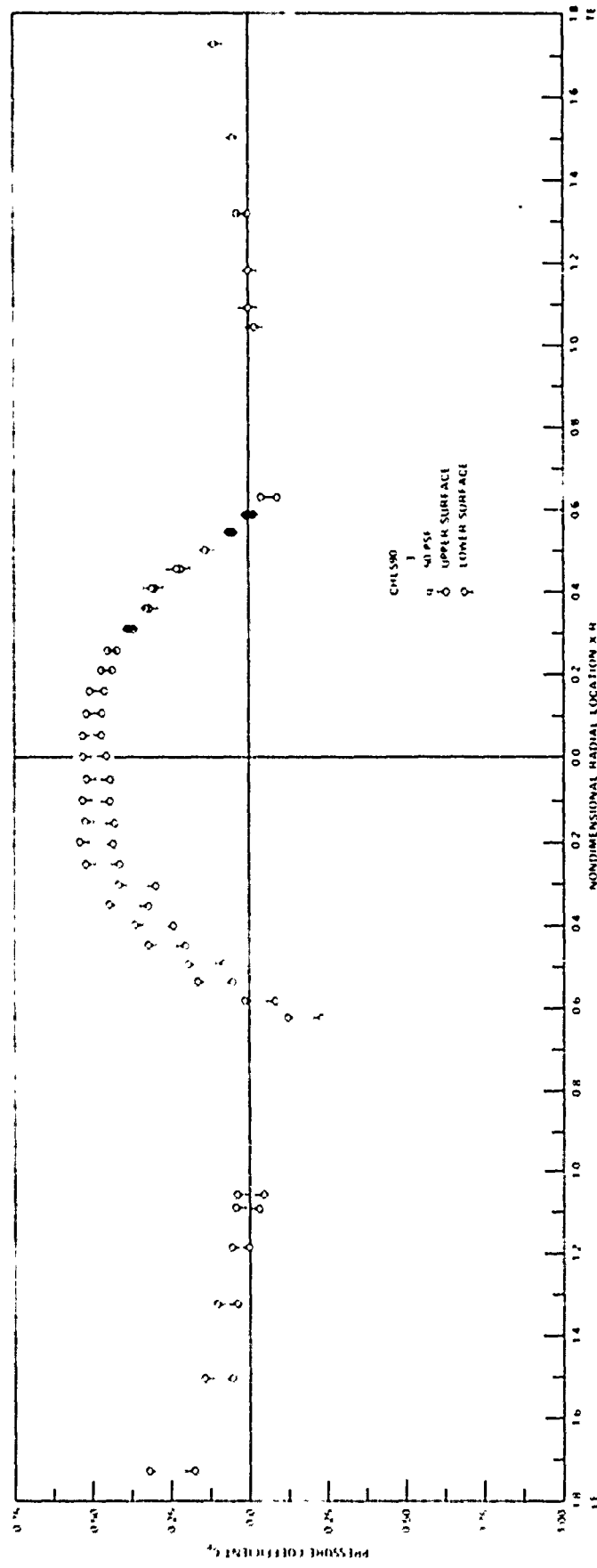


Figure 11 - (Continued)

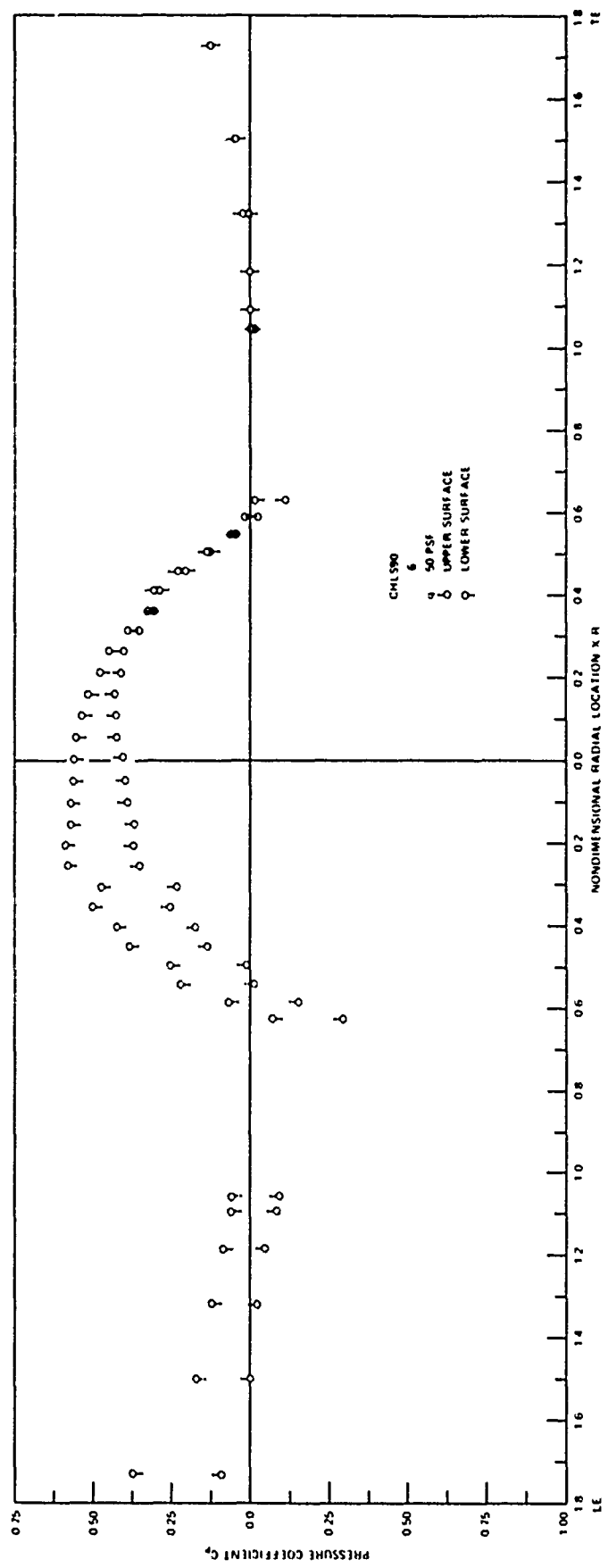


Figure 11 — (Continued)

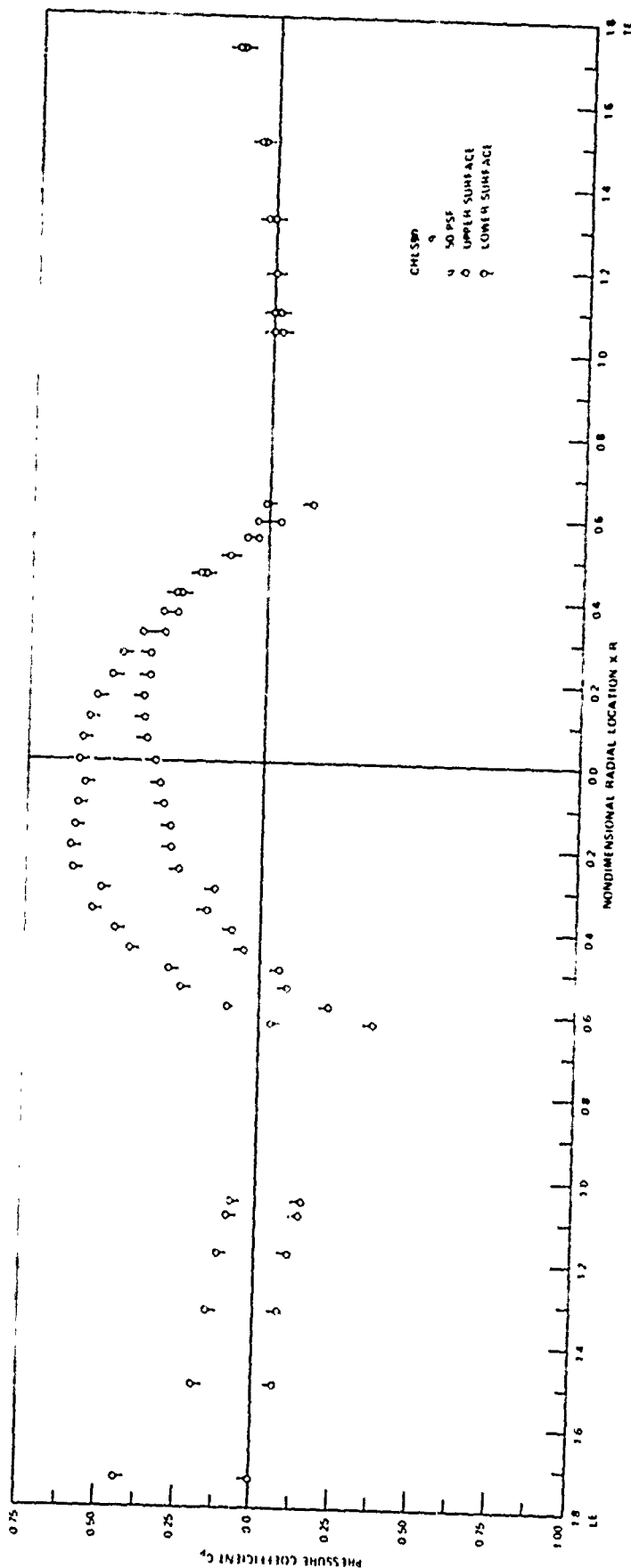
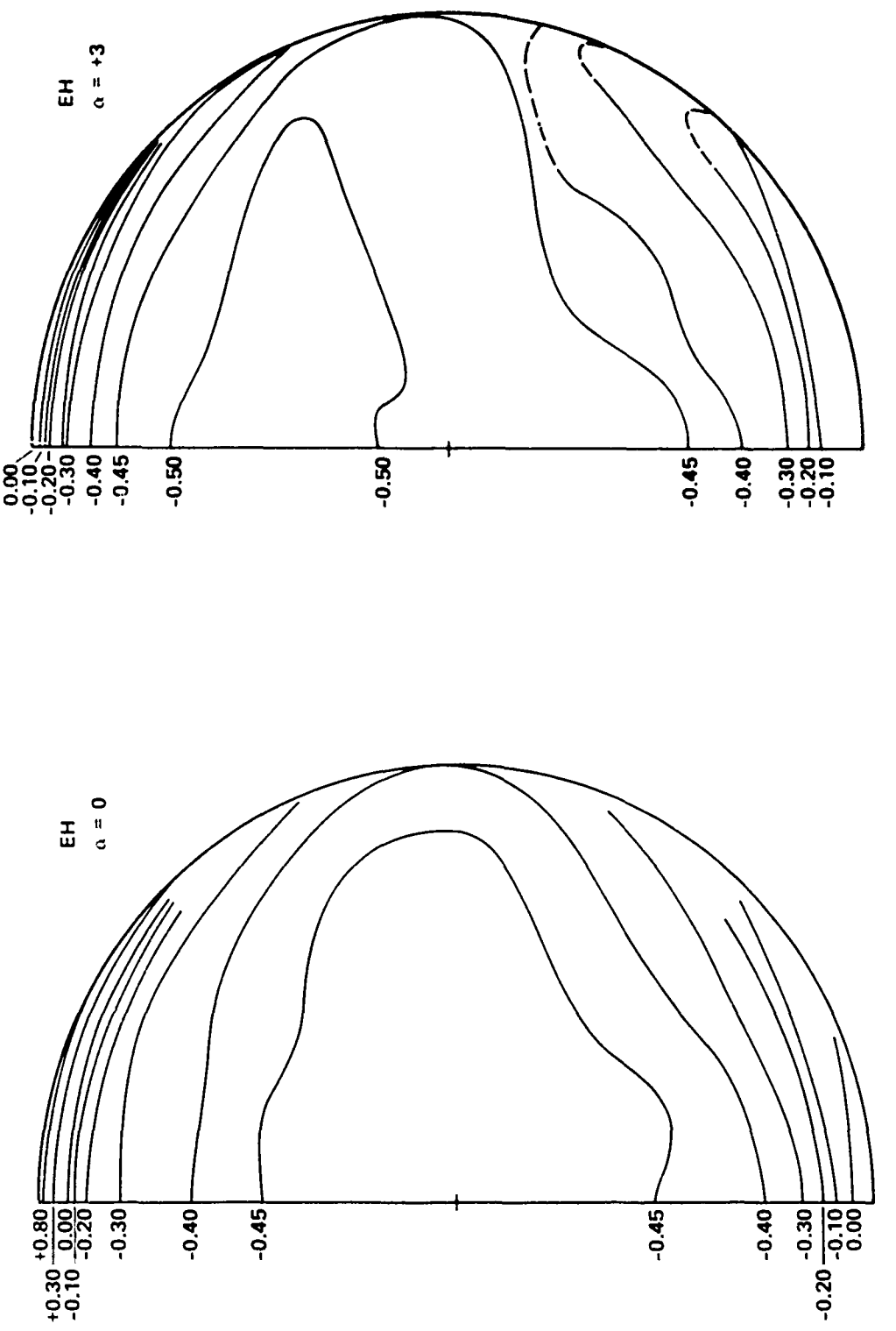


Figure 11 - (Concluded)

Figure 12 - Pressure Coefficient Contours on the Upper Surface of the Hub
Turbine at a Dynamic Pressure of 50 Pounds Per Square Foot



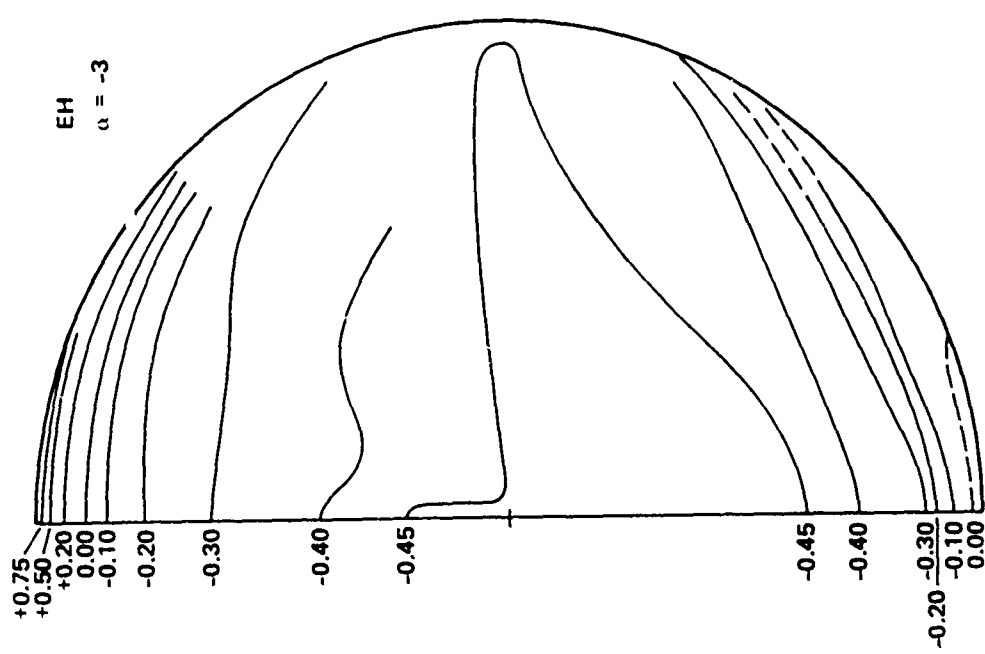
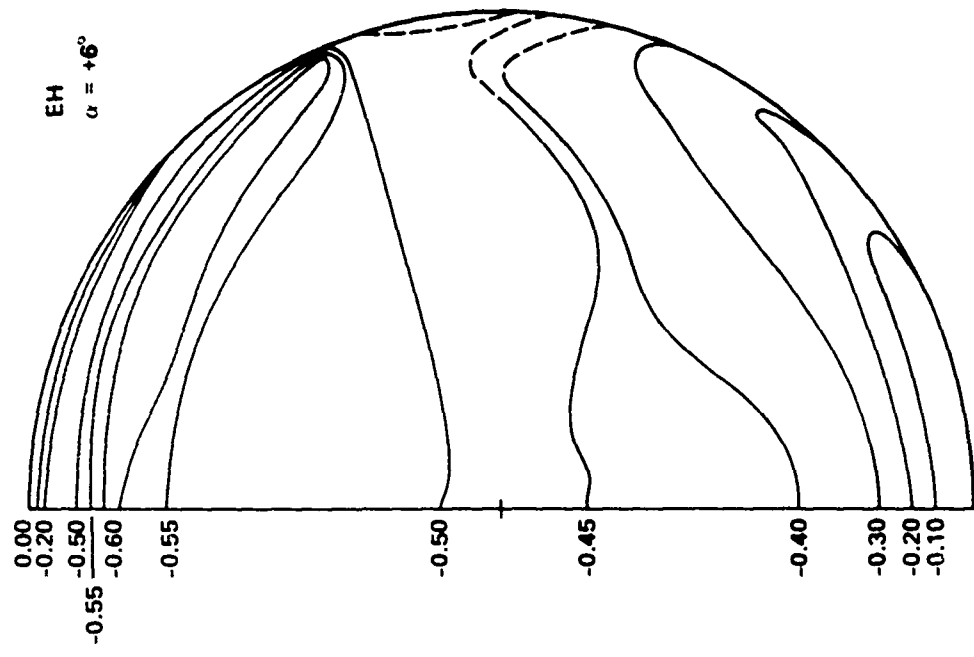


Figure 12 — (Continued)

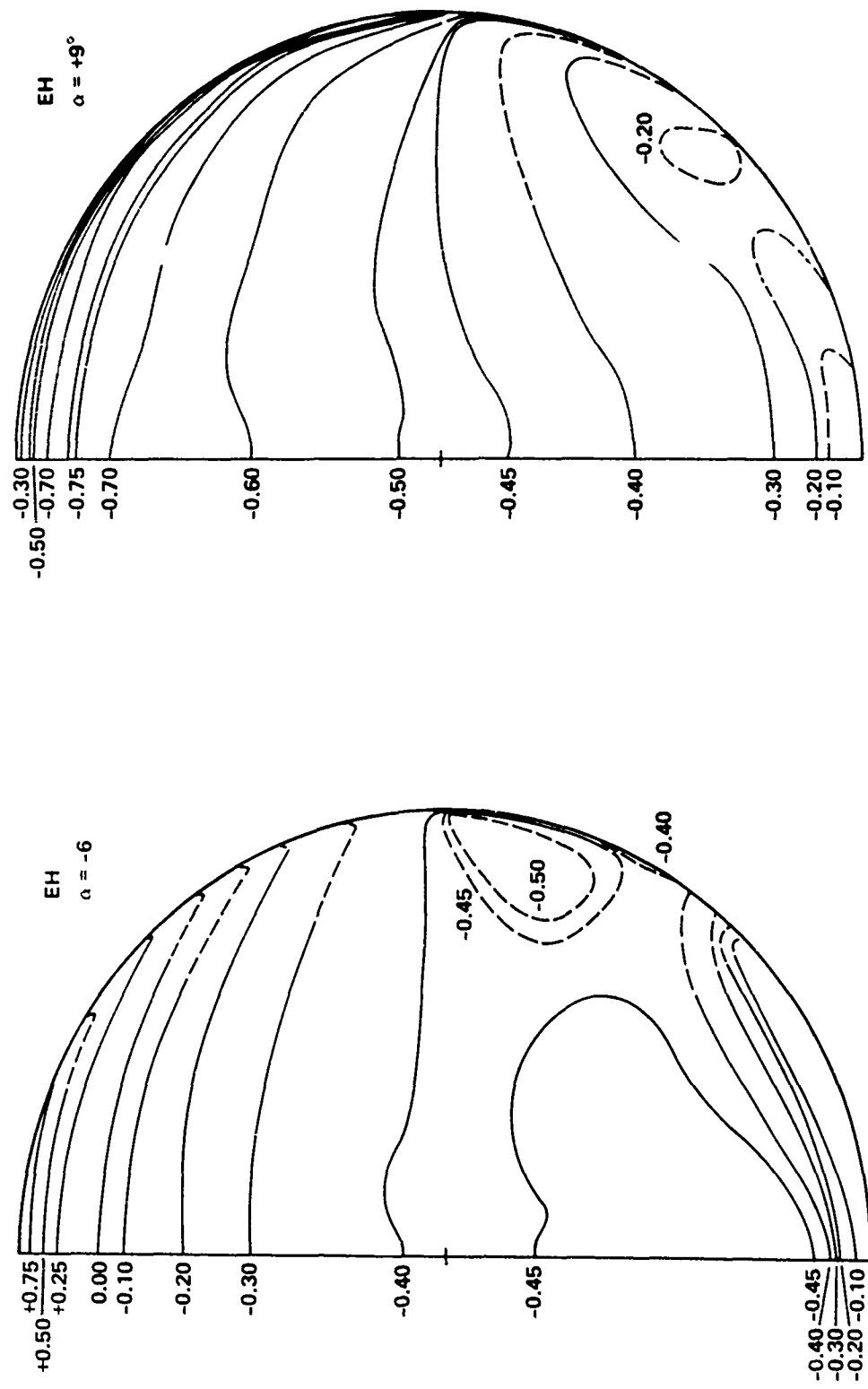


Figure 12 -- (Continued)

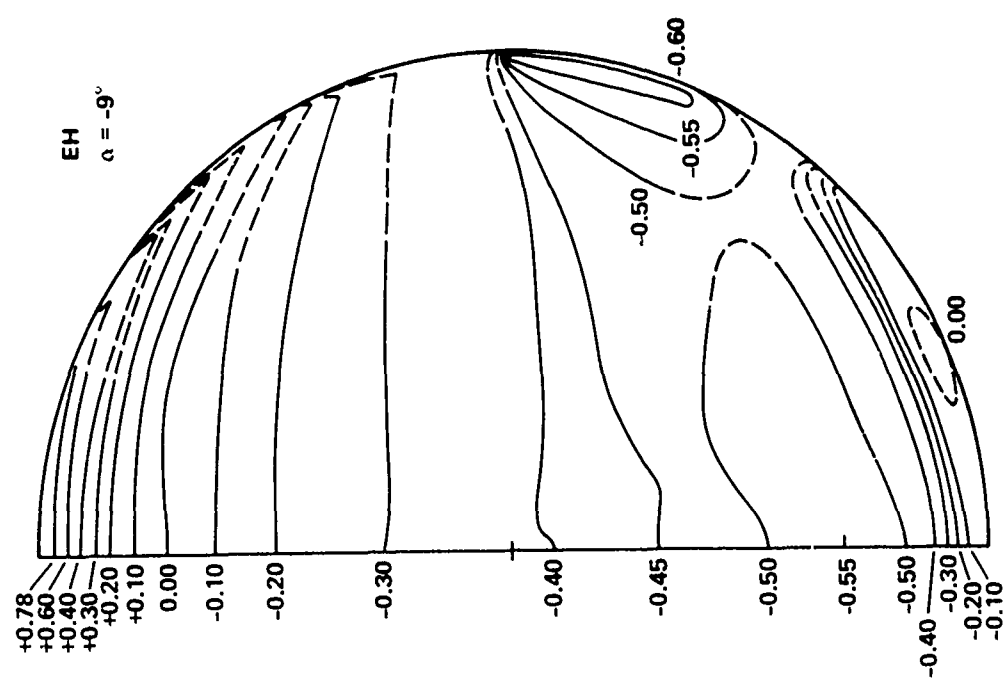
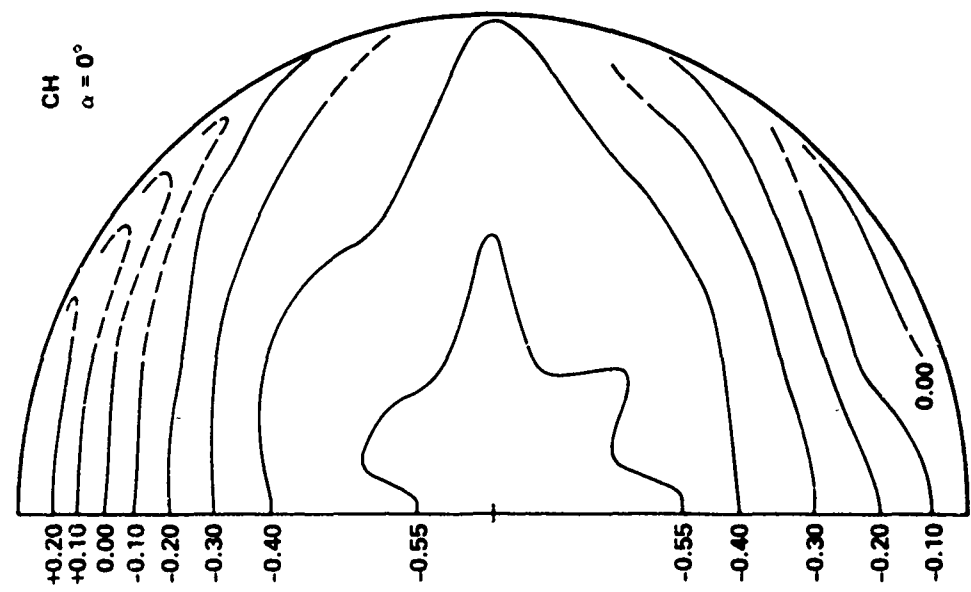


Figure 12 – (Continued)

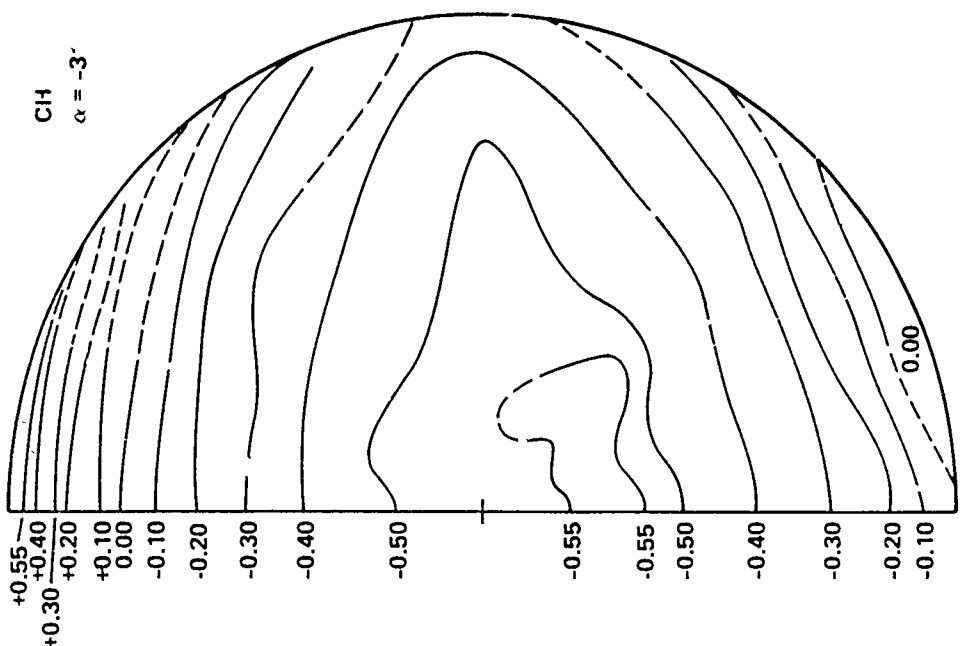
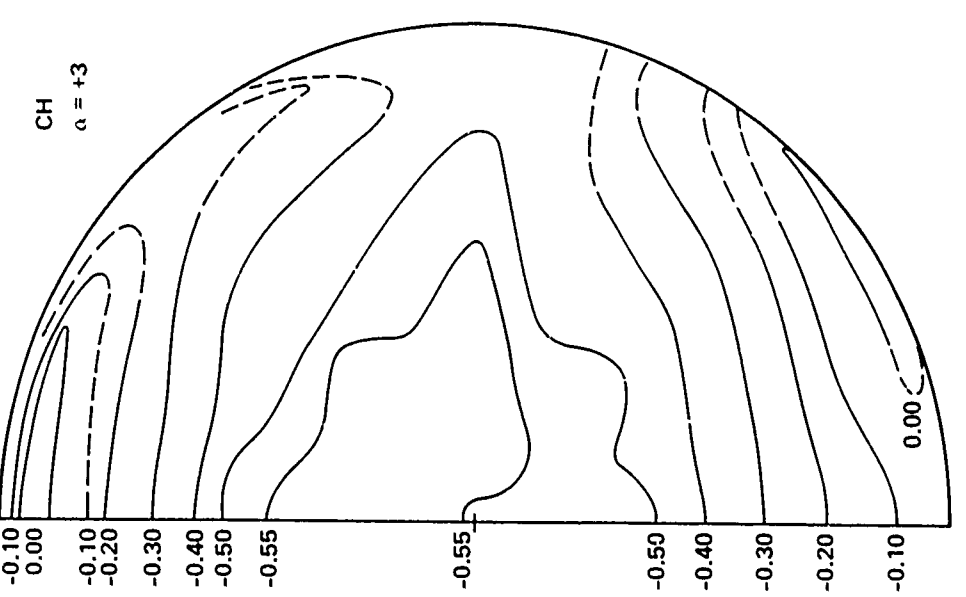


Figure 12 -- (Continued)

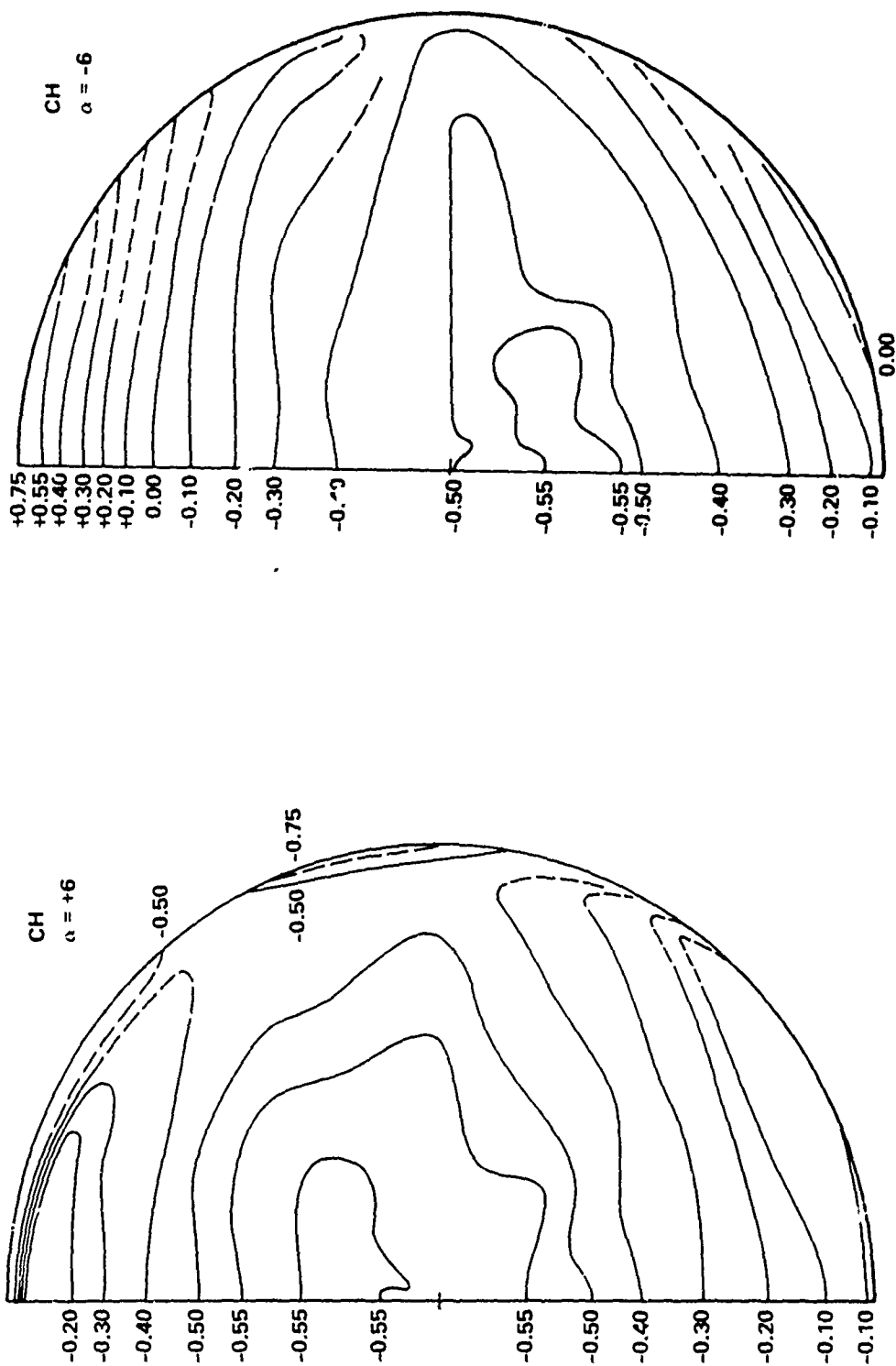


Figure 12 – (Continued)

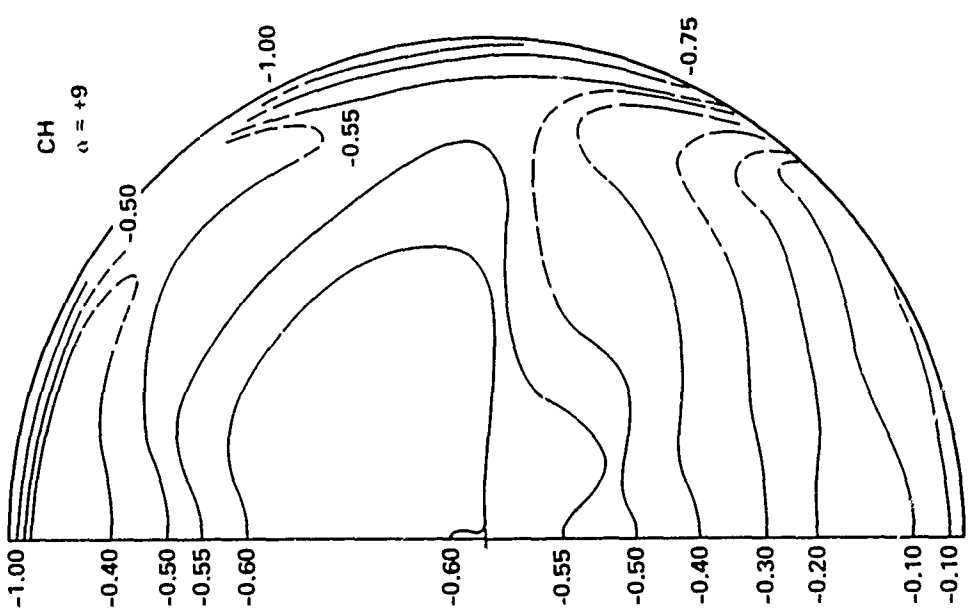
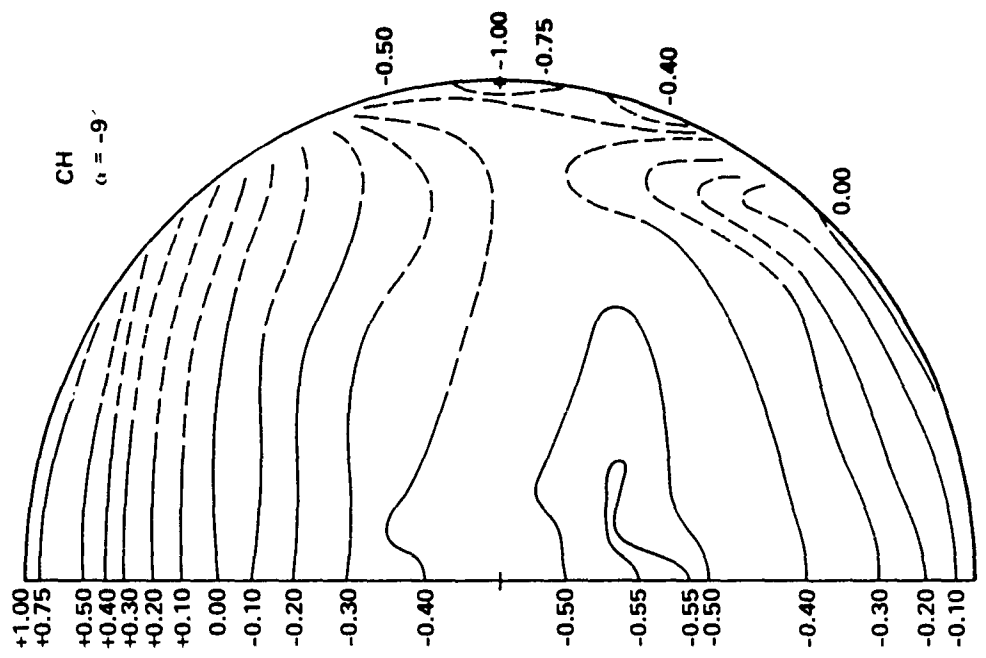


Figure 12 – (Continued)

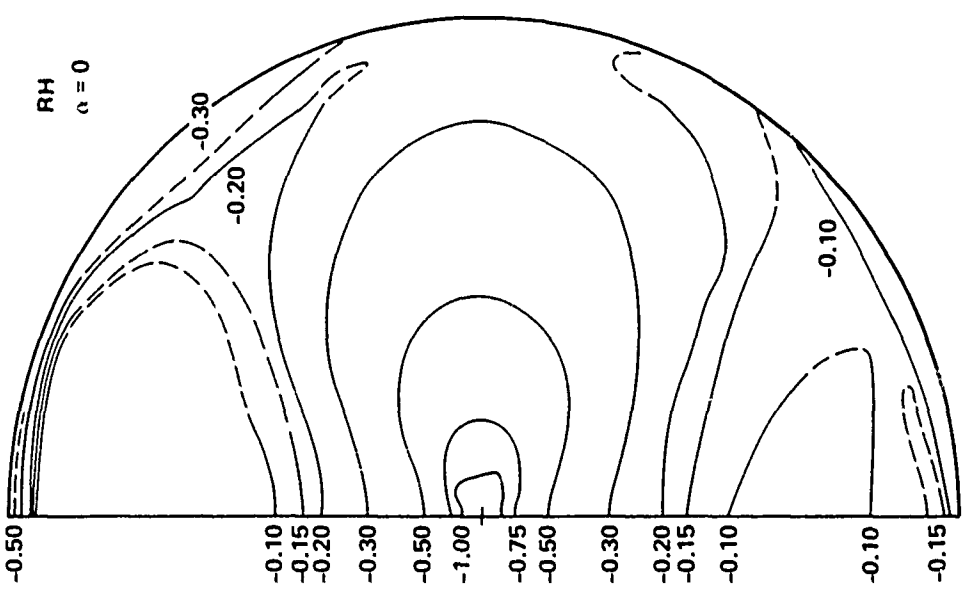
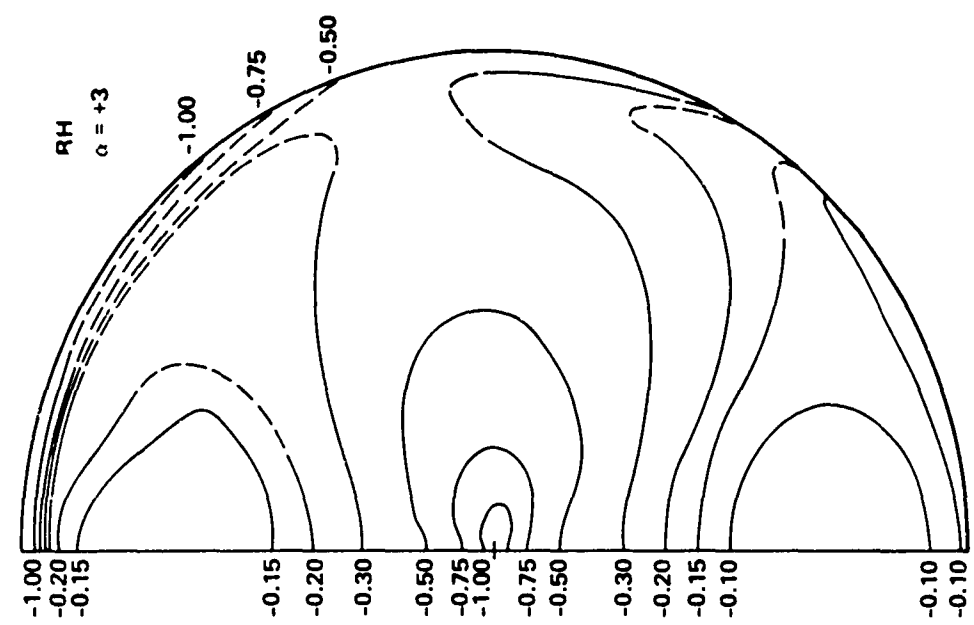


Figure 12 – (Continued)

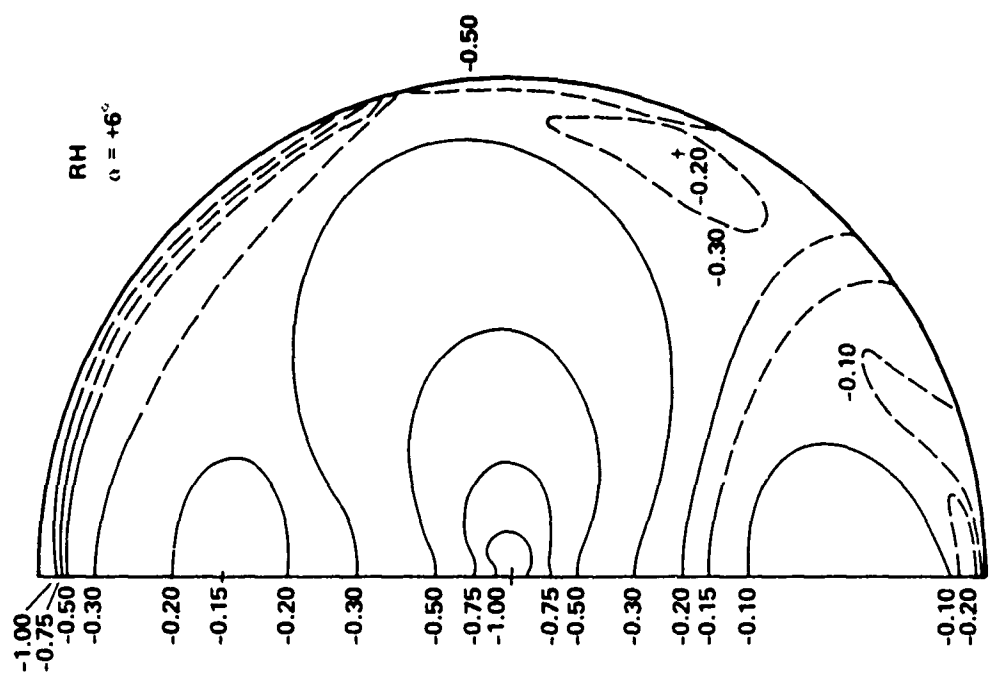
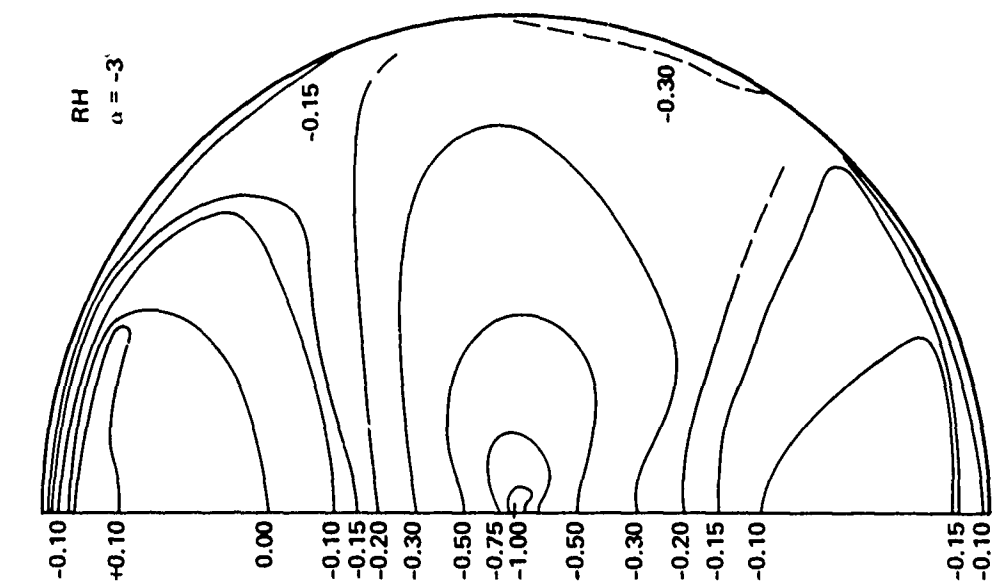


Figure 12 – (Continued)

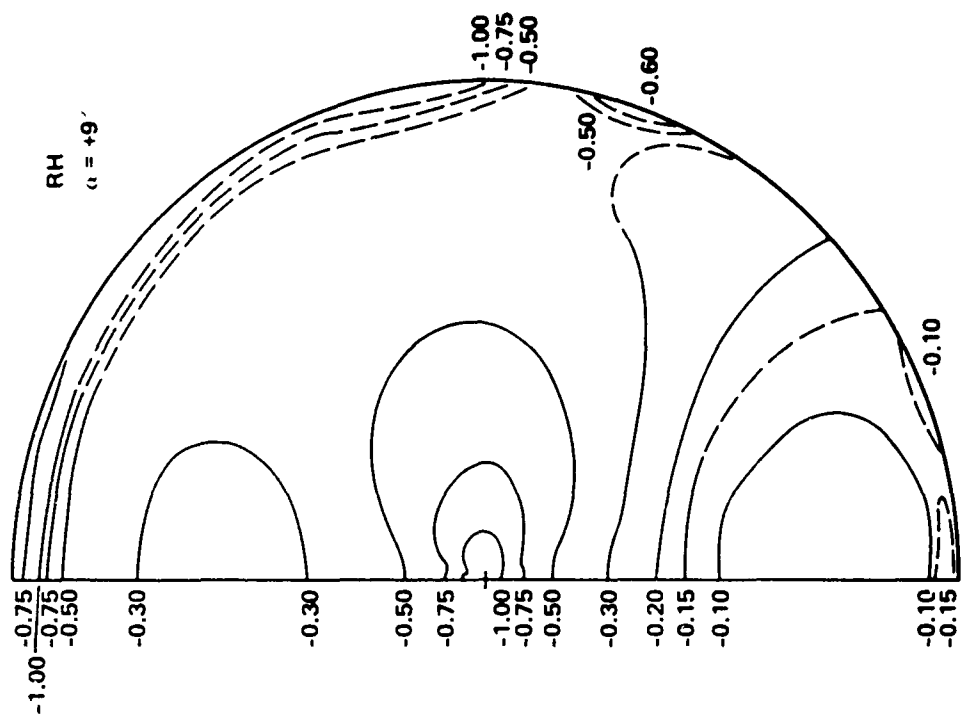
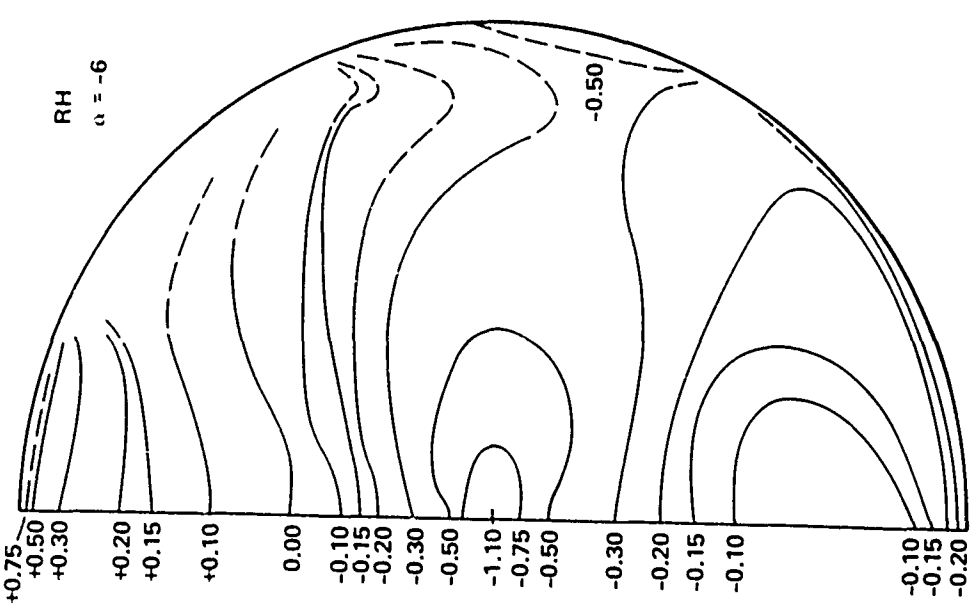


Figure 12 – (Continued)

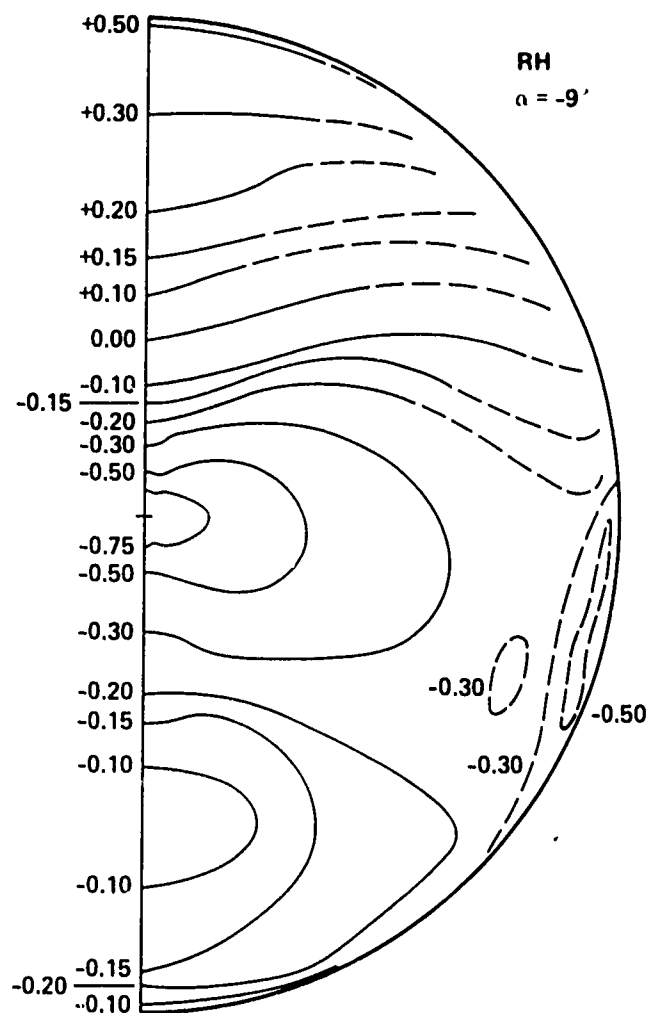
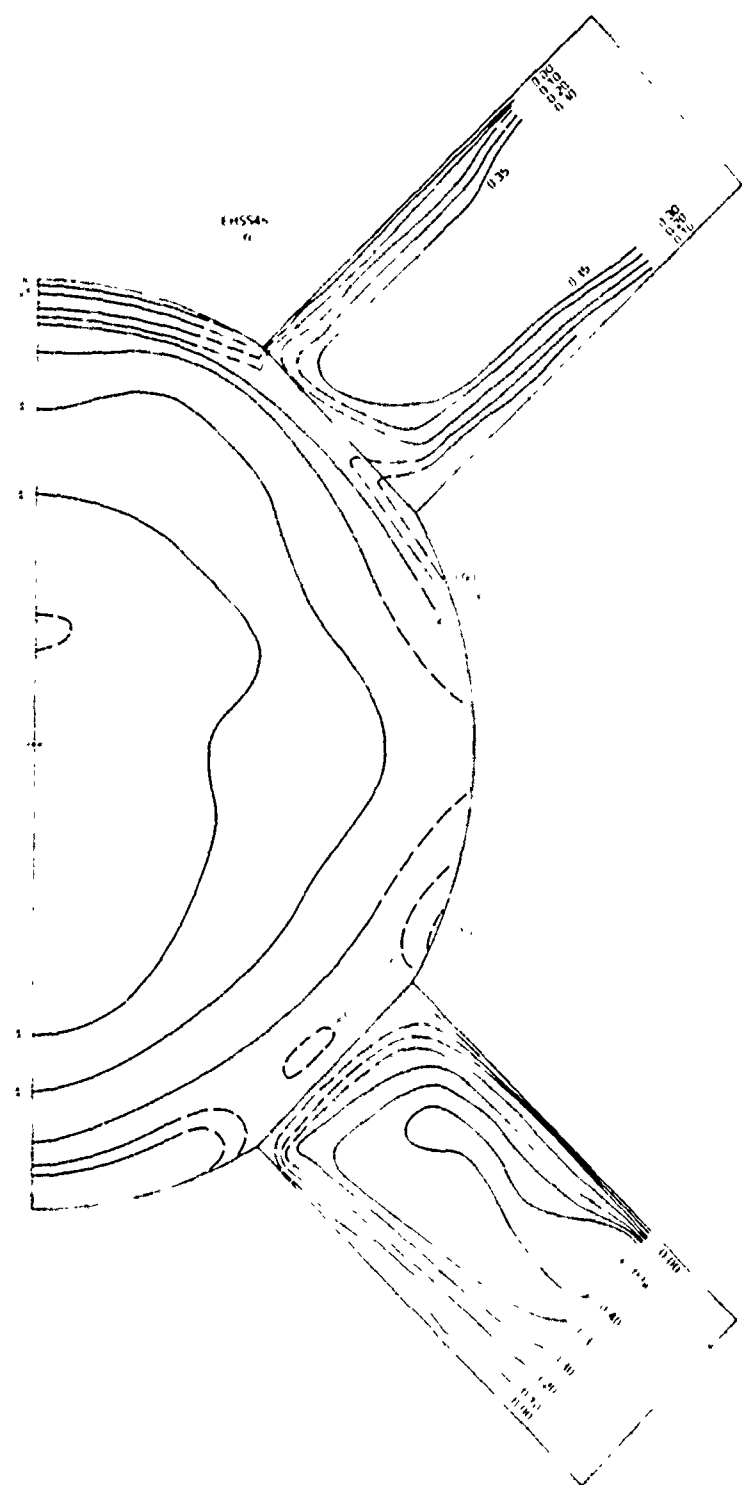


Figure 12 – (Concluded)

Figure 13 – Pressure Coefficient Contours on the Upper Surface of the
Elliptical Hub - Small Shank Fairing Configurations at a Dynamic
Pressure of 50 Pounds Per Square Foot



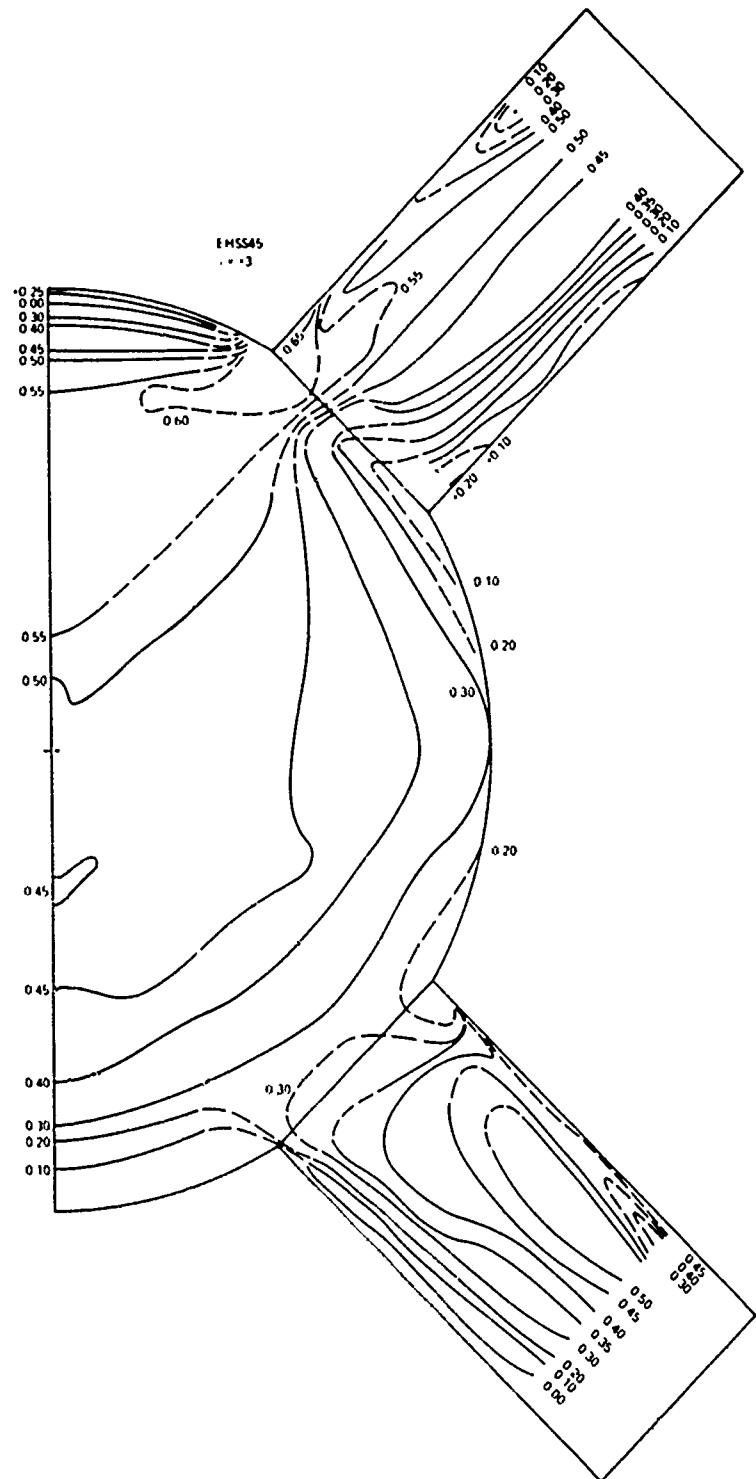


Figure 13 – (Continued)

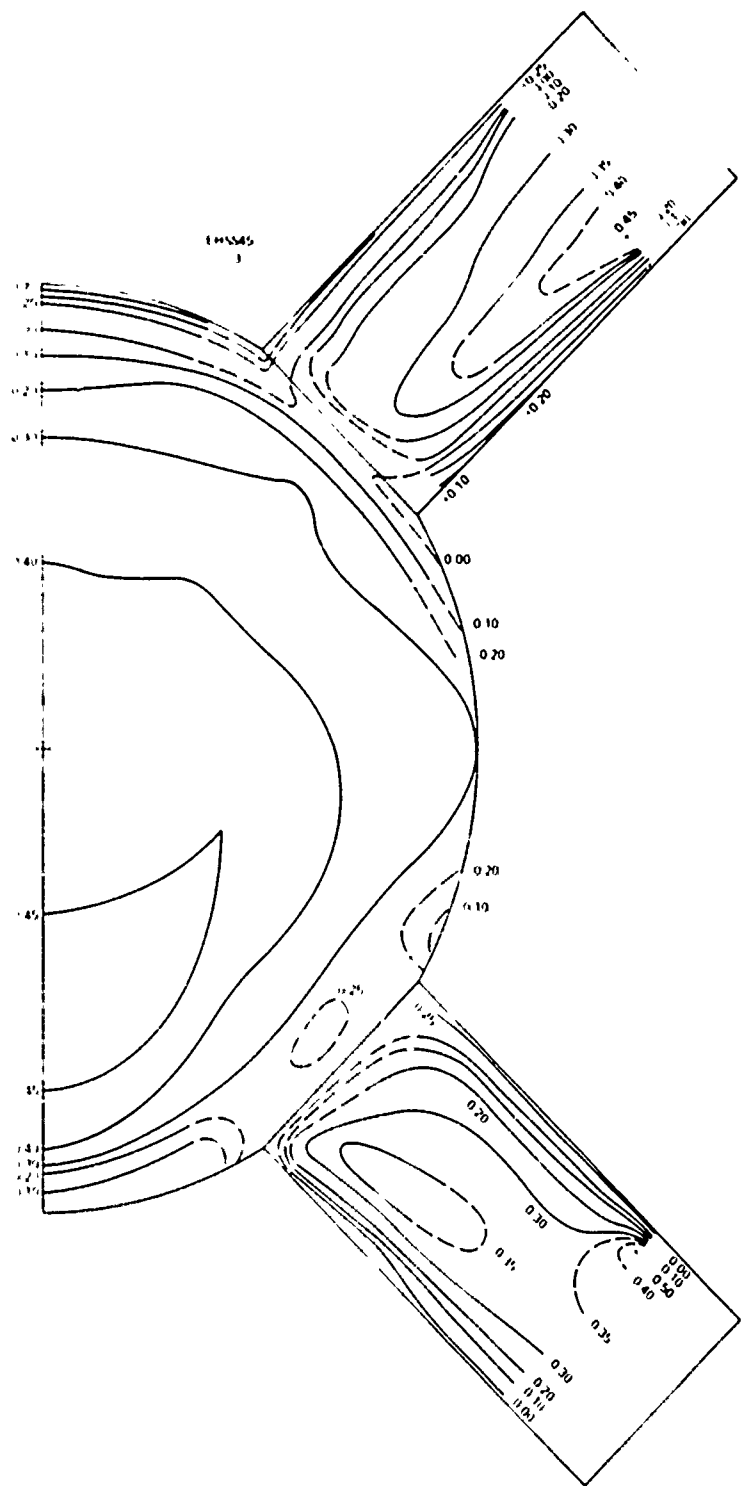


Figure 13 – (Continued)

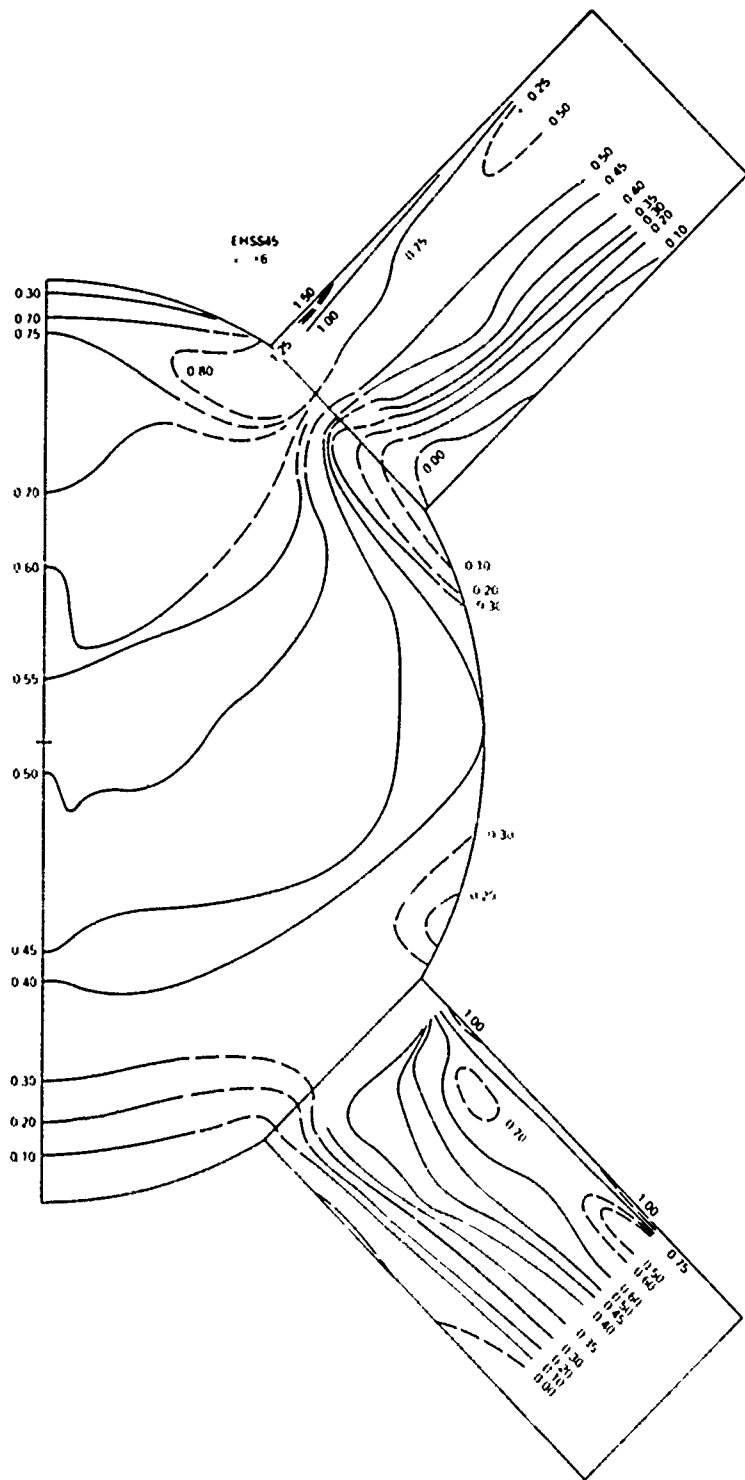


Figure 13 – (Continued)

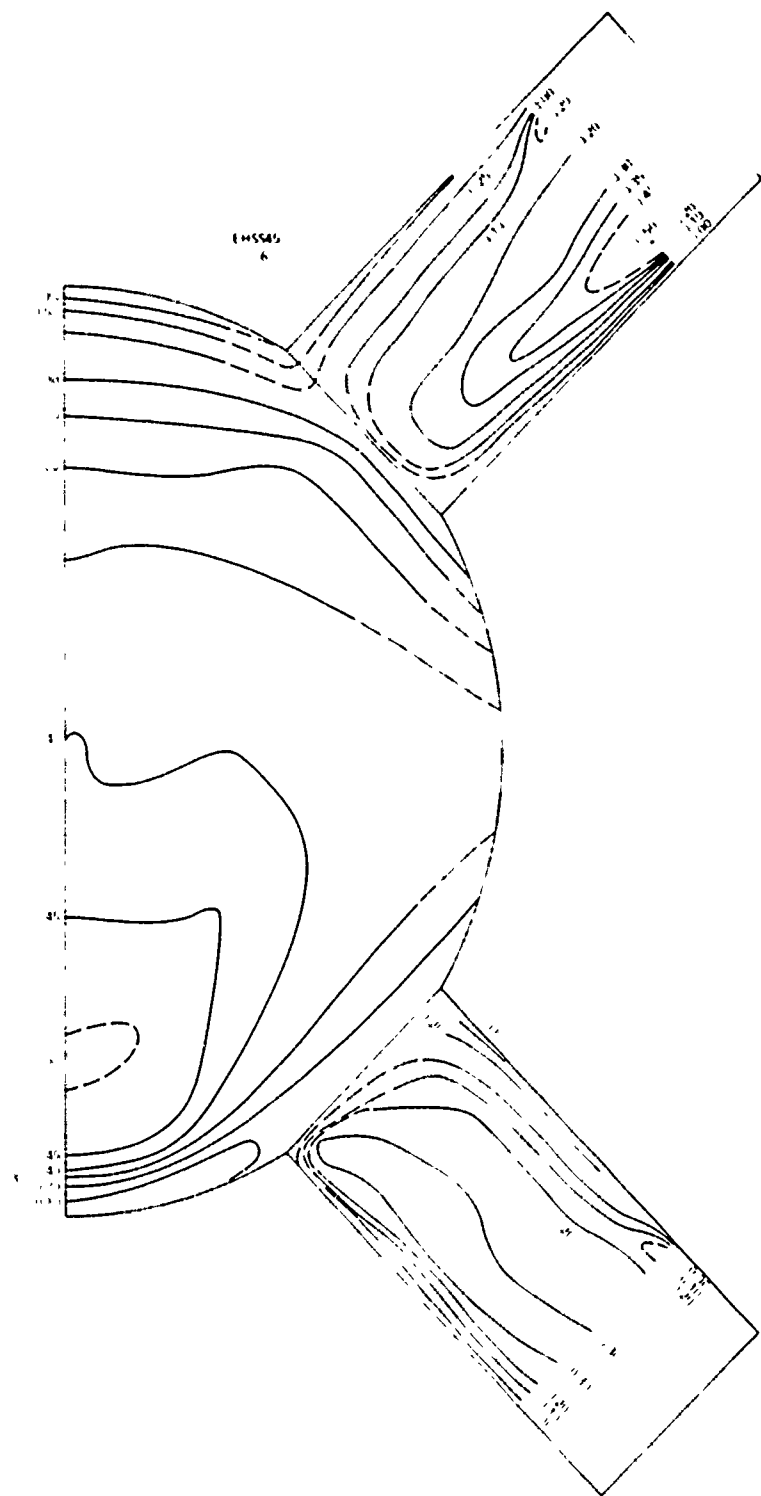


Figure 13 – (Continued)

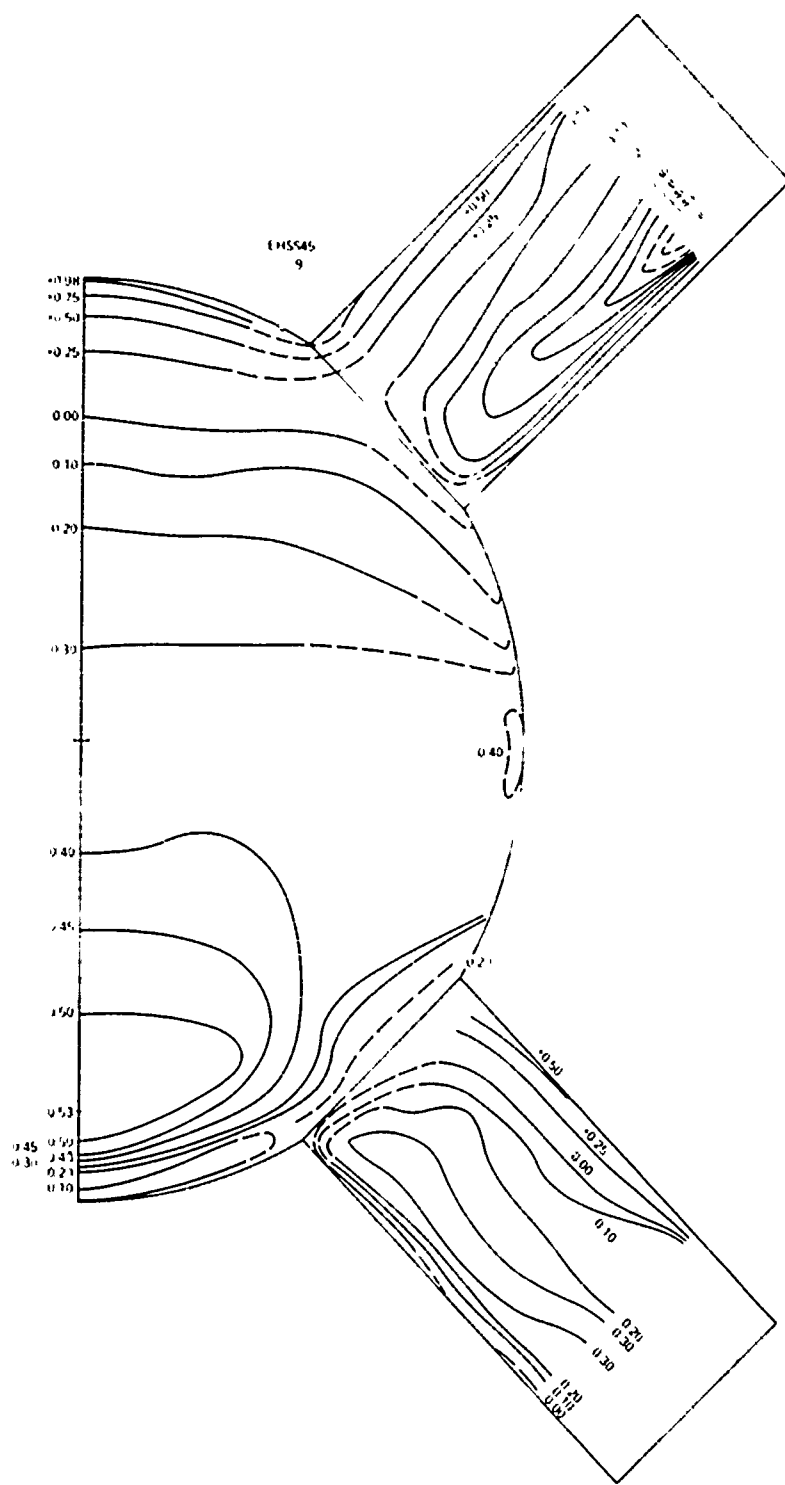


Figure 13 – (Continued)

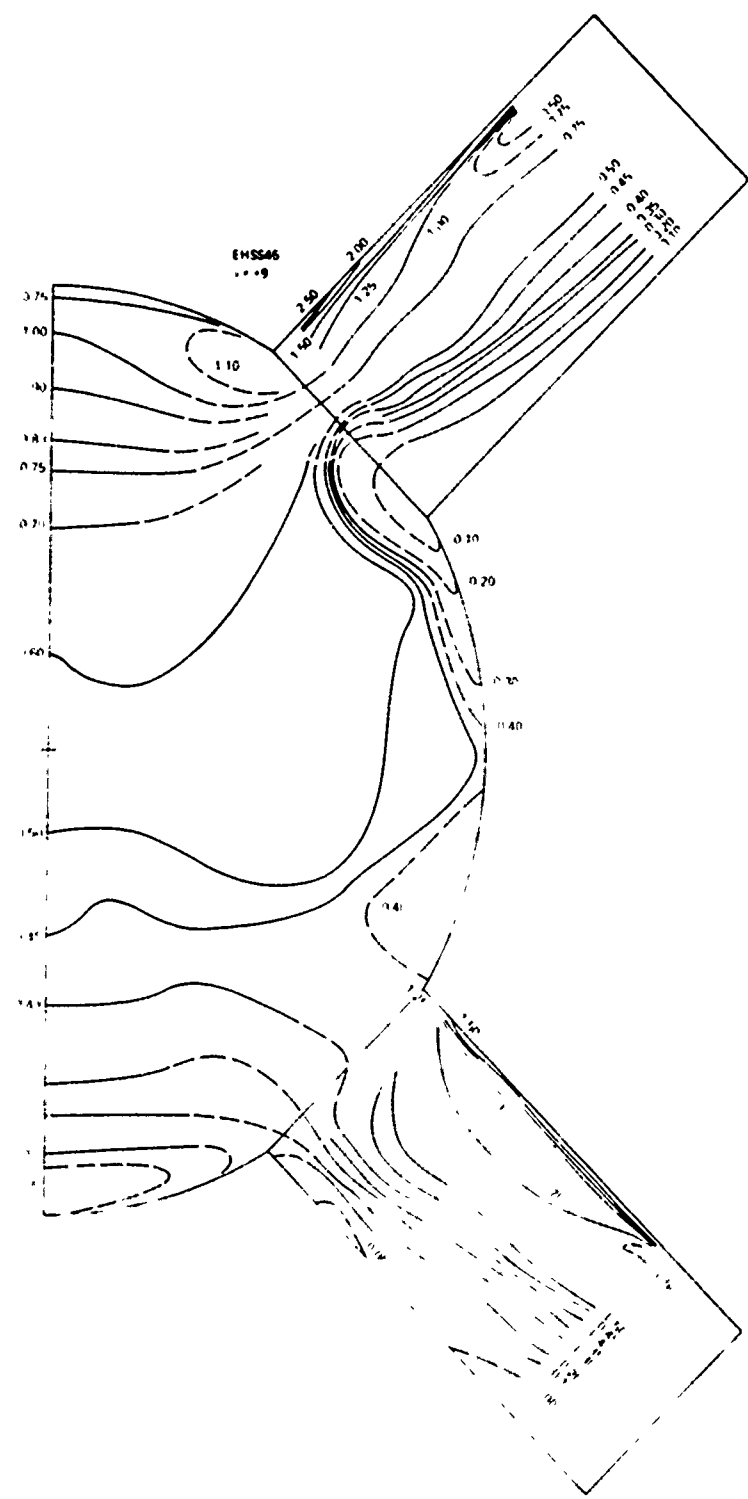


Figure 13 - (Continued)

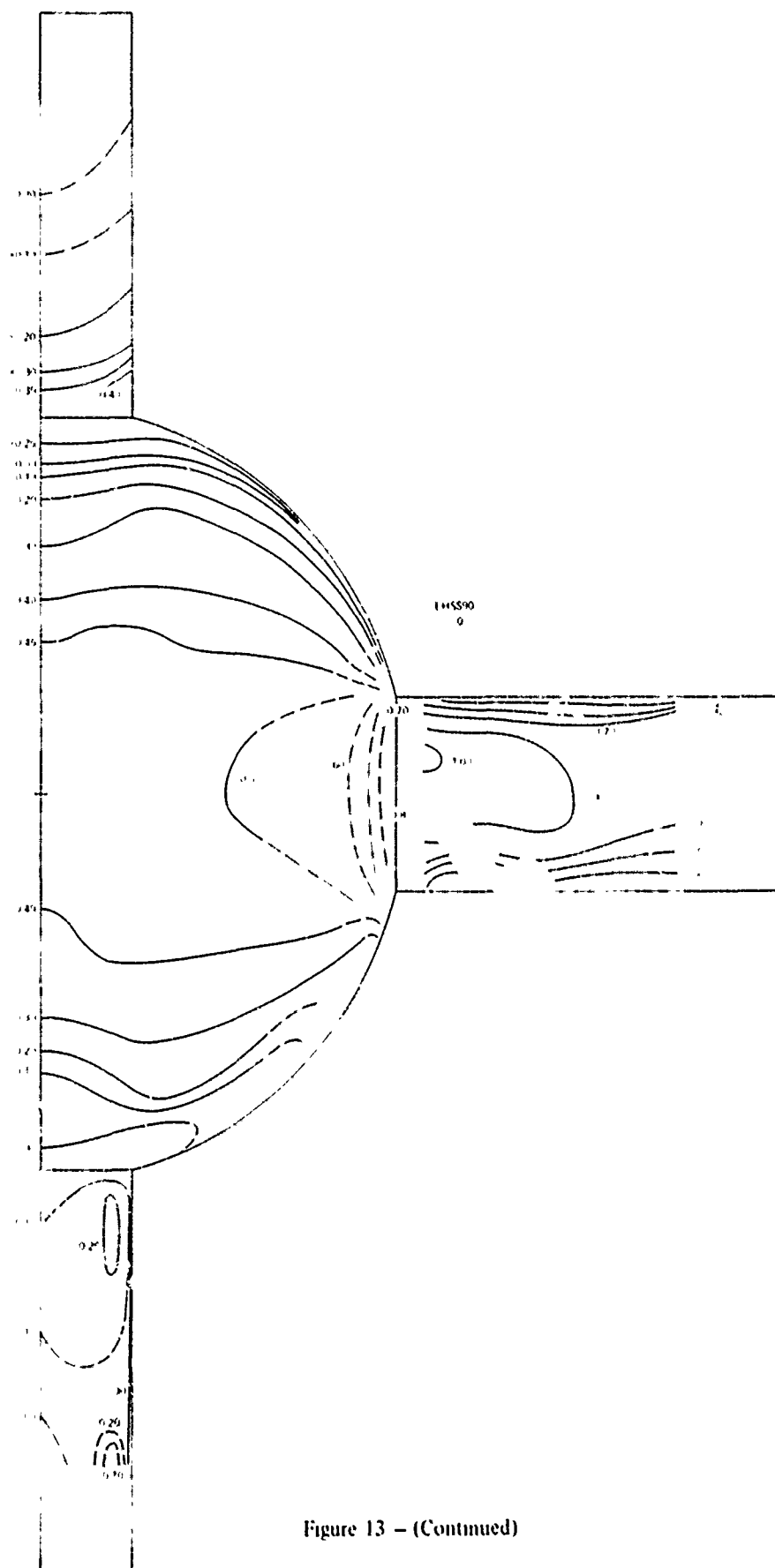


Figure 13 – (Continued)

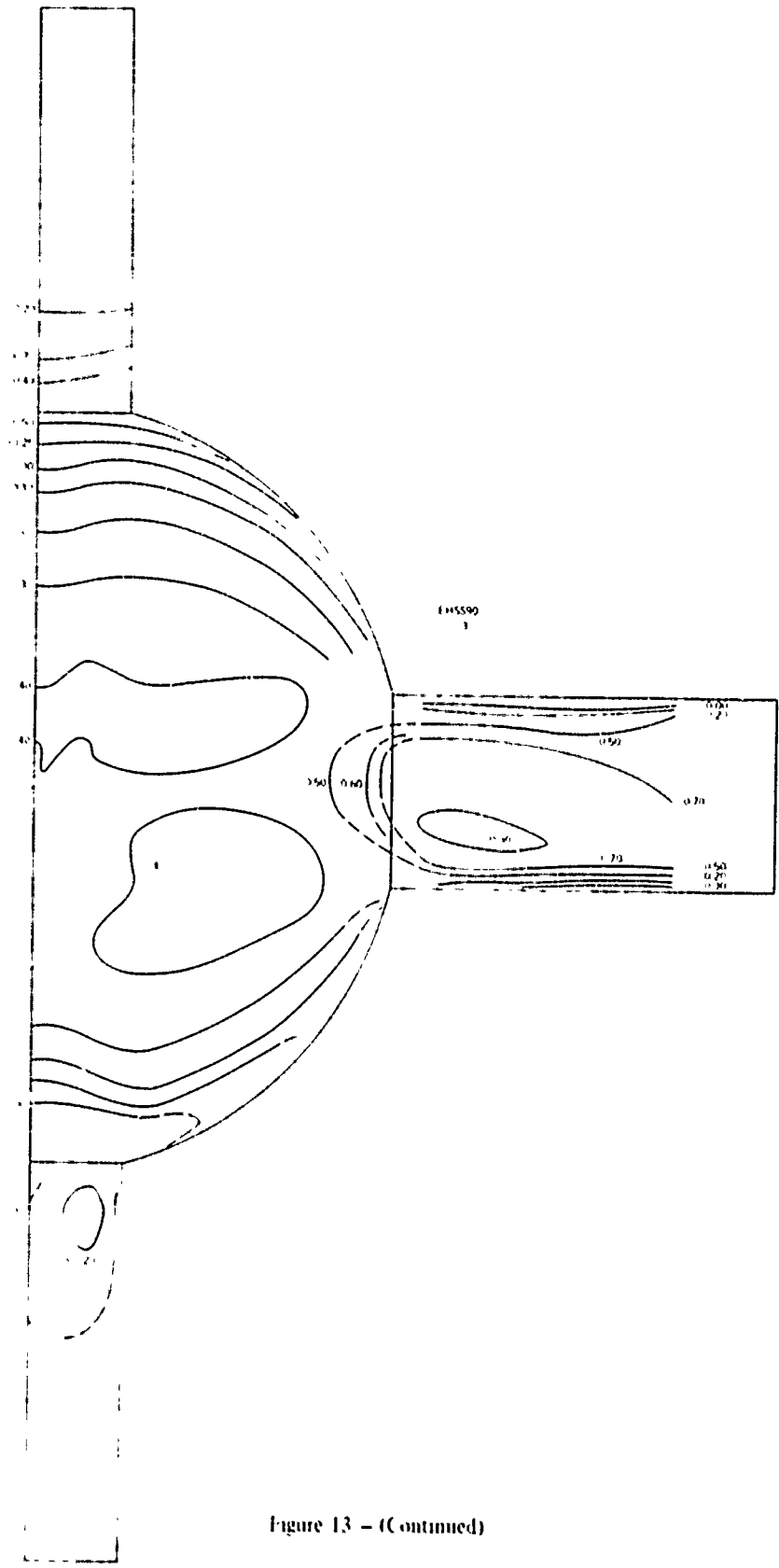
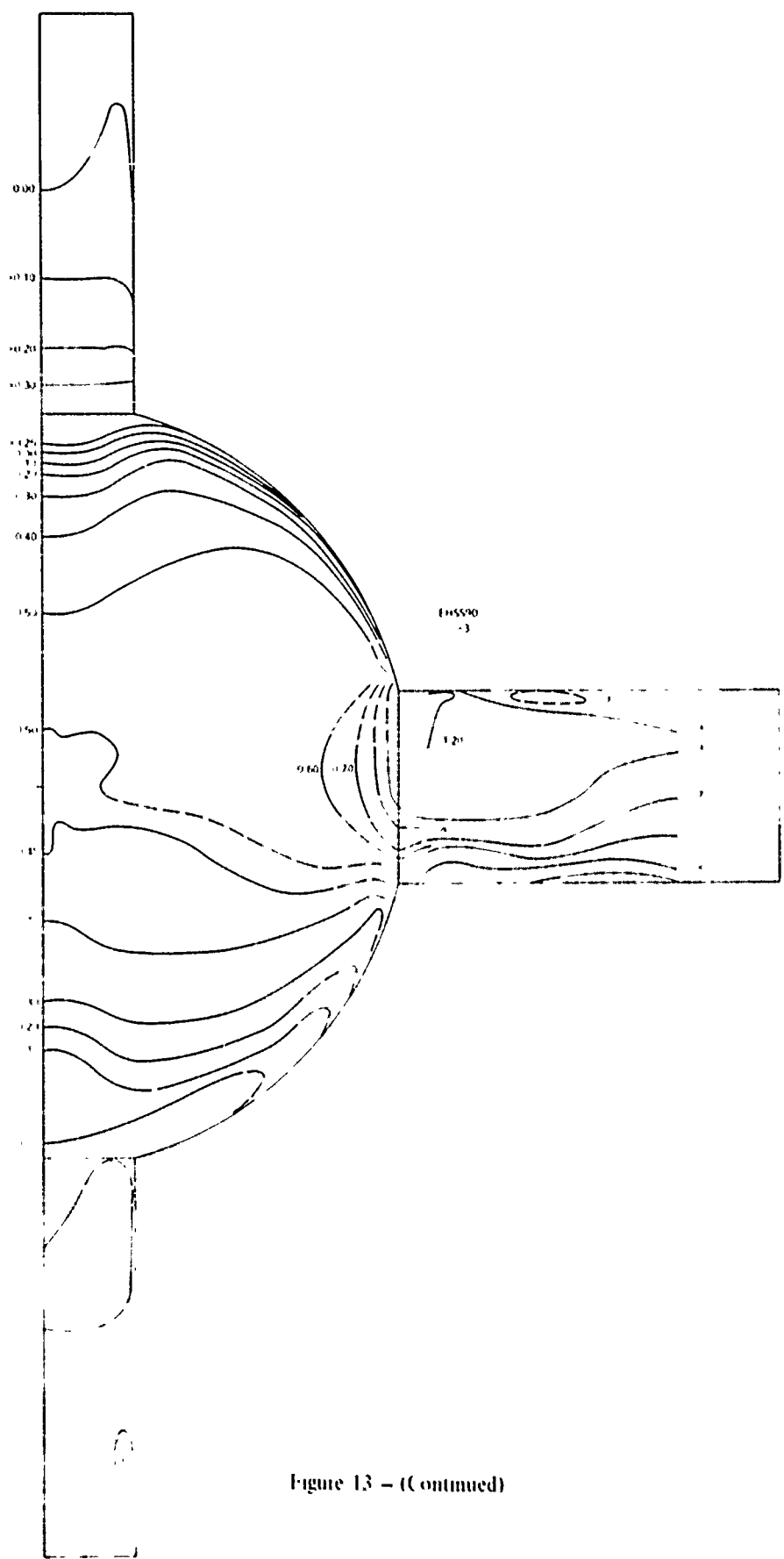


Figure 13 – (Continued)



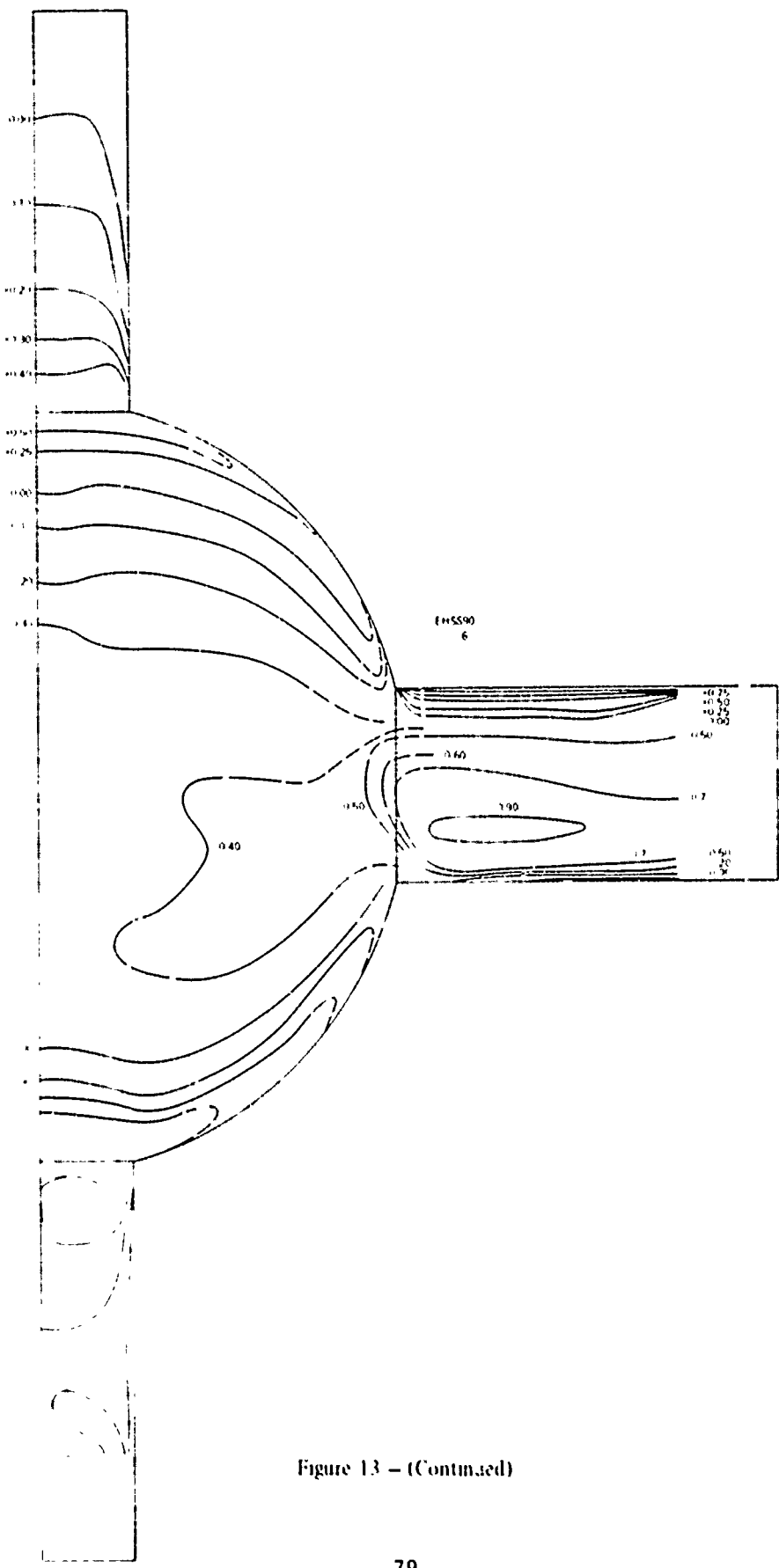
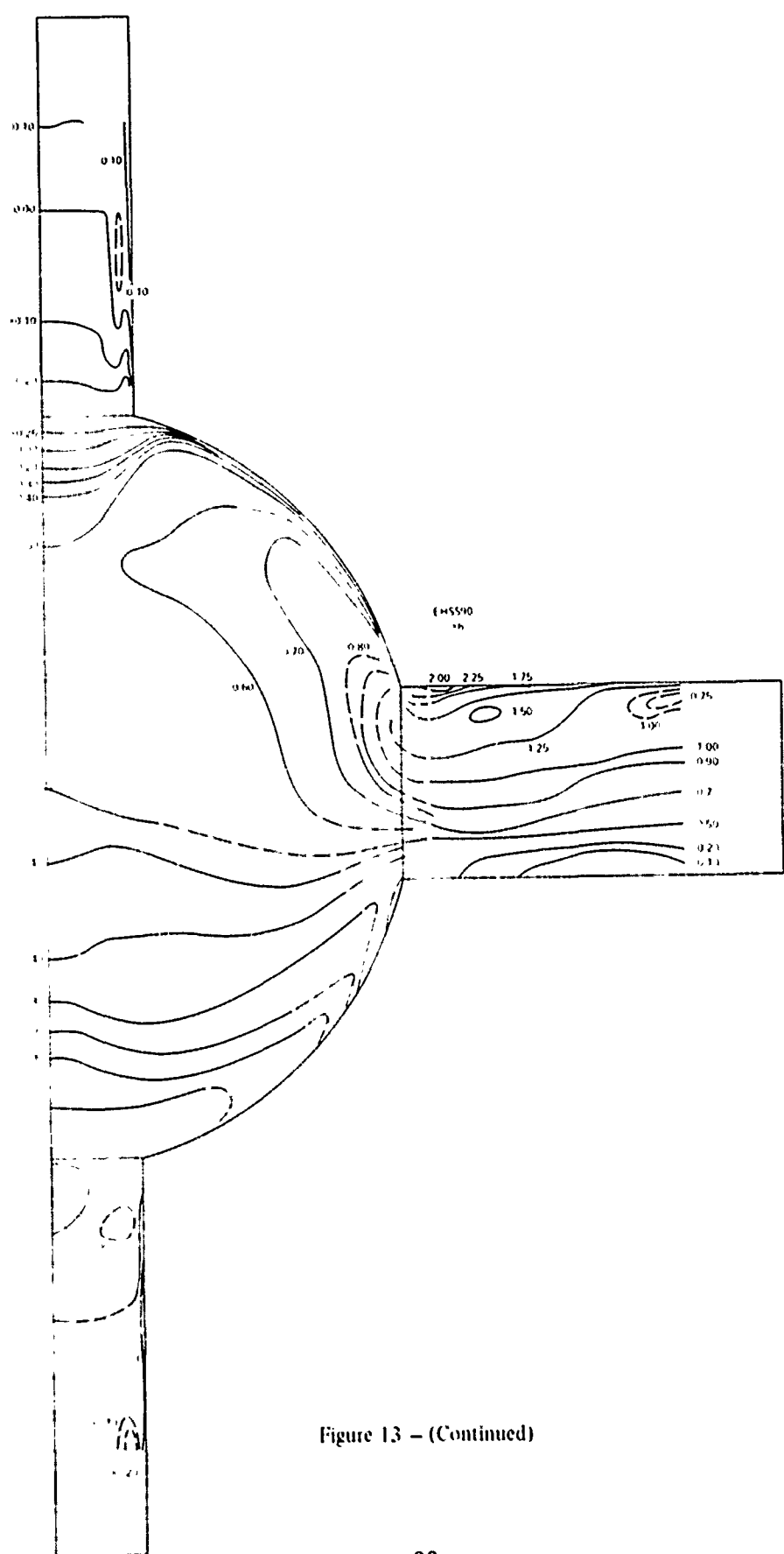


Figure 13 - (Continued)



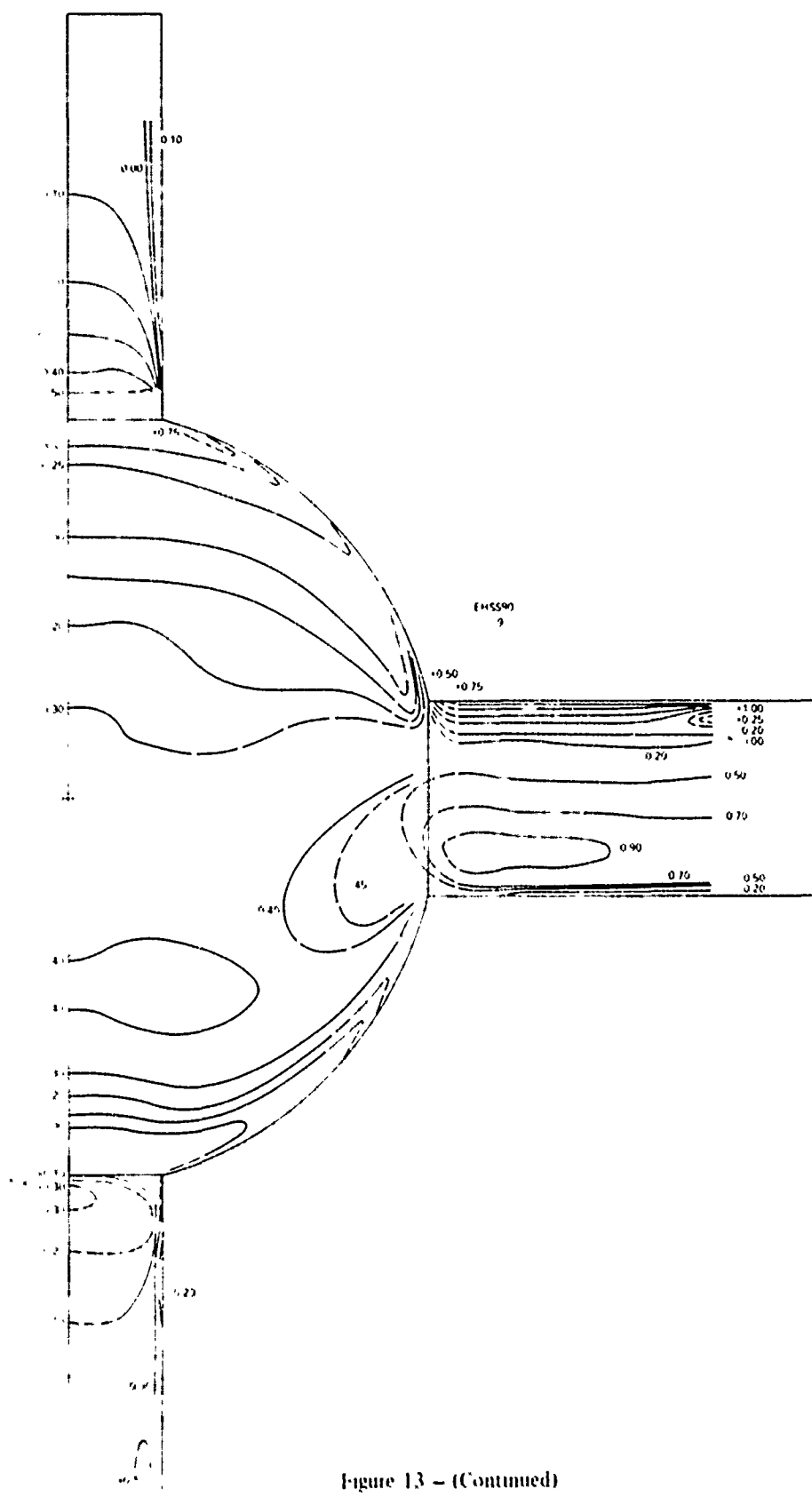


Figure 13 - (Continued)

